NASA Contractor Report 3542

Moisture Processes Accompanying Convective Activity

Meta E. Sienkiewicz and James R. Scoggins

CONTRACT NAS8-33776
APRIL 1982

NASA

NASA Contractor Report 3542

Moisture Processes Accompanying Convective Activity

Meta E. Sienkiewicz and James R. Scoggins
Texas A&M University
College Station, Texas

Prepared for
Marshall Space Flight Center
under Contract NAS8-33776

National Aeronautics
and Space Administration

**Scientific and Technical
Information Branch**

1982

ACKNOWLEDGMENTS

The authors thank Drs. Phanindramohan Das and Charles Asmuth for their review of the manuscript. Also, thanks are extended to the students who participated in the research. This contract is under the auspicies of the Atmospheric Sciences Division, NASA Marshall Space Flight Center, Huntsville, Alabama. The authors appreciate the advice and support of personnel in this division.

TABLE OF CONTENTS

TABLE OF CONTENTS (Continued)

LIST OF FIGURES

LIST OF FIGURES (Continued)

LIST OF FIGURES (Continued)

LIST OF TABLES

LIST OF SYMBOLS

Symbol		Unit
A	Area over which integration is performed	cm^2
g	Acceleration of gravity	$cm\ s^{-2}$
L	Boundary of area of integration	cm
q_L	Precipitable water	$g\ cm^{-2}$
q	Specific humidity or mixing ratio	$g\ g^{-1}$
R	Residual term integrated in vertical	$g\ cm^{-2} s^{-1}$
S	Residual term	$g\ cm^{-3} s^{-1}$
T	Time difference between observations	s
u	Wind component in x direction	$cm\ s^{-1}$
v	Wind component in y direction	$cm\ s^{-1}$
$\vec{V}$	2-dimensional vector wind	$cm\ s^{-1}$
$\vec{V}_3$	3-dimensional vector wind	$cm\ s^{-1}$
V_n	Wind component normal to boundary	$cm\ s^{-1}$
ρ	Density of air	$g\ cm^{-3}$
ρ_L	Density of liquid water	$g\ cm^{-3}$
ρ_v	Density of water vapor	$g\ cm^{-3}$
$\vec{\nabla}$	2-dimensional del operator	cm^{-1}
$\vec{\nabla}_3$	3-dimensional del operator	cm^{-1}
ω	Kinematic vertical motion	$\mu bar\ s^{-1}$

1. INTRODUCTION

a. Statement of the problem

The distribution of moisture in the atmosphere is important, as the availability of moisture controls the initiation and maintenance of convective activity. The moisture distribution is quite variable, especially in regions where convective activity is taking place. This is because the activity acts to modify the moisture distribution.

Time scales of convective activity are typically on the order of a few hours at most. Ordinary 12-hr synoptic-scale data are unable to adequately resolve features of convective activity and its interrelationships with larger-scale weather systems. Data taken at 3-hr intervals are better able to resolve the smaller-scale systems. The calculation of moisture budgets with 3-hr rawinsonde data allows the determination of changes in the distribution of moisture in the atmosphere, and some of the processes that act to produce these changes.

b. Previous studies

Researchers have found moisture budgets to be useful in investigating characteristics of storms and storm areas. Many have used simplified budget equations because of the inadequacies of the data available. Spar (1953) used a moisture budget to forecast precipitation by equating the moisture convergence of a region to the maximum possible increase in precipitable water. In this forecast method, the entire vertical column would have to become saturated before precipitation could occur, and so the method was found useful in locating regions of large expected rainfall although forecast amounts failed to verify.

Bradbury (1957) computed water budgets for three kinds of storms. Her method of computation was similar to Spar's, but she improved the formulation by using a local rate-of-change of moisture

computed from soundings spaced at intervals of 6 hr rather than requiring saturation conditions. The budgets were computed over large areas encompassing the storms, and integrated from the surface to 400 mb so that it was possible to neglect vertical divergence. Her results showed a fair agreement between observed and computed precipitation. She also was able to show differences in rainfall potential between the storms.

Palmén and Holopainen (1962) used a simple form of the moisture budget equation in analyzing an extratropical cyclone over the central United States. They found that horizontal moisture convergence, the dominant term, nearly balanced the observed precipitation.

A number of researchers have used moisture budgets in the tropics for convective parameterization (e.g., Yanai, et al., 1973; Ogura and Cho, 1973; and Cho, 1977). However, Fritsch et al. (1976) have shown that the synoptic-scale budgets in middle latitudes would likely underestimate precipitation if used for convective parameterization. In their study of an Oklahoma squall line, they found that the synoptic-scale moisture convergence was much smaller than the rate of comsumption of water vapor by mesoscale systems, and it explained only 20% of the rainfall rate. They concluded that mesoscale organization and development can generate substantially larger moisture flux into convective clouds than that indicated by the synoptic-scale moisture convergence.

Scott and Scoggins (1977) analyzed the moisture budget for two squall lines that occurred during the Spring of 1975. By using observations spaced at 3 and 6 hr, they found that moisture accumulation by moisture convergence occurred in regions downstream from the strongest convective activity; future development was favored in these regions. Good relationships existed between the local rate-of-change of moisture and convection observed by radar 3 hr later. The computed moisture sink terms were in fairly good agreement with observed precipitation.

Other studies have concentrated on observations taken on a smaller scale. Sanders and Paine (1975) made a composite analysis of an Oklahoma squall line by grouping observations with respect to their distance from the surface wind shift line. They explained sources and sinks of moisture in terms of physical processes occurring in the area. The calculated moisture sink, however, did not balance the measured precipitation, and they attributed this to the transport of liquid water through the boundary of their analysis area. Bradberry (1981) analyzed another squall line by the same method but could not evaluate the local rate-of-change term. However, the magnitudes and locations of sources and sinks of moisture were compatible with the earlier study.

Williams and Scoggins (1979) used a number of observations from the Texas HIPLEX area to develop water budget models for storms. Results were stratified according to the presence, type, depth, and areal coverage of radar echoes. The largest residuals were found for deep convection and for echo coverage greater than 50%. A nearly linear relationship was found between the residual moisture sink term and precipitation, with the best agreement occurring when the precipitation was the heaviest.

c. Objectives of research

The objective of this research is to determine the moisture balance in convective and non-convective areas using 3-hr rawinsonde data from synoptic and sub-synoptic scale rawinsonde networks. Specific items to be investigated include the depth of the environmental energy (moisture) source for the convective activity, the rate of vertical transport and redistribution of environmental moisture due to large-scale vertical motion, and the combined influence of environmental and convective transports on the redistribution of moisture accompanying large areas of convective activity.

The approach used will be:

1) Determine convective and non-convective areas using radar

facsimile charts and convert the coordinates of the charts to grid space.

2) Using 3-hr rawinsonde data, evaluate the following moisture budget terms:
   a) local rate-of-change of moisture,
   b) horizontal moisture divergence,
   c) vertical moisture divergence, and
   d) residual term.
3) Interpret calculated moisture budget terms to determine the part each term plays in maintaining large-scale moisture balance in regions of convective activity.

2. DATA

Rawinsonde data used in this research were collected during two Atmospheric Variability Experiments (AVE) in the Spring of 1978 and 1979. The first of the two experiments, AVE VII, was conducted on 2-3 May 1978 (Davis *et al.*, 1978). Twenty-four rawinsonde stations in the south central United States participated in AVE VII. Their locations are shown in Fig. 1. Observations were taken at eight times: 0000, 1200, 1500, 1800, and 2100 GMT on 2 May 1978; and 0000, 0300, and 1200 GMT on 3 May 1978.

The second experiment, AVE-SESAME I, was conducted as a part of the Severe Environmental Storms and Mesoscale Experiment during the spring of 1979. Forty-two rawinsonde stations participated in AVE-SESAME I, conducted on 10-11 April 1979 (Gerhard *et al.*, 1979). Locations of the participating stations are shown in Fig. 2. Soundings were taken at nine observation times during AVE-SESAME I: 1200, 1500, 1800, and 2100 GMT on 10 April, 1979, and 0000, 0300, 0600, 0900, and 1200 GMT on 11 April 1979.

The processing method for the rawinsonde data was developed by Fuelberg (1974). The recorded data and processing procedures were carefully checked for errors to assure the highest possible accuracy in the sounding data. Estimates of the RMS errors in thermodynamic quantities are given in Table 1 (Fuelberg, 1974).

The maximum RMS errors in scalar wind speed and wind direction are given in Table 2. These errors are for wind measurements computed at 30-sec intervals. The accuracy of winds at 25-mb intervals used in this report is probably greater than that stated because of the smoothing and interpolation that was performed in the data processing. The RMS errors given are for elevation angles of 10^{o} and 40^{o}.

Other data used in this report (surface observations, cumulative precipitation totals, and radar summary charts) were obtained

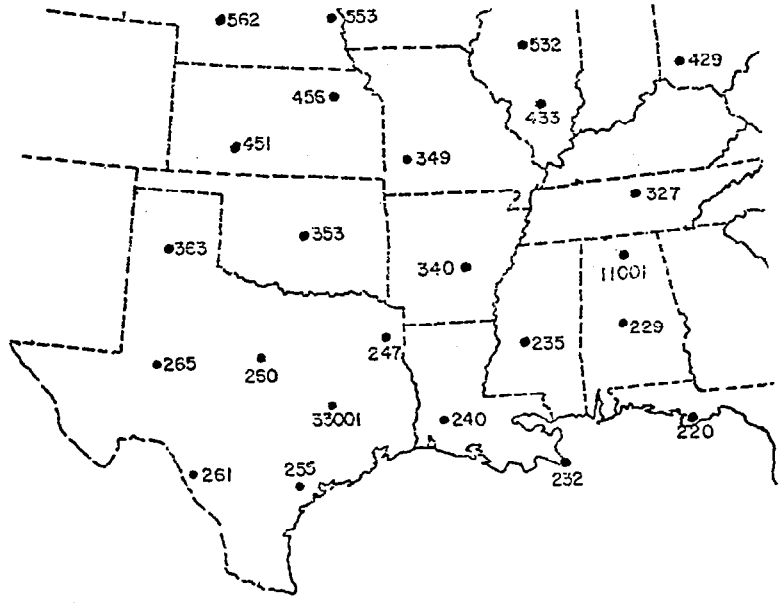

Fig. 1. Locations of rawinsonde stations participating in AVE VII.

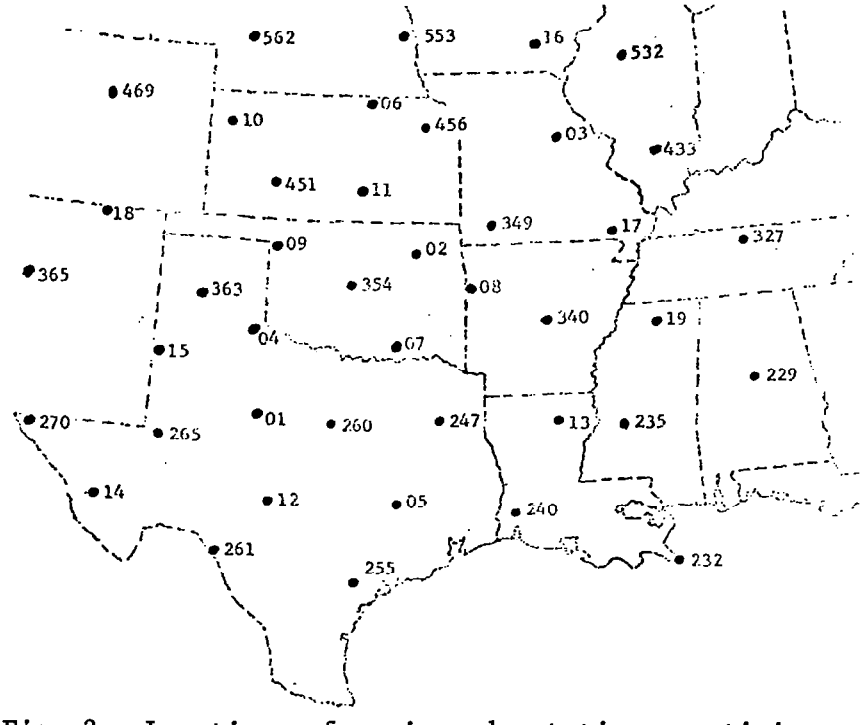

Fig. 2. Locations of rawinsonde stations participating in AVE-SESAME I.

Table 1. Estimates of RMS errors in thermodynamic data (after Fuelberg, 1974).

Parameter	Approximate RMS Error
Temperature	0.5°C (Fuelberg's value is 1°C)
Pressure	1.3 mb from surface to 400 mb; 1.1 mb between 400 and 100 mb; 0.7 mb between 100 and 10 mb.
Humidity	10 percent
Pressure Altitude	10 gpm at 500 mb; 20 gpm at 300 mb; 50 gpm at 50 mb.

Table 2. Estimates of RMS errors in wind speed and direction (after Fuelberg, 1974).

	RMS errors ($m\ s^{-1}$) in speed		RMS errors (deg) in direction	
Pressure	10 deg el.	40 deg el.	10 deg el.	40 deg el.
700	2.5	0.5	9.5	1.3
500	4.5	0.8	13.4	1.8
300	7.8	1.0	18.0	2.5

from routine teletype reports and facsimile charts produced by the National Weather Service and archived at Texas A&M University.

3. SYNOPTIC CONDITIONS

Figure 3 shows synoptic charts for 0000 GMT on 3 May 1978. During the AVE VII experiment, a cold-core low which intensified with height moved eastward from Arizona across the Texas Panhandle. At the surface, a cold front moved southward to the Gulf Coast and became stationary.

The low-level flow from the south brought warm and moist air from the Gulf into the Texas area. The combination of the warm influx in lower levels with cold air in upper levels associated with the upper-level low, created conditions that were favorable for the development of severe convective activity.

Radar summary charts showing areas and intensity of convective activity during the AVE VII experiment are contained in Appendix B. A large area of showers and thunderstorms developed in the western part of the analysis area under the influence of the upper-level low. As time progressed, these storms moved eastward as the upper-level low moved into the Texas Panhandle. An additional area of storms developed in the east over southern Mississippi and eastern Louisiana midway through the experiment in the vicinity of the surface front. This area of storms did not move with time.

Synoptic charts for 0000 GMT on 11 April 1979 are shown in Fig. 4. These figures are reproduced from Williams et al. (1980) with some modifications. During the AVE-SESAME I experiment, southerly and southeasterly winds advected warm and moist Gulf air northward in lower layers south of a weak warm front. The moist air was overlain by a layer of southwest winds that advected warm and dry air from the Mexican plateau into Texas which created a capping inversion that inhibited convection early in the experiment. Convective activity developed north of the warm front fairly early in the experiment as a result of lifting of the air over the frontal surface. A cold front associated with a deepening low approached

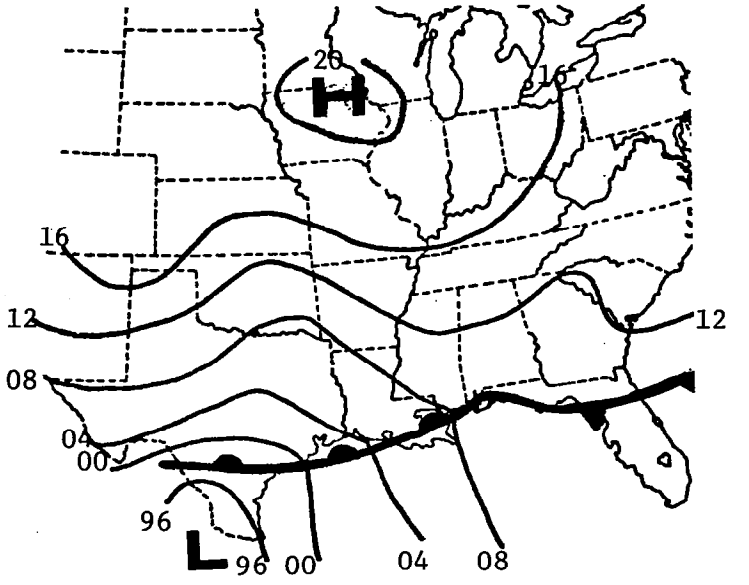

a. Surface

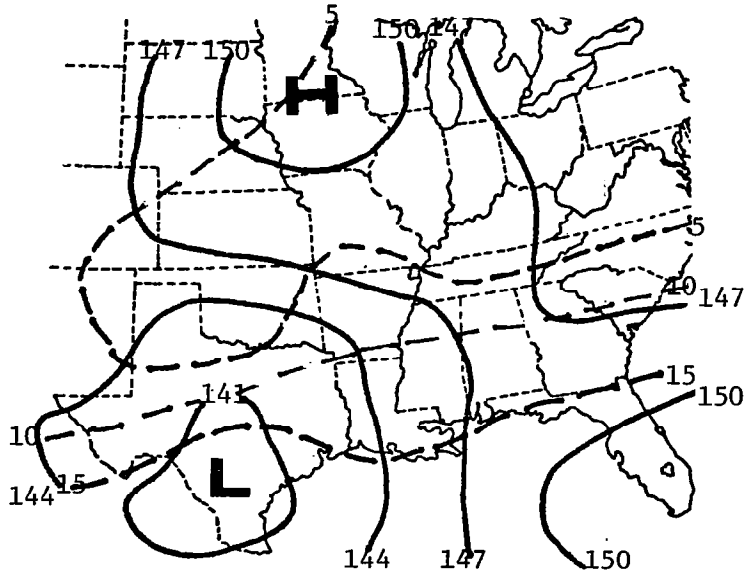

b. 850 mb

Fig. 3. Synoptic charts for 0000 GMT on 3 May 1978.

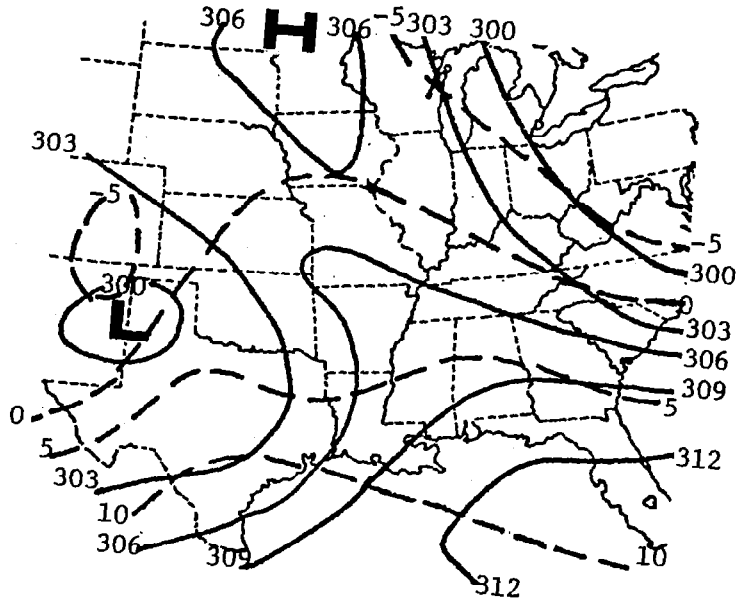

c. 700 mb

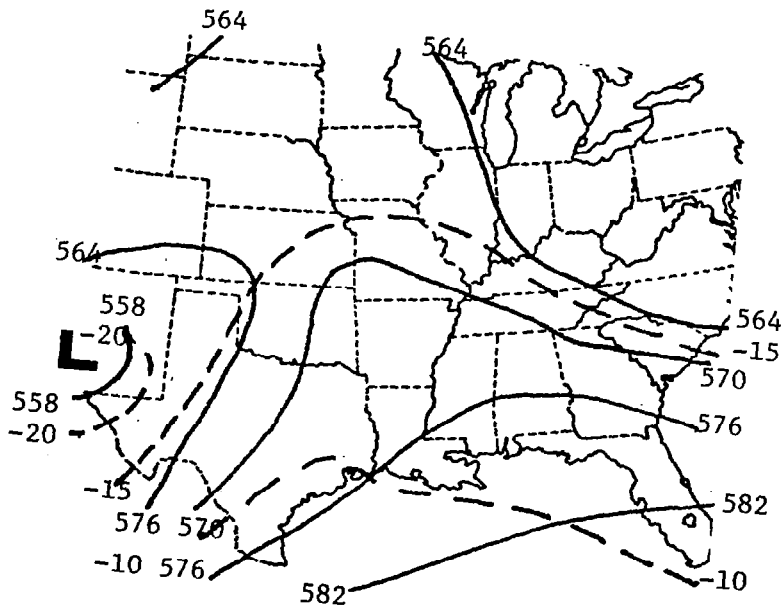

d. 500 mb

Fig. 3. (continued)

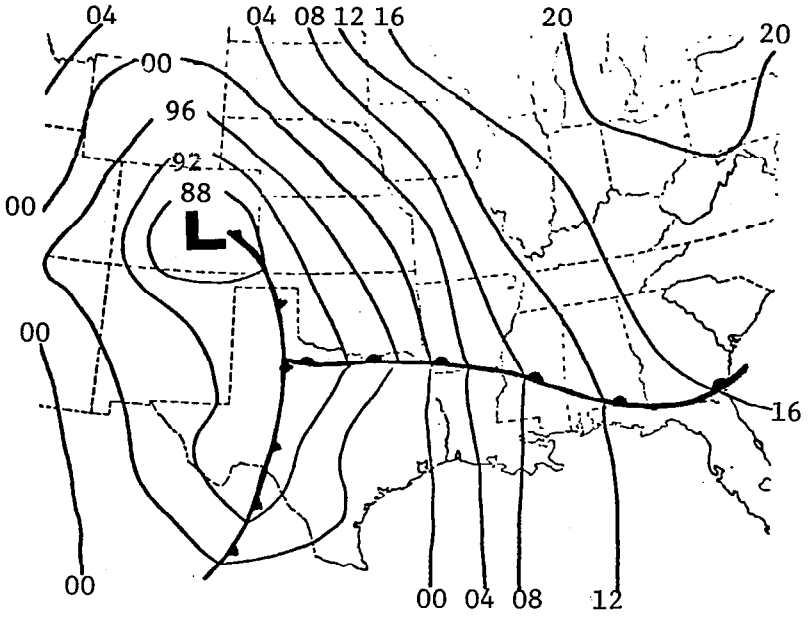

a. Surface

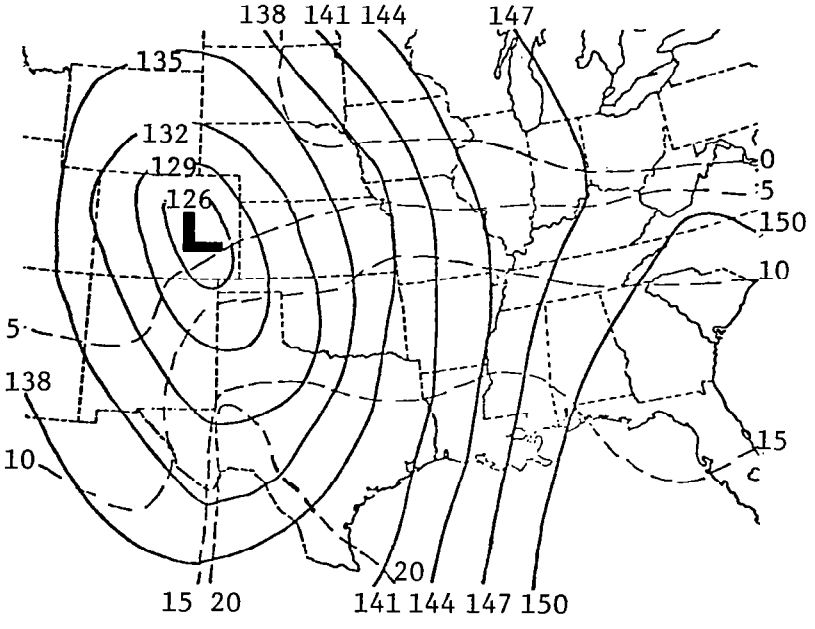

b. 850 mb

Fig. 4. Synoptic charts for 0000 GMT on 11 April 1979.

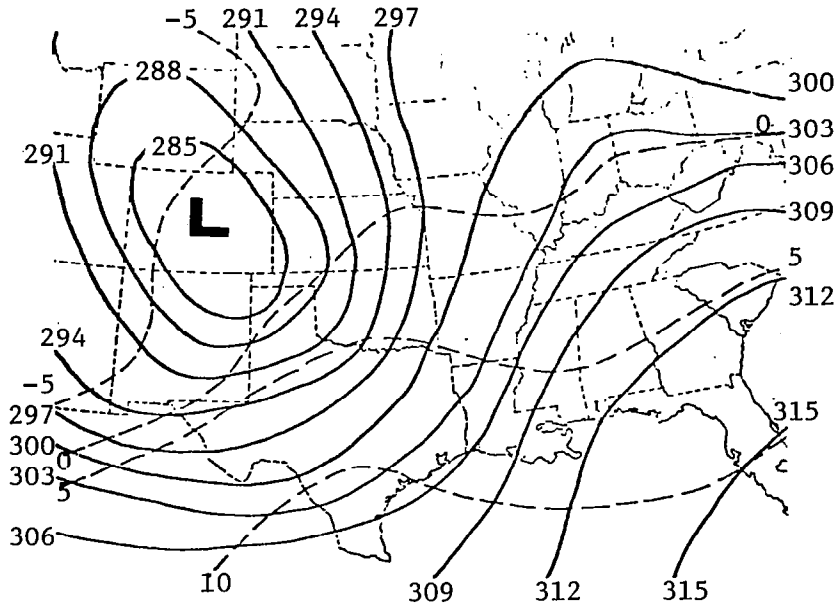

c. 700 mb

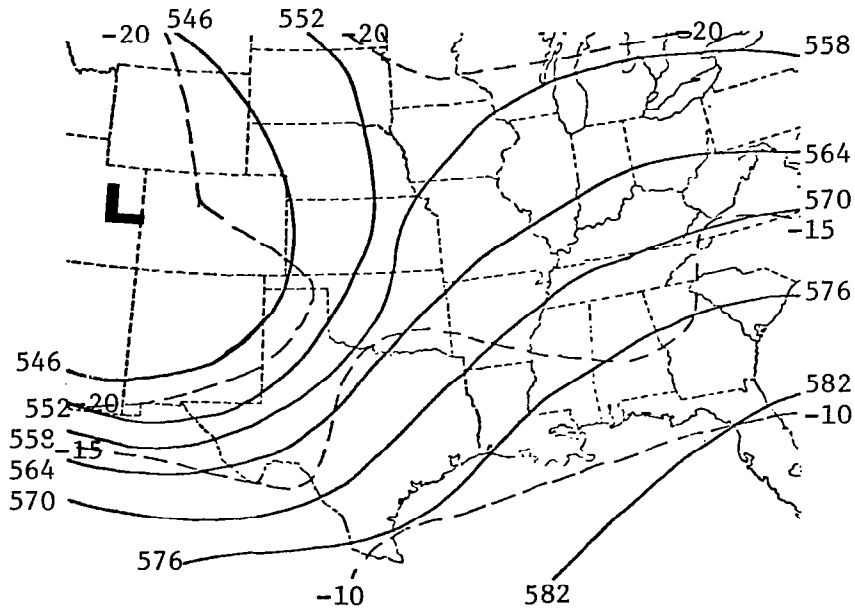

d. 500 mb

Fig. 4. (continued)

from the west. As the cold front and low center moved eastward the southwesterly flow from Mexico also shifted eastward, moving the capping inversion eastward and permitting strong convective activity to develop in squall lines in Texas and Oklahoma by 0000 GMT on 11 April 1979. The warm and cold fronts became occluded, and the entire system, along with its associated convective activity, moved eastward with time.

4. THEORETICAL DEVELOPMENT OF THE MOISTURE BUDGET EQUATION

Scott and Scoggins (1977) used a moisture budget equation similar to the one used in this research. Their equation was altered in order to resolve some problems with the local rate-of-change term. The reason for the alteration is discussed in Section 8. The development of the moisture budget equation parallels their work.

The equation of continuity for water vapor is (see list of symbols for explanation)

$$\frac{\partial \rho_v}{\partial t} + \vec{\nabla}_3 \cdot \rho_v \vec{V}_3 = S, \tag{1}$$

where S represents sources and sinks of water vapor, such as evaporation and condensation. Substitution of the definition of ρ_v ($\rho_v \equiv \rho q$) and expansion of the resulting equation yields

$$\rho\left(\frac{\partial q}{\partial t} + \vec{V}_3 \cdot \vec{\nabla} q\right) + q\left(\frac{\partial \rho}{\partial t} + \vec{\nabla}_3 \cdot \rho \vec{V}_3\right) = S. \tag{2}$$

The second term on the left-hand side (LHS) is equal to zero because of mass continuity. Using the equation of continuity in isobaric coordinates, (2) can be written as

$$\rho\left(\frac{\partial q}{\partial t} + \vec{\nabla} \cdot \vec{V} q + \frac{\partial \omega q}{\partial p}\right) = S \tag{3}$$

which represents the balance of moisture at a single point in space. If the equation is integrated in the vertical, and the hydrostatic assumption is made, the result is:

$$\frac{1}{g} \int_{p_2}^{p_1} \left(\frac{\partial q}{\partial t} + \vec{\nabla} \cdot (\vec{V} q) + \frac{\partial \omega q}{\partial p}\right) dp = R, \tag{4}$$

where R is the vertically integrated source term and represents the effects of evaporation, condensation, and precipitation.

Upon integration of the vertical divergence term (third term on the LHS), the equation becomes

$$\frac{1}{g}\int_{p_2}^{p_1}\frac{\partial q}{\partial t}dp + \frac{1}{g}\int_{p_2}^{p_1}\vec{\nabla}\cdot(\vec{V}q)dp + \frac{1}{g}[(\omega q)_{p_1} - (\omega q)_{p_2}] = R. \quad (5)$$

The terms in this equation were integrated over an area three grid distances square centered on each grid point. The resulting equation is

$$\frac{1}{gA}\int_A\int_{p_2}^{p_1}\frac{\partial q}{\partial t}dpdA + \frac{1}{gA}\int_A\int_{p_2}^{p_1}\vec{\nabla}\cdot(\vec{V}q)dpdA +$$

$$\frac{1}{gA}\int_A[(\omega q)_{p_1} - (\omega q)_{p_2}]dA = \frac{1}{A}\int_A RdA \quad (6)$$

where terms have been normalized by division by A, the area. By use of the divergence theorem, the second term on the LHS can be expressed as a boundary flux term and the equation becomes

$$\frac{1}{gA}\int_A\int_{p_2}^{p_1}\frac{\partial q}{\partial t}dpdA + \frac{1}{gA}\oint_L\int_{p_2}^{p_1}qV_n dpdL +$$

$$\frac{1}{gA}\int_A[(\omega q)_{p_1} - (\omega q)_{p_2}]dA = \frac{1}{A}\int_A RdA \quad (7)$$

where V_n is the outwardly directed normal velocity to the boundary L.

Equation 7 is the moisture budget equation used by Scott and Scoggins (1977). To reach the form of the moisture budget equation used in the present study, an additional integration is performed

with respect to time. This allows the local rate-of-change term to be evaluated in a more appropriate manner. The equation becomes

$$\frac{1}{gAT}\int_{A}\int_{p_2}^{p_1}(q_{t_2}-q_{t_1})dpdA+\frac{1}{gAT}\int_{t_1}^{t_2}\oint_{L}\int_{p_2}^{p_1}qV_n dpdLdt\ +$$

$$\frac{1}{gAT}\int_{t_1}^{t_2}\int_{A}[(\omega q)_{p_1}-(\omega q)_{p_2}]dAdt\ =\ \frac{1}{AT}\int_{t_1}^{t_2}\int_{A}RdAdt, \tag{8}$$

where $T = (t_2 - t_1)$. The terms are, from left to right, the local rate-of-change, horizontal moisture divergence, vertical moisture divergence, and residual.

This equation is the theoretical form of the moisture budget equation used in this study. Since continuous observations were not possible, the equation was evaluated using finite-difference techniques (discussed in the next section) so that the values of the terms are, in effect, not continuous integrals but rather averages of grid point values.

5. METHODS OF EVALUATION OF MOISTURE BUDGET TERMS

a. Gridding procedure

Values of u- and v-components of wind and mixing ratios were interpolated to a grid using an objective analysis technique developed by Barnes (1964). The grid was superimposed on a conformal conic projection map true at 30^{o} and 60^{o} N latitude. Map factors were small and were neglected. The 18x18 grid analysis areas had a grid spacing of approximately 158 km with the grid points oriented north-south along 105^{o} W longitude. These areas and grids are shown in Figs. 5 and 6.

Data at 50-mb intervals were interpolated to the grid. Observations were allowed to influence grid points within a radius of three grid distances. Four iterations of successive corrections to the gridded values were applied in order to retain subsynoptic scale features (< 600 km) without amplifying smaller-scale noise. The resulting fields were smoothed with a light nine-point filter developed by Shuman (1957) to remove additional small-scale noise in the analysis.

Because the rawinsonde stations were concentrated in the southwest part of the grid, only a portion of the grid area could be used in the analyses. The solid black lines in Figs. 5 and 6 correspond to the boundaries of the analyses presented in this research.

b. Local rate-of-change

To evaluate the local rate-of-change term, values of mixing ratio at each grid point were subtracted from corresponding grid point values at the next observation time. The resulting amount was divided by the difference in time between the two observations (usually three hours). This can be expressed as

$$\frac{\partial q}{\partial t} \cong \frac{q_{t_2} - q_{t_1}}{t_2 - t_1} .$$

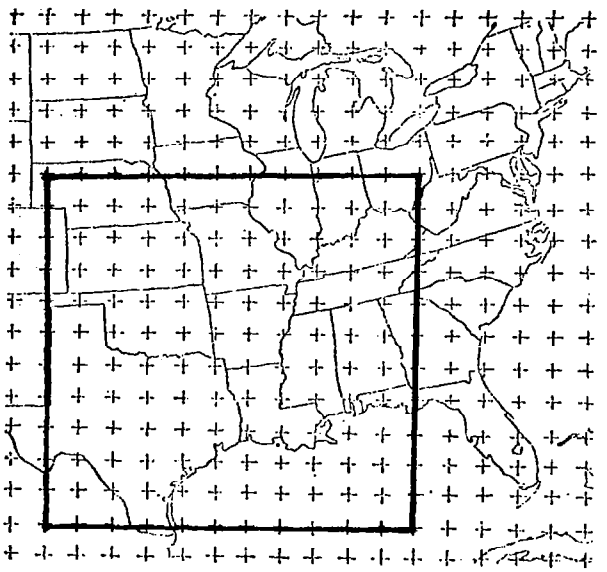

Fig. 5. Grid used for numerical computations with AVE VII data.

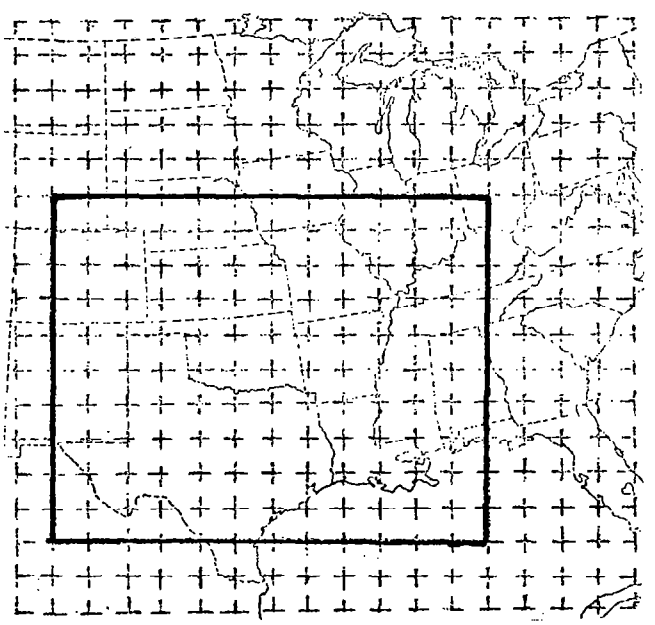

Fig. 6. Grid used for numerical computations with AVE-SESAME I data.

Vertical integration was performed for layers 50-mb thick by the trapezoidal rule; taking the average value of grid points at the top and bottom of the 50-mb layer and multiplying by the thickness of the layer. The equation for the trapezoidal method for integration with respect to pressure is of the form

$$\int_{p_2}^{p_1} f \, dp \simeq (f_{p_1} - f_{p_2}) \frac{\Delta p}{2}$$

where, in this case, f is the local rate-of-change of moisture.

The area integration was performed by summing each grid point value with the values at the eight adjacent grid points, assuming each grid point value was representative of an area one grid distance square. This integration over area can be expressed in finite difference form as

$$\int_A f \, dA \simeq \sum_{j=1}^{9} f_j \, d^2.$$

The resulting value was divided by the area $A=(3d)^2$ over which the integration was performed and by gravity to complete the evaluation of the term.

c. Vertical moisture divergence

Vertical motion used in this research was computed by the kinematic method and corrected to adiabatic values at 100 mb by a correction scheme developed by O'Brien (1970). To evaluate the vertical divergence for each 50-mb thick layer, the product of mixing ratio and vertical motion was found at the gridded levels 50 mb apart. The value at the top of each 50-mb layer was then subtracted from the value at the next lower level. This term was integrated over area as described above. The average value at each grid point between adjacent observation times was calculated by adding values at each time together and dividing by 2. Division by area and gravity completed the evaluation of the term.

d. Horizontal moisture divergence

To compute horizontal moisture divergence, the products of mixing ratio and u- and v-components of the wind were found at each grid point for each level. Each of these products was integrated over 50-mb layers by the method described above in the section on local rate-of-change of moisture. These pressure-integrated fields were used to compute the horizontal moisture divergence for the same three grid distance square areas used in computing the other terms. The diagram below represents this area. Each side of the boundary

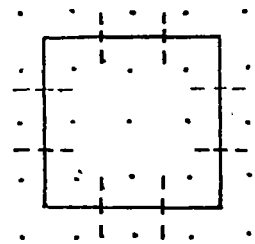

was divided into three segments and qV_n, the horizontal boundary flux of moisture, was calculated for each segment and summed around the boundary. The flux across each segment was taken to be the average of the flux (qu or qv as appropriate) at the two grid points adjacent to the segment. Each average was multiplied by the length of the segment, d (one grid distance), over which it was assumed to apply. The signs of qu and qv on the west and south sides of the area, respectively, were adjusted so that they were positive when the velocity was directed out of the area. The resulting term was divided by area and gravity, and the average of each grid point value at adjacent observation times was taken to complete the evaluation of the term.

e. Residual term

The source term, or residual term was computed as the sum of the three terms on the left-hand side of the moisture budget equation. The term represents the effects of sources and sinks of moisture such as evaporation, condensation, precipitation, small-scale transports not resolved in these analyses, and computational error.

This term was calculated for each layer. Values in all layers were added together to form the total residual for the atmosphere between 900 and 450 mb. These totals were summed over 6-hr periods and converted to equivalent inches of rainfall so that they could be compared to hand analyzed maps of 6-hr cumulative precipitation totals that had been similarly smoothed.

The cumulative precipitation analysis used for comparison was obtained by manual interpolation of hand analyzed precipitation charts to the analysis grid, integration over the 9 grid square area, and hand analysis of the grid point values obtained. The resulting fields represent precipitation averaged over the same areas as the moisture budget terms.

6. RESULTS

To aid in interpretation of the calculated moisture budget terms, the values integrated over 50-mb layers were combined into two deeper layers from which contoured plots were produced.

The first layer (900-750 mb) includes the moist areas of the lower troposphere. The second layer (600-500 mb) was chosen to be representative of middle tropospheric conditions. The contoured plots for the moisture budget terms in these layers are in Appendix A. Radar summary charts for time periods close to the sounding observation times are in Appendix B. The data contained in these figures will be used in the following discussions.

One representative time period from each experiment was analyzed in greater detail, and radar summary charts, contoured plots, and vertical cross sections of moisture terms for these time periods are included in this section. Figures 7-11 show convective activity and moisture budget terms for 2100-0000 GMT on 2-3 May 1978, during AVE VII. Figures 12-16 show convective activity and moisture budget terms for 0000-0300 GMT on 11 April 1979, during AVE-SESAME I.

The vertical cross sections (Figs. 10-11 and 15-16) were taken along rows and columns of the analysis grid, and are oriented roughly north-south and east-west. The lines along which the cross sections were taken are indicated on the radar summary charts (Figs. 7 and 12).

a. Local rate-of-change of moisture

Values of the local rate-of-change of moisture were quite variable. In the lower layer (900-750 mb) in convective areas the term was generally negative as a rule, though in areas where storms were developing at the end of the time interval, positive values were present. These characteristics show up well on the contoured plots in Figs. 8 and 13. Comparison with convective activity depicted in Figs. 7 and 12 shows generally negative values in the convective areas, except between Midland and Abilene where strong convection developed between 2235 and 0235 GMT on 10-11 April 1979.

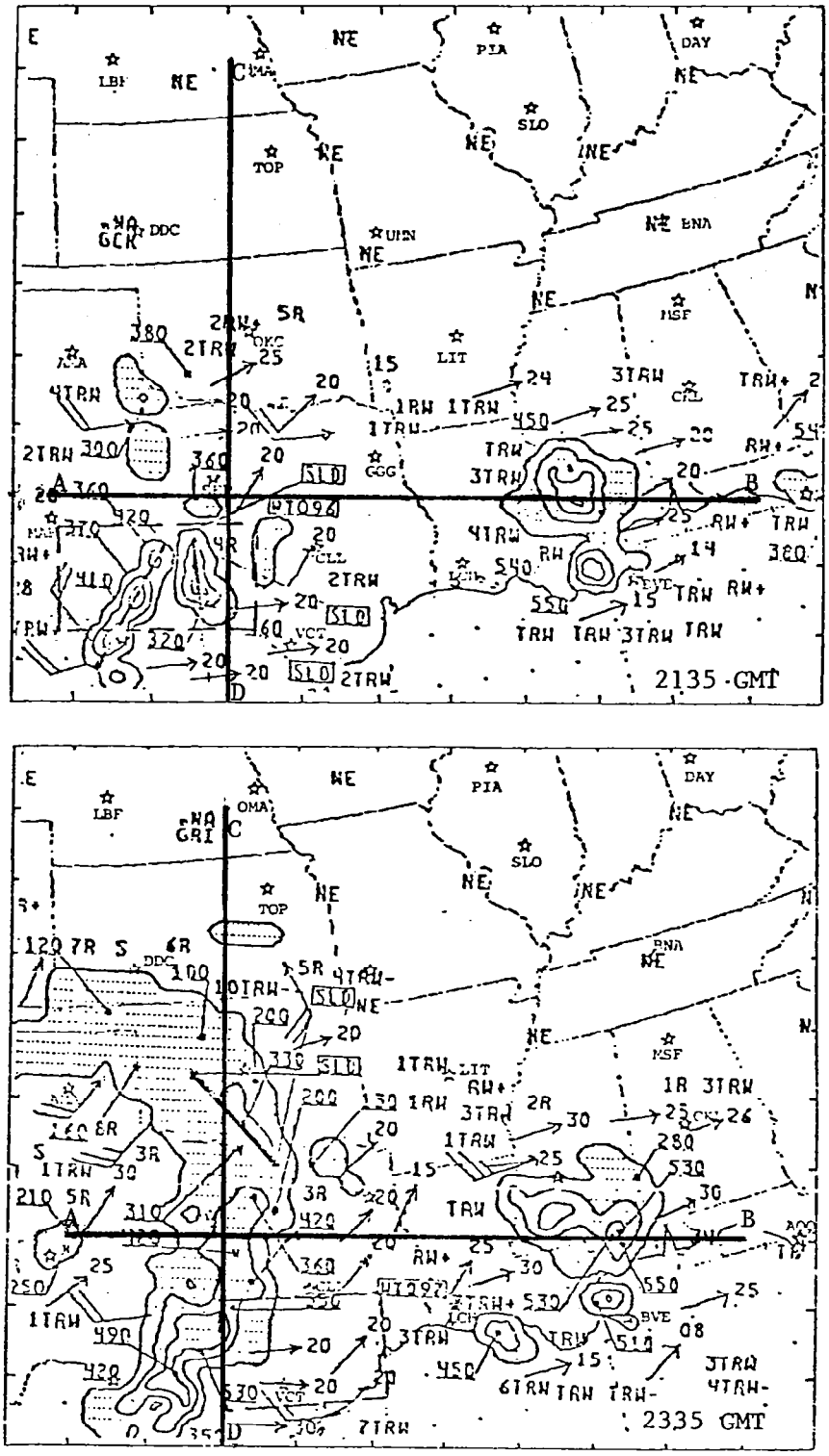

Fig. 7. Radar summary charts at 2135 and 2335 GMT on 2 May 1978.

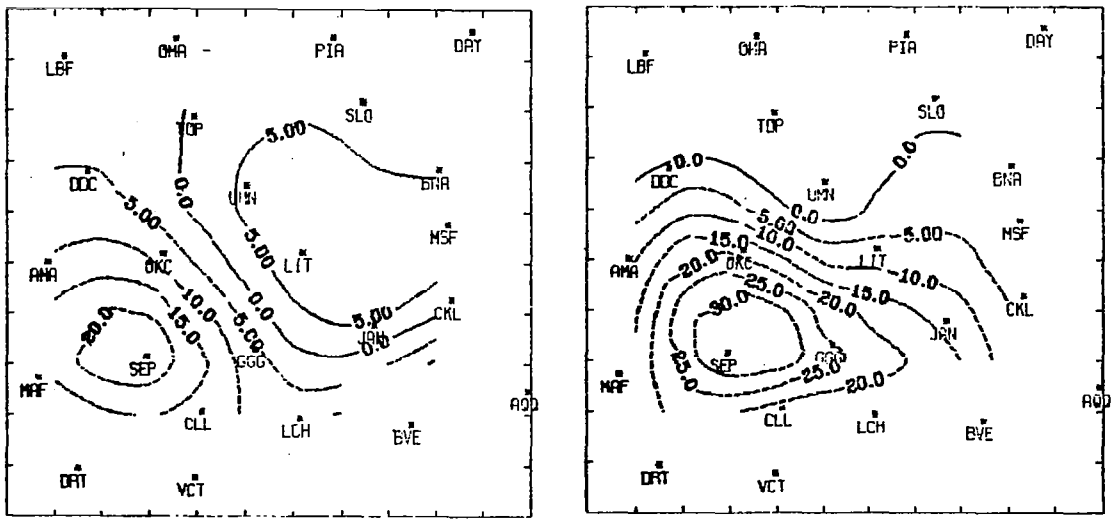

a. Local rate-of-change

b. Horizontal divergence

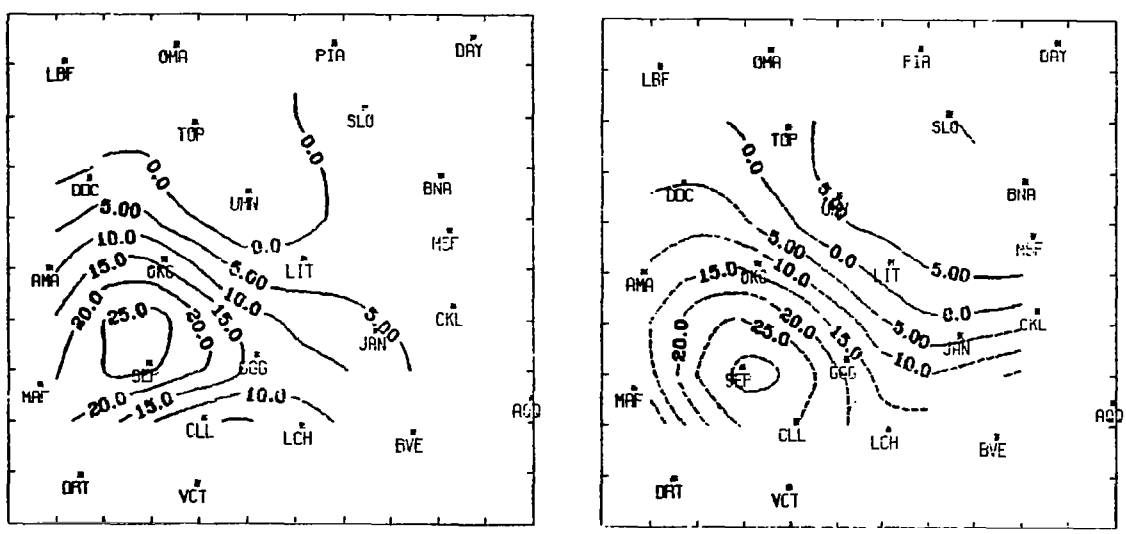

c. Vertical divergence

d. Residual

Fig. 8. Moisture budget terms (g $cm^{-2}s^{-1}$ x 10^{-6}) in the 900-750 mb layer for 2100-0000 GMT on 2-3 May 1978.

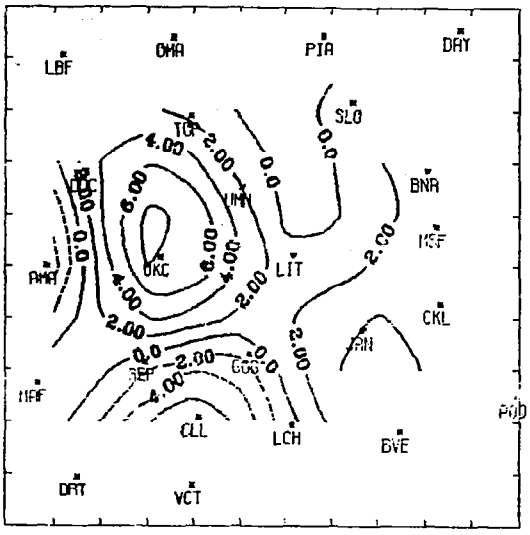

a. Local rate-of-change

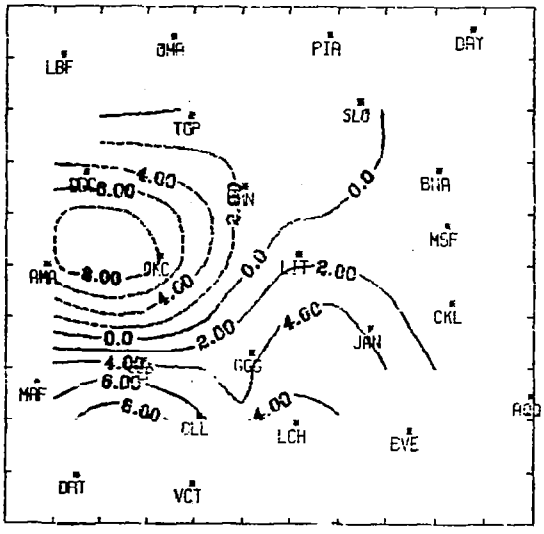

b. Horizontal divergence

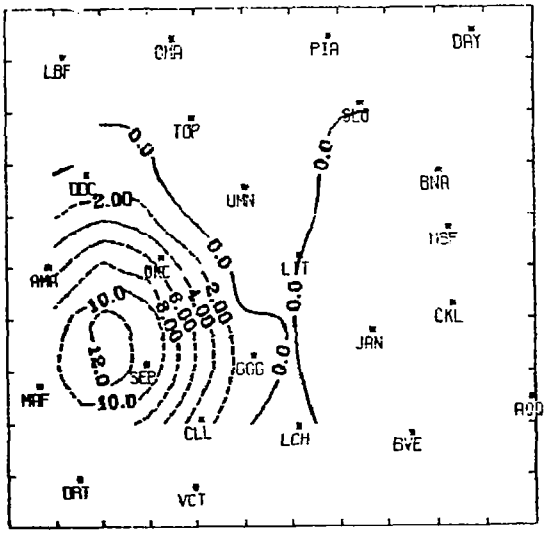

c. Vertical divergence

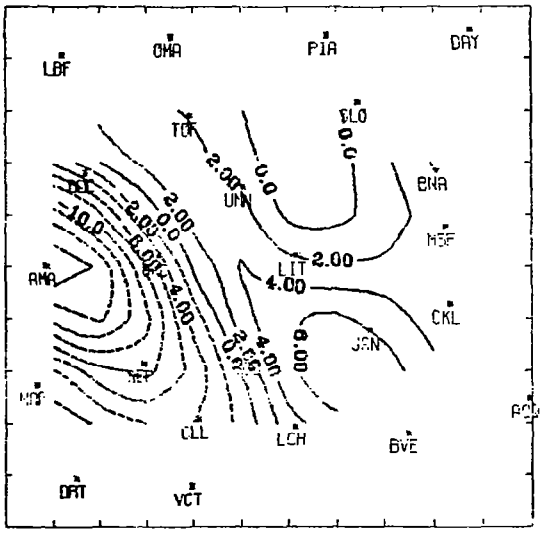

d. Residual

Fig. 9. Moisture budget terms (g $cm^{-2} s^{-1} \times 10^{-6}$) in the 600-500 mb layer for 2100-0000 GMT on 2-3 May 1978.

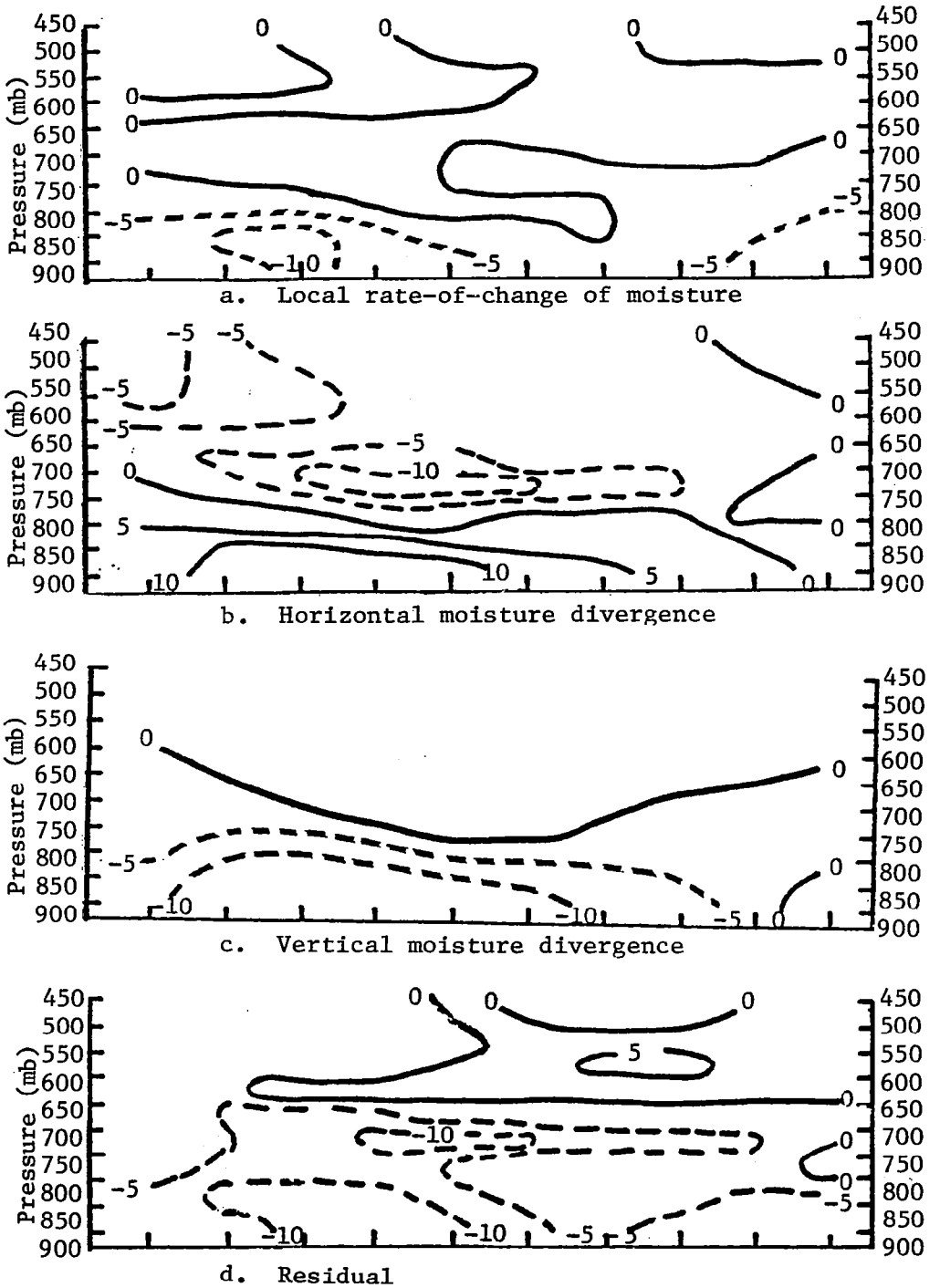

Fig. 10. Vertical cross section of moisture budget terms (g $cm^{-2}s^{-1}x\ 10^{-6}$) along line A-B for the time period 2100-0000 GMT on 2-3 May 1978.

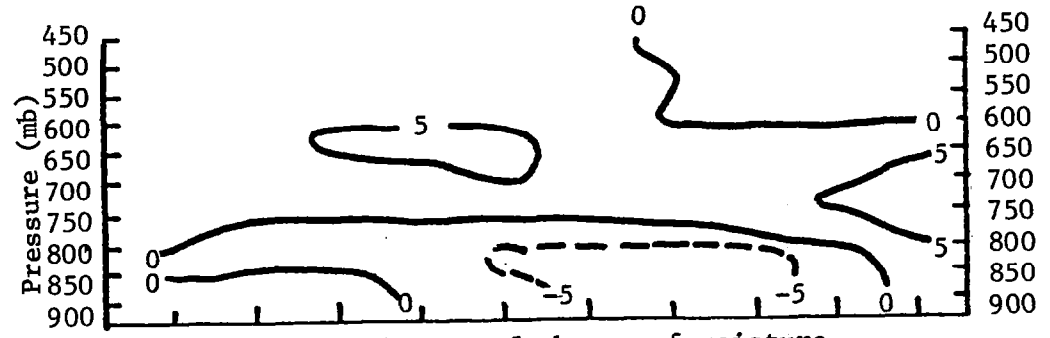

a. Local rate-of-change of moisture

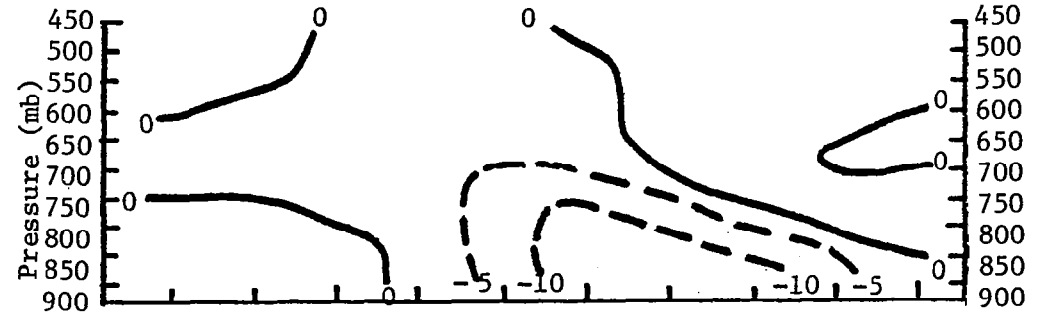

b. Horizontal moisture divergence

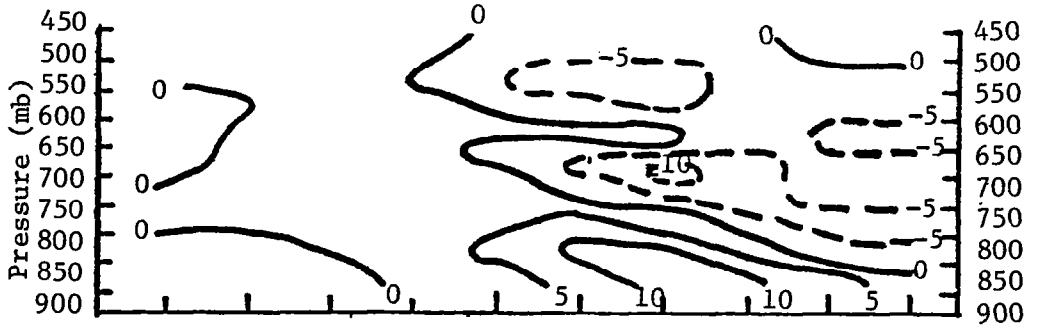

c. Vertical moisture divergence

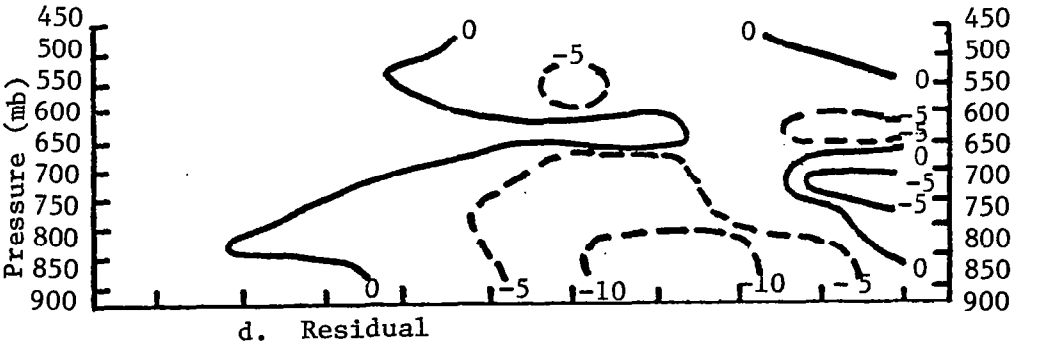

d. Residual

Fig. 11. Vertical cross section of moisture budget terms (g $cm^{-2}s^{-1}x\ 10^{-6}$) along line C-D for the time period 2100-0000 GMT on 2-3 May 1978.

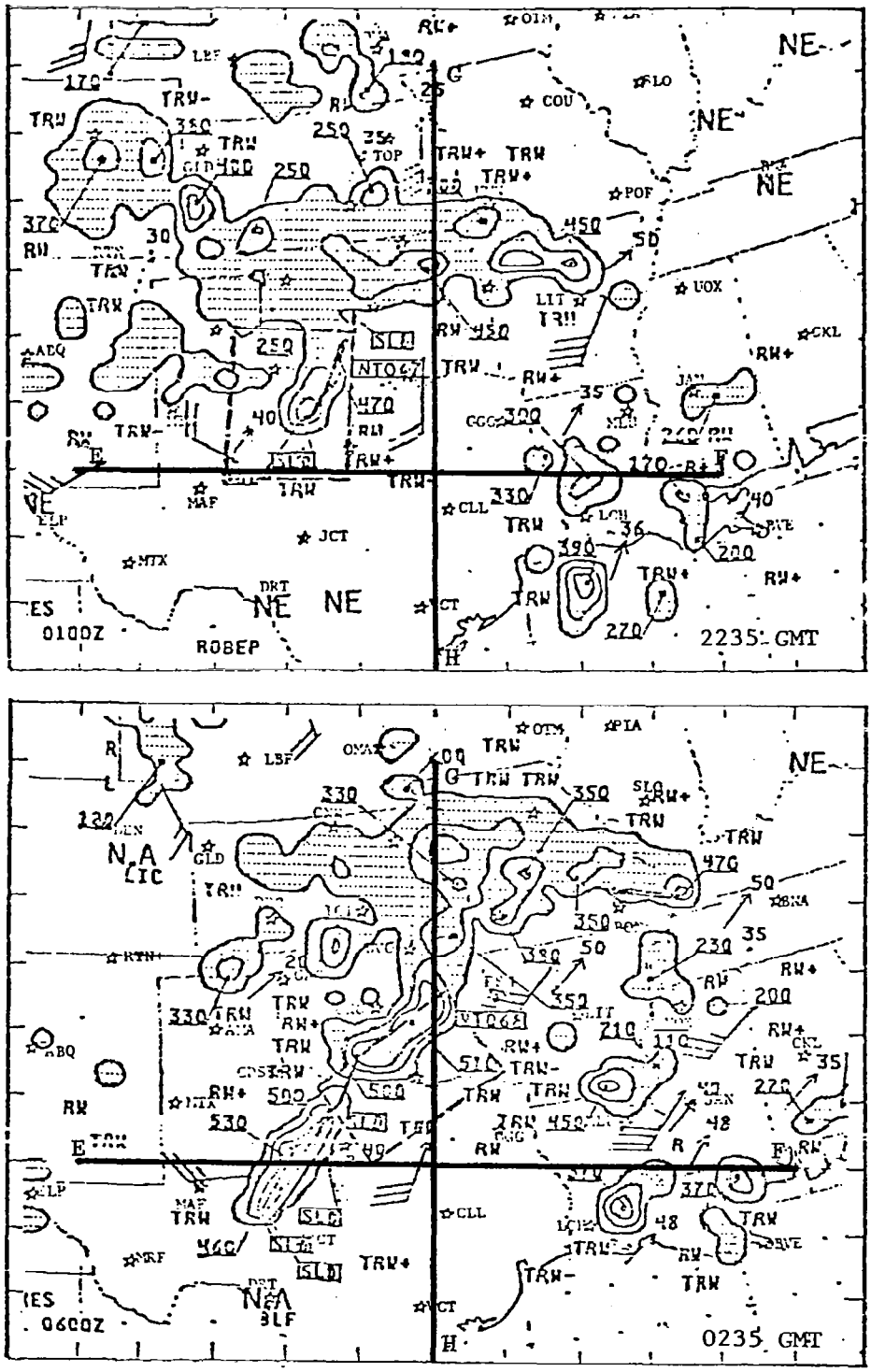

Fig. 12. Radar summary charts at 2235 and 0235 GMT on 10-11 April 1979.

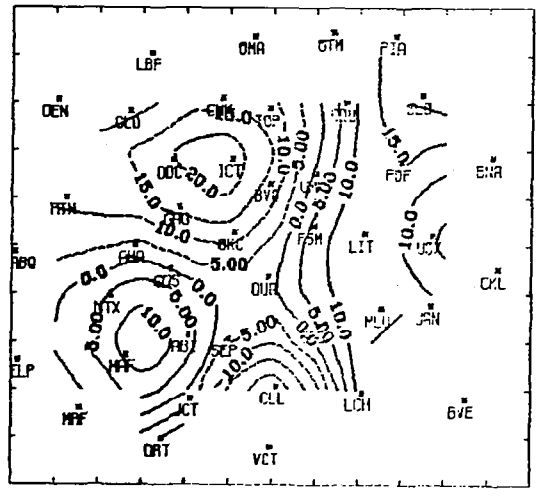

a. Local rate-of-change

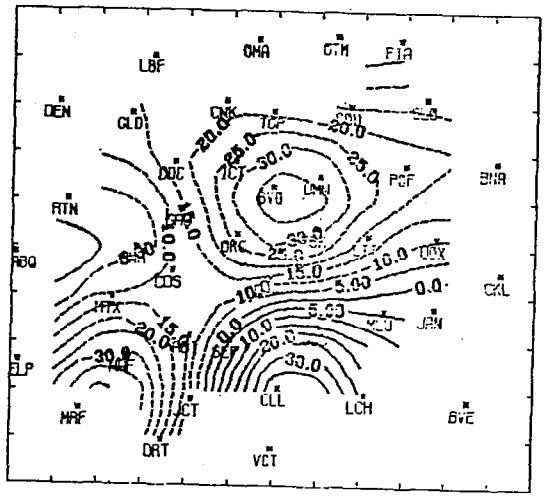

b. Horizontal divergence

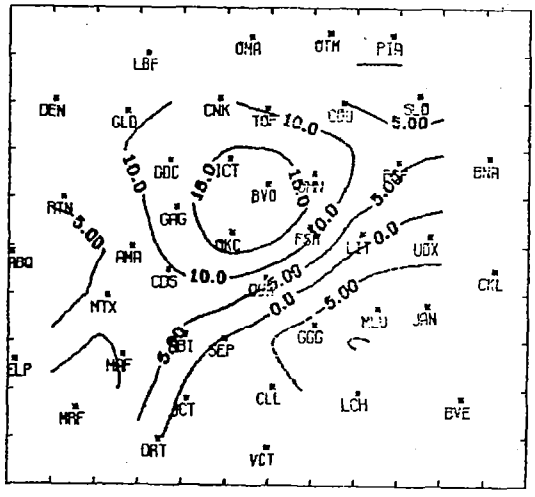

c. Vertical divergence

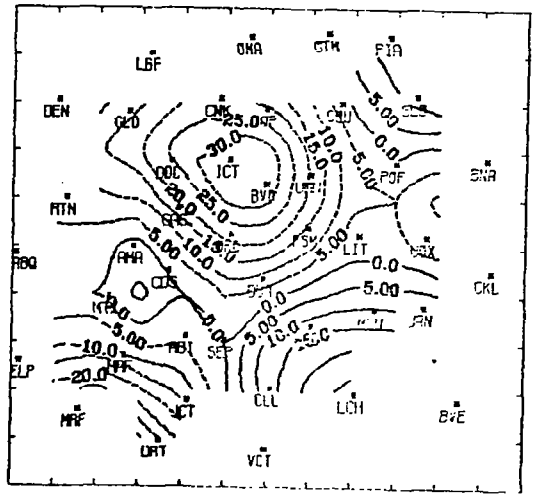

d. Residual

Fig. 13. Moisture budget terms (g $cm^{-2}s^{-1}$ x 10^{-6}) in the 900-750 mb layer for 0000-0300 GMT on 11 April 1979.

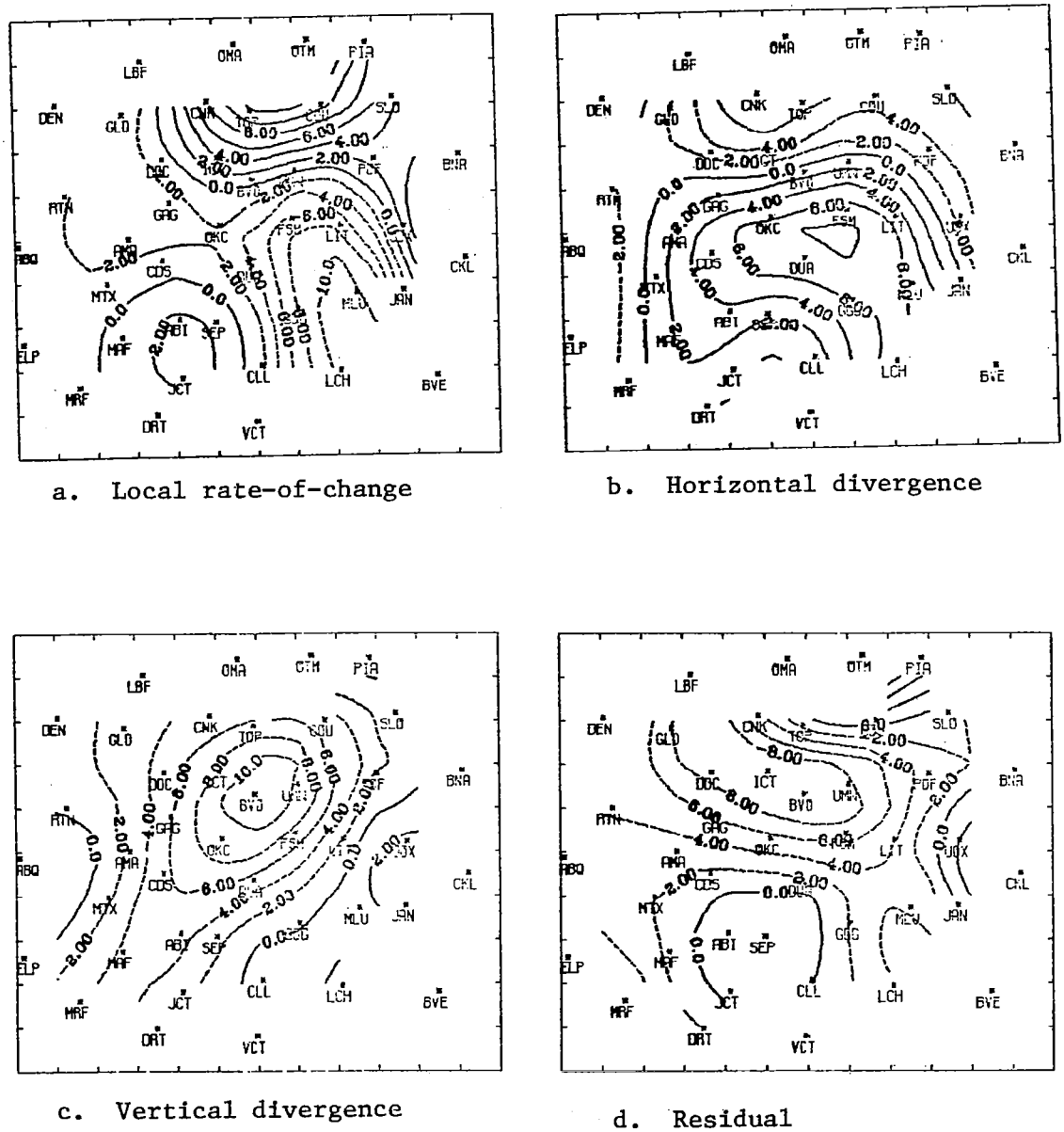

Fig. 14. Moisture budget terms (g $cm^{-2} s^{-1}$ x 10^{-6}) in the 600-500 mb layer for 0000-0300 GMT on 11 April 1979.

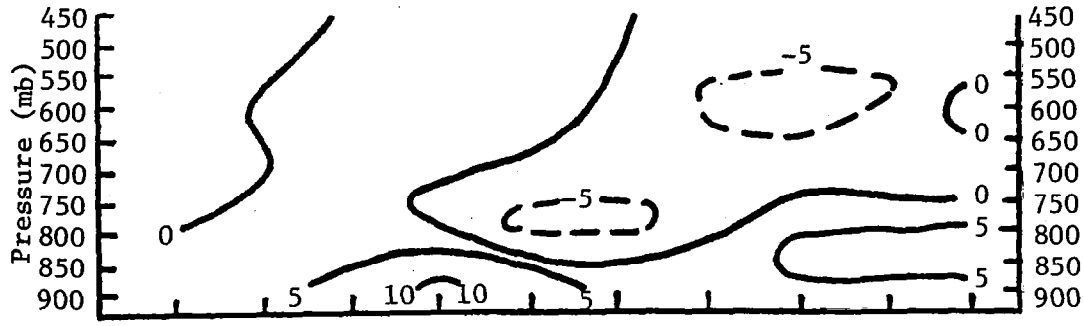

a. Local rate-of-change of moisture

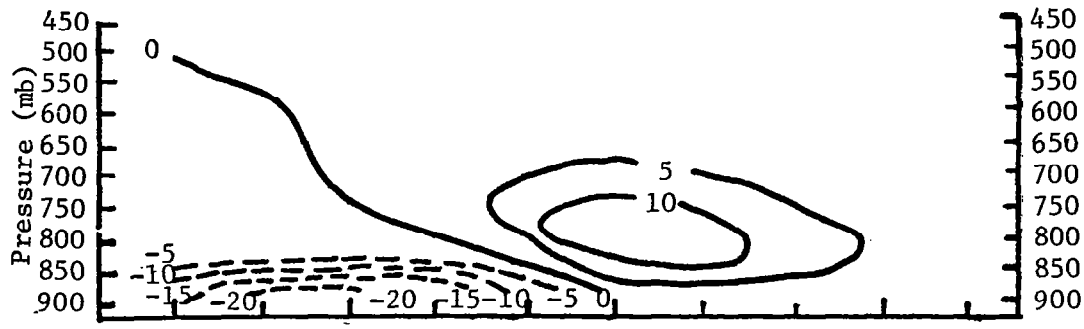

b. Horizontal moisture divergence

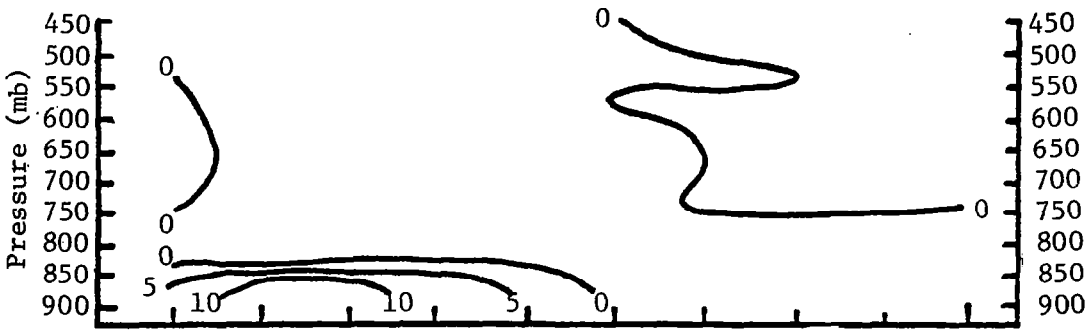

c. Vertical moisture divergence

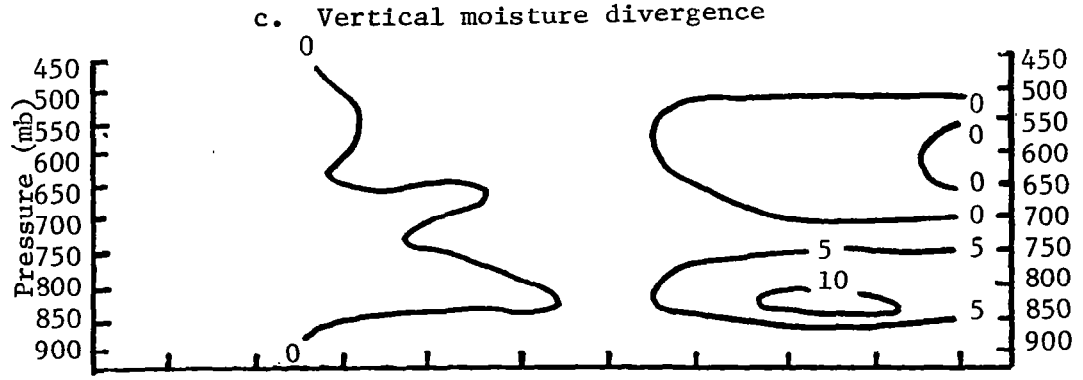

d. Residual

Fig. 15. Vertical cross sections of moisture budget terms (g $cm^{-2}s^{-1}x\ 10^{-6}$) along line E-F for the time period 0000-0300 GMT on 11 April 1979.

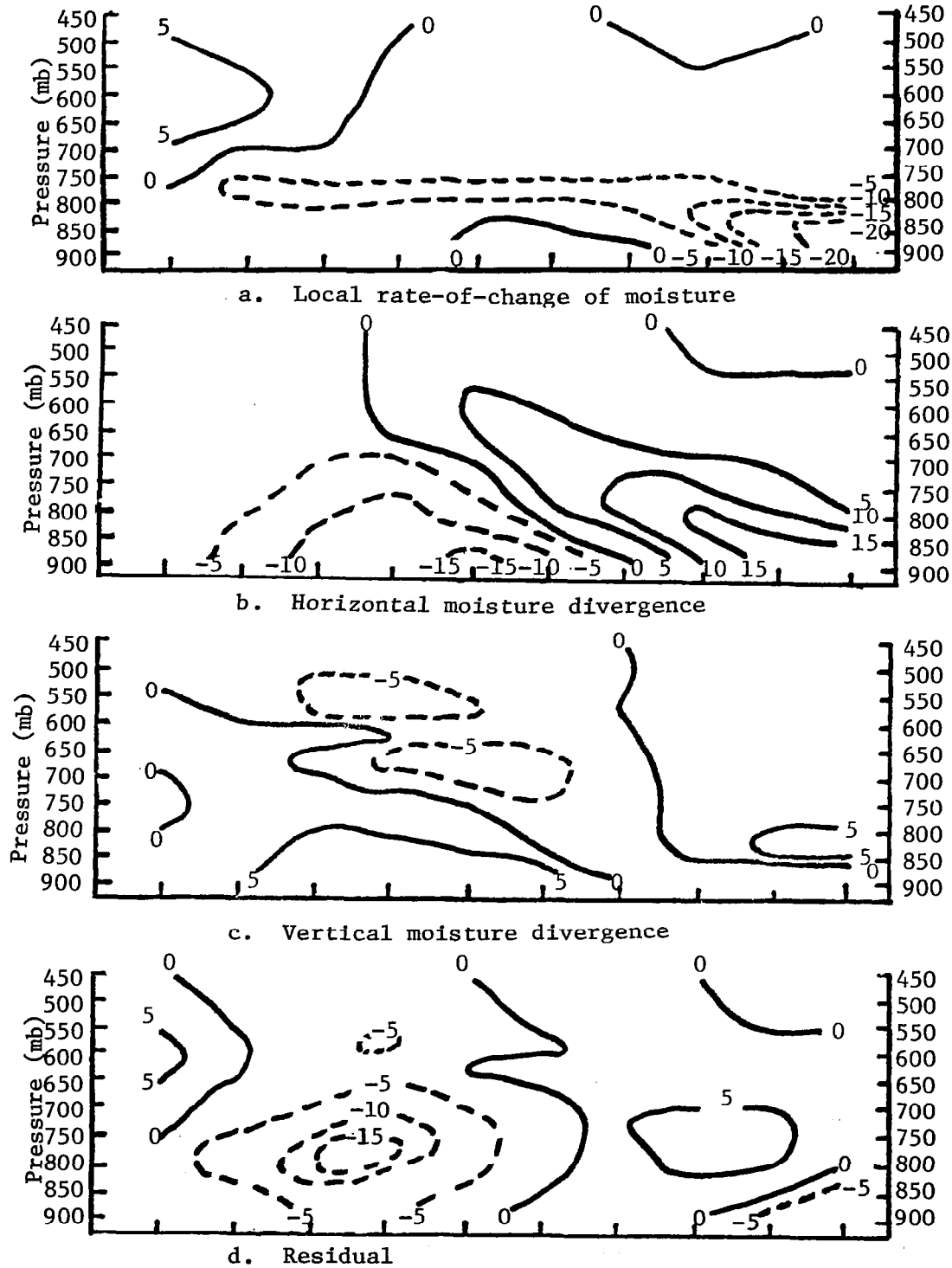

Fig. 16. Vertical cross sections of moisture budget terms (g $cm^{-2}s^{-1}x\ 10^{-6}$) along line G-H for the time period 0000-0300 GMT on 11 April 1979.

The negative values in convective areas dominated in the vertical cross sections shown in Figs. 10-11 and 15-16.

Higher in the atmosphere, values of the local rate-of-change term were quite dependent on convective activity development and movement. This layer was very dry in both experiments, except in areas where clouds and precipitation were developing. Large changes of moisture content in this layer occurred in areas where coverage of convective activity changed during a time interval (See the contoured plots in Figs. 9 and 14). The negative center in the east in Fig. 14 is not well explained by the radar charts, but the first chart did not exactly coincide with the 0000 GMT observation time. The vertical cross sections in Figs. 10-11 and 15-16 show more detailed distributions of this term in the vertical than the contoured plots.

b. Horizontal moisture divergence

The contoured plots of horizontal moisture divergence in Figs. 8 and 13 clearly show the major characteristics of the term in lower layer: moisture convergence in areas with convective activity, and some moisture divergence in other areas. These characteristics are also borne out by the cross section plots in Figs. 10-11 and 15-16. The divergence behind the storm line in AVE-SESAME I becomes more intense in later time periods.

It is interesting to note the northward slope with height of the moisture convergence centers in the vertical cross sections in Figs. 11 and 17. This is most pronounced in the plot for 0000-0300 GMT on 11 April 1979. The horizontal divergence and transport of moisture northward occurred as wind speeds increased form south to north.

Divergence is present in upper layers over storm areas with convergence present to the north of the storm areas (Figs. 9 and 14). This could be the result of moisture advection away from the storm in middle layers by the southerly winds. This is consistent with the northward slope of convergence centers in the convective areas.

c. Vertical moisture divergence

The vertical moisture divergence term is characterized by moisture divergence in lower layers and moisture convergence in middle layers in regions of convective activity. This is readily seen from the contoured plots and the cross section plots (Figs. 8-11 and 13-16). The largest values of this term occurred when convective activity covered a large area; a result of the resolution limitations of the data. Figure 10 shows two maxima of vertical moisture convergence, one near 700 mb and the other centered near 500 mb. The lower center, which is spread over a larger horizontal extent than the higher-level center, marks the boundary between moist air in lower layers and drier air in higher levels. The higher convergence center results from decreasing vertical motion with height and is located over the area of strongest convective activity in this figure.

The horizontal and vertical moisture divergence work together to concentrate moisture by horizontal motions in lower layers, and transport this moisture upward and concentrate it in middle levels by the aid of vertical air motions.

d. Residual term

The residual term was computed as a combination of the terms on the left-hand side of the moisture budget equation. Values of the residual were negative in the lower layers in areas with convective activity (Figs. 8 and 13). The magnitude of the horizontal moisture divergence was greater than the vertical moisture divergence in this layer, so that the large-scale transport of moisture resulted in net gains of moisture in this layer. The local rate-of-change term in this layer in areas of convection was generally negative, however, indicating losses. Thus, the residual term in this layer is negative and there is a net moisture sink in the lower layers in areas of convective activity.

In higher layers the values of the residual in convective areas are more variable (Figs. 9 and 14). The vertical divergence term is generally negative in the upper layer in areas of convective activity. However, the horizontal moisture divergence may be of

either sign, depending on whether or not the grid point is on the downwind side of the precipitation area. Addition of the local rate-of-change term makes the residual value even more variable, since the local rate-of-change of moisture is highly influenced by small-scale, short-period fluctuations in moisture that occur in the vicinity of convective activity.

The vertical cross sections show that in areas of convective activity most of the moisture sink (negative residual) is contained in layers below 650 mb.

e. Comparison of residual with cumulative precipitation totals

The cumulative precipitation totals and corresponding residual values for six hour periods during AVE VII and AVE-SESAME I are shown in Figs. 17 and 18. The precipitation totals, like the moisture budget terms, were integrated over an area three grid distances square.

Comparison of measured precipitation with the moisture budget residual shows very similar patterns. The maximum center of precipitation in the west during the AVE VII case (Fig. 17) matched well with the computed residual although the residual center was too far south. Likewise, in the AVE-SESAME I case (Fig. 18), the residual term corresponded well with the precipitation center even if the magnitude of the term was too small.

In both cases the actual precipitation plots showed a second maximum of precipitation in the Louisiana area associated with a small area of convective activity. The scale of this activity was too small to be adequately resolved by the gridded data in this study. This could account for the positive residual value in those areas even though precipitation had fallen.

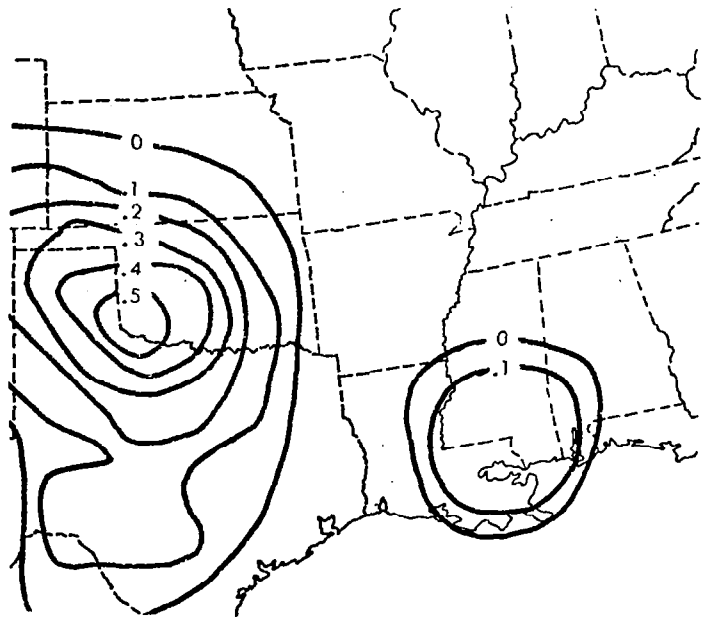

a. Measured precipitation

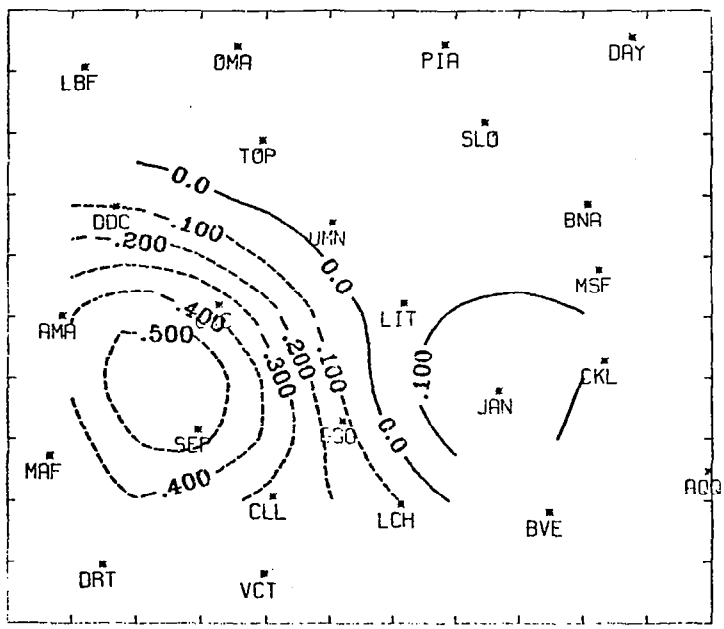

b. Equivalent precipitation from residual

Fig. 17. Cumulative precipitation (in) integrated over 9 grid square area, and total moisture budget residual term (in) for layer 900-450 mb for 1800-0000 GMT on 2-3 May 1978.

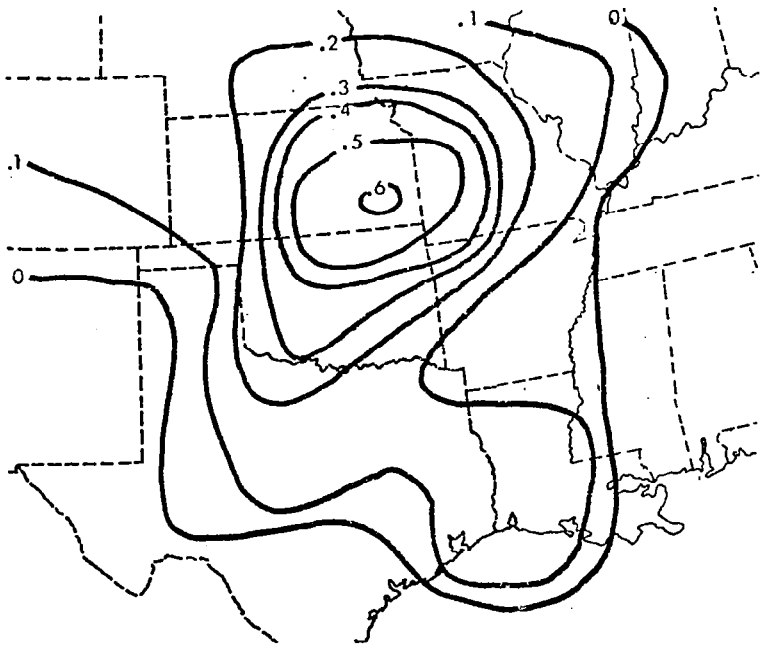

a. Measured precipitation

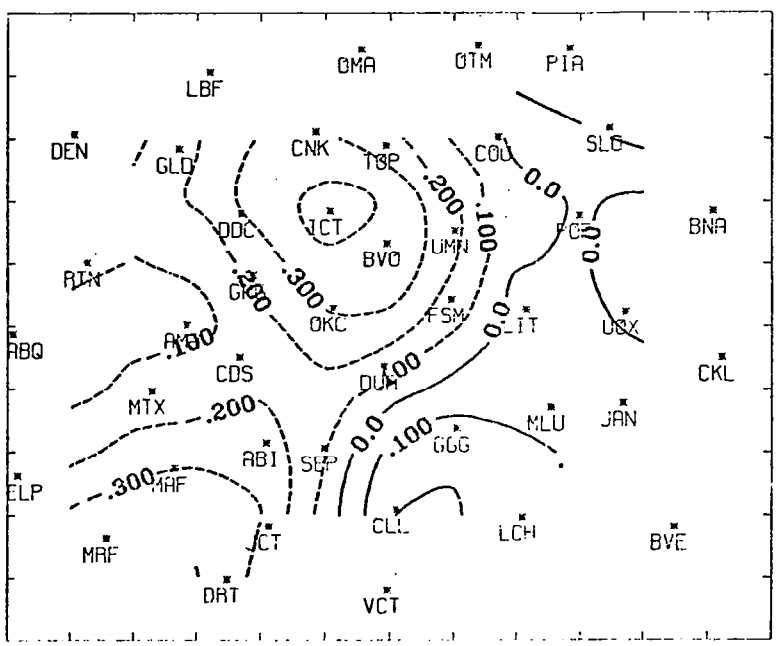

b. Equivalent precipitation from residual

Fig. 18. Cumulative precipitation (in) integrated over 9 grid square area, and total moisture budget residual term (in) for layer 900-450 mb for 0000-0600 GMT on 11 April 1979.

7. MODELS OF MOISTURE BUDGET PROCESSES

Figures 19 and 20 show some qualitative models of the moisture budget terms in the 900-750-mb and 600-500-mb layers used in the analyses in both experiments. These models show the general behavior of the moisture budget terms in the vicinity of convective activity. Some of the drawings are oriented in a specific direction related to environmental wind fields or movement of storm areas; other drawings are more general.

a. The 900-750-mb layer:

The local rate-of-change term shows decreasing moisture in the 900-750-mb layer in areas where storms are moving away or dissipating (Fig. 20). Increases of moisture accompany storm movement or initiation in an area.

Horizontal moisture convergence is the largest term in the lower layer in areas of convective activity. Moisture was being concentrated by low-level winds in areas of convective activity. Outside the convective areas, divergence was prevalent.

Vertical moisture divergence transports moisture out of the lower layer into layers above 700 mb. The loss of moisture in this layer due to vertical motions comes about because upward vertical motion increases in magnitude through this layer.

The combination of terms on the LHS shows a net moisture sink (the residual term) in convective areas. The presence of the moisture sink can be attributed to precipitation.

Net losses of moisture in this layer (from the local rate-of-change term) occurred despite the concentration of moisture in the layer due to horizontal and vertical air motions.

b. The 600-500-mb layer:

The plots for the 600-500 mb layer are shown in Fig. 20. Again, moisture increased in areas into which storms moved, and decreased in areas in which storms moved away or dissipated.

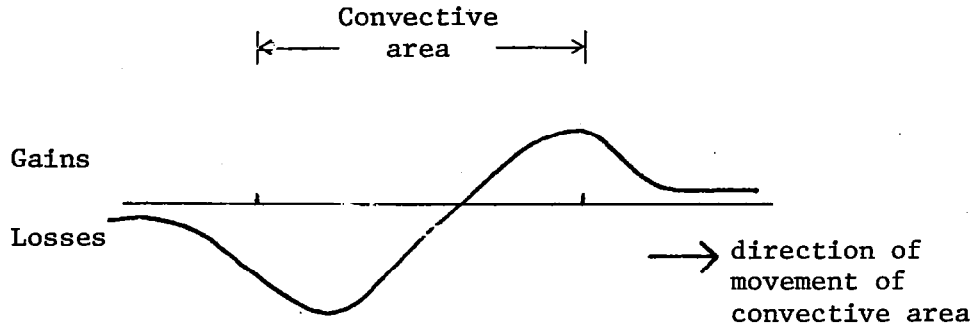

a. Local rate-of-change of moisture

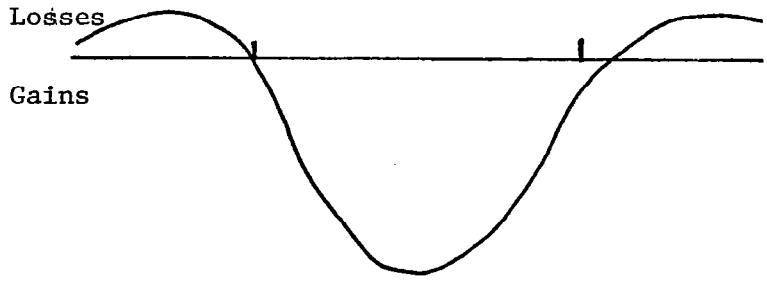

b. Horizontal moisture divergence

c. Vertical moisture divergence

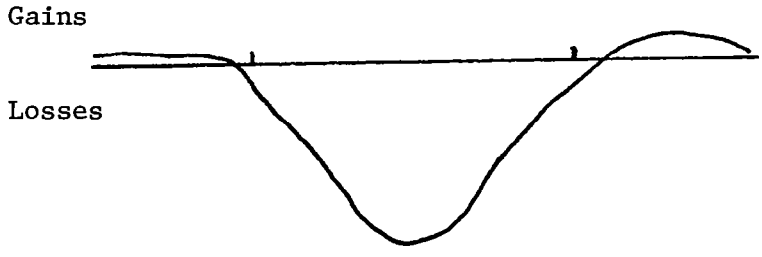

d. Residual

Fig. 19. Qualitative models of moisture budget terms in the 900-750-mb layer.

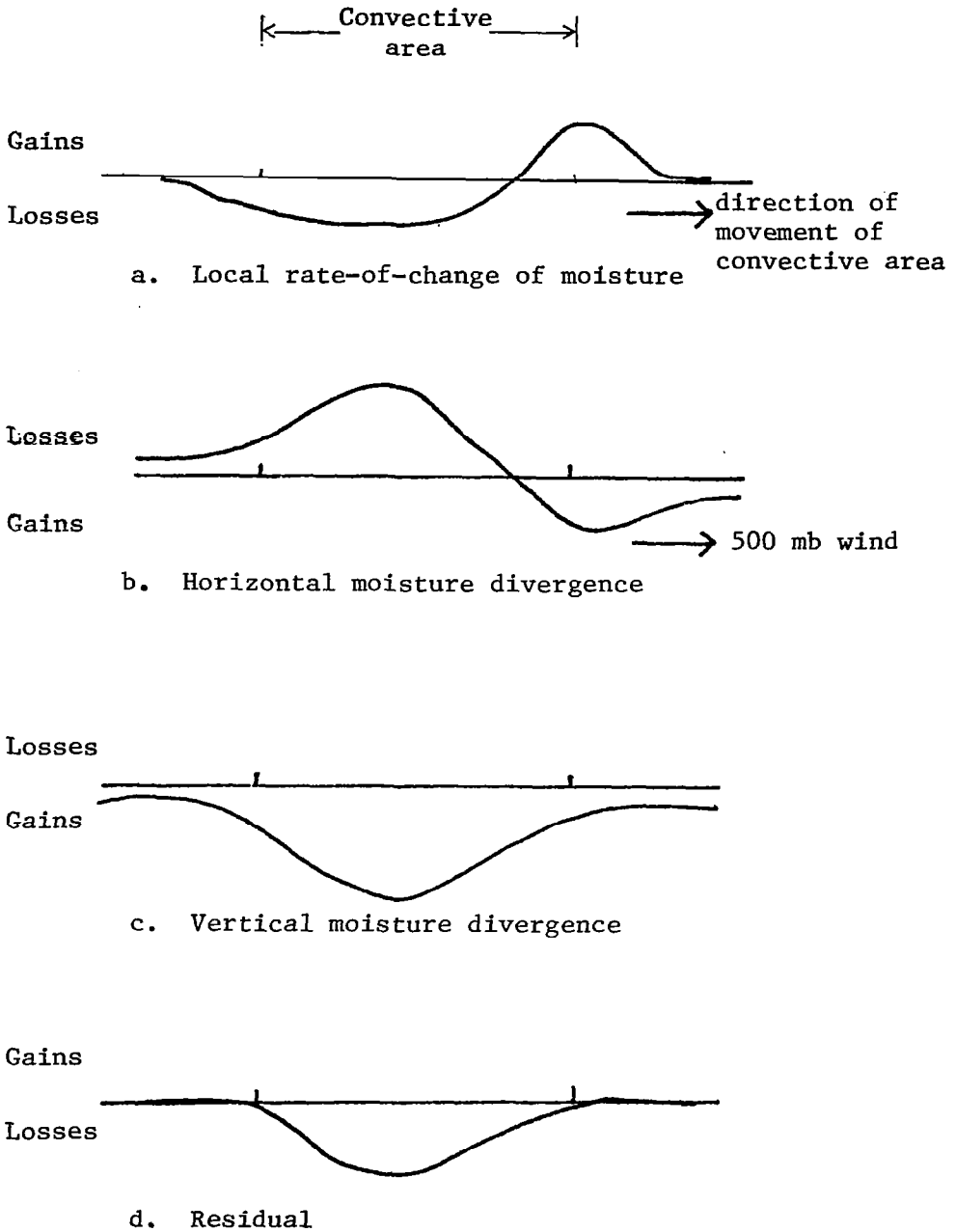

Fig. 20. Qualitative models of moisture budget terms in the 600-500-mb layer.

The horizontal moisture divergence showed both positive and negative values in the vicinity of convective activity. Moisture convergence occurred upstream (with respect to 500-mb winds) of the storms.

Vertical moisture convergence was present in the 600-500 mb layer in convective areas. In this layer upward vertical motions and specific humidity decreased with height. In this manner, more moisture was transported into the bottom of this layer than escaped through the top of the layer. Thus, the vertical motions served to concentrate moisture in this layer.

Signs and values of the residual term in this layer were quite variable since the magnitudes of the other terms that are combined to compute the residual source term also were variable. Generally, this term had negative values which could be explained by precipitation from this layer. Yet, sometimes the local rate-of-change term would become large and dominate the residual term at this level. At these times a positive center of residual in a convective area could be attributed to evaporation of liquid water transported into this layer, or to smaller-scale transports.

The distribution of moisture terms in the convective areas during most of the time periods agreed with these models. The exceptions generally occurred when the convective area was small and could not be well depicted by the analysis scheme.

8. EFFECTS OF THREE HOUR DIFFERENCING SCHEME

Figures 21 and 22 show the time variation of moisture content in the layer from 600-500 mb at Stephenville, Texas, during the two experiments. These graphs were constructed using actual sounding data rather than data interpolated to a grid. The top graph in each figure shows precipitable water in the 600-500 mb layer, here denoted by q_L. The formula for this is given by

$$q_L = \int_{z_{600mb}}^{z_{500mb}} \rho_v dz = \frac{1}{g} \int_{600mb}^{500mb} \rho_L \, q \, dp$$

where ρ_L is density of liquid water (1 g cm^{-3}). This term was evaluated using the trapezoidal rule with a step size of 50 mb. The local rate-of-change of moisture was calculated as the difference in q_L from soundings spaced three and six hours apart divided by the corresponding difference in time between the soundings. The figures show that moisture content in the 600-500 mb layer is quite variable, even over a 3-hr period.

Scott and Scoggins (1977) used a centered difference formulation for computation of the local rate-of-change of moisture that used data taken at the observation times before and after the observation time for which the derivative was computed. This local rate-of-change was then summed with the divergence terms at the given observation time to obtain a residual term. A problem with this approach is that the time difference involved in the calculation of the derivative was at least six hours or even as much as twelve hours. This meant that the resulting derivative was highly smoothed, and much of the variability of the moisture was not taken into account.

What this amounts to is that in that study divergence terms at a single time were being used with a term that expressed changes over six hours of time. The calculated rate-of-change represents

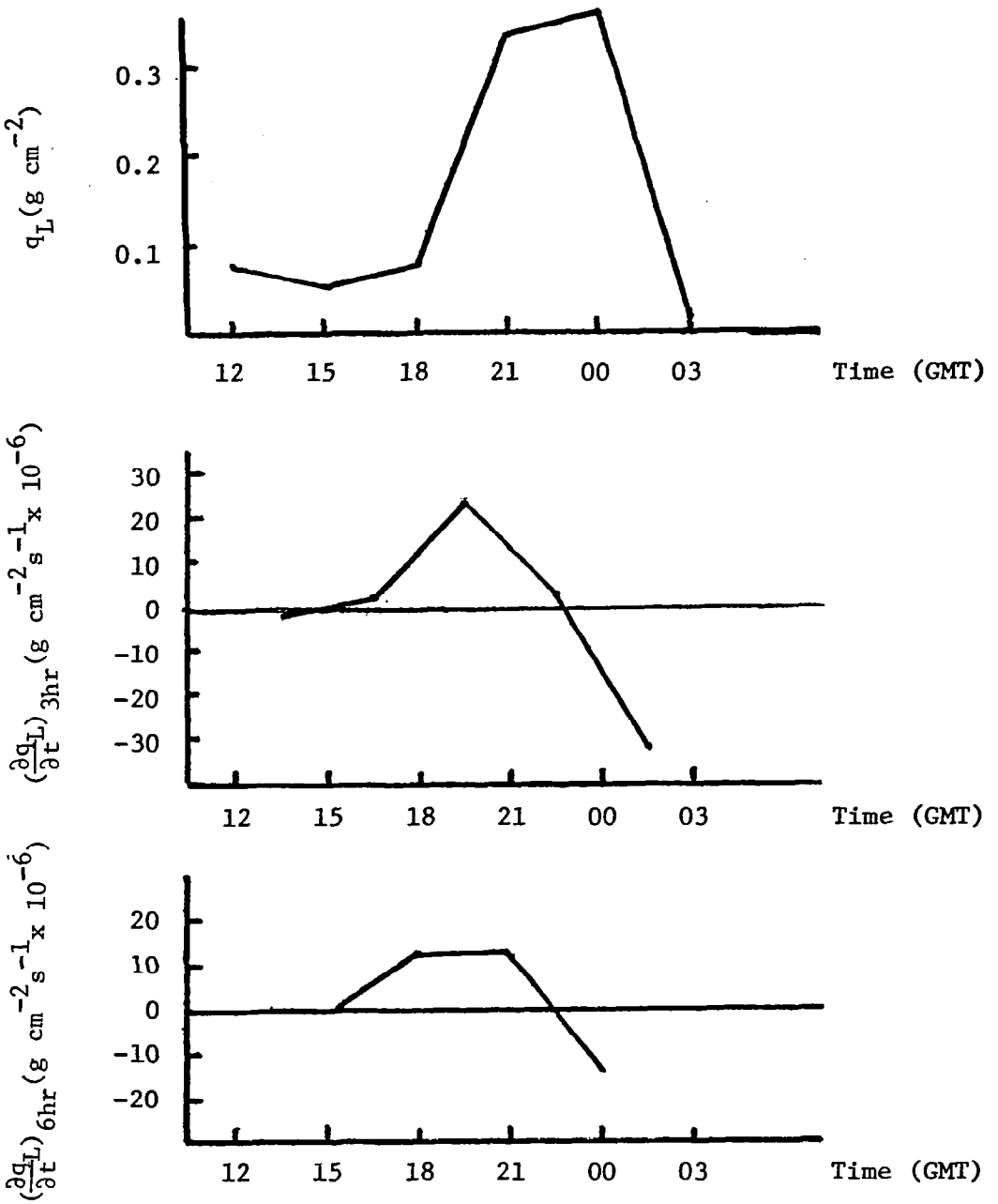

Fig. 21. Moisture content (q_L) and changes in moisture over 3- and 6-hr in the layer 600-500 mb at Stephenville, Texas, on 2-3 May 1978.

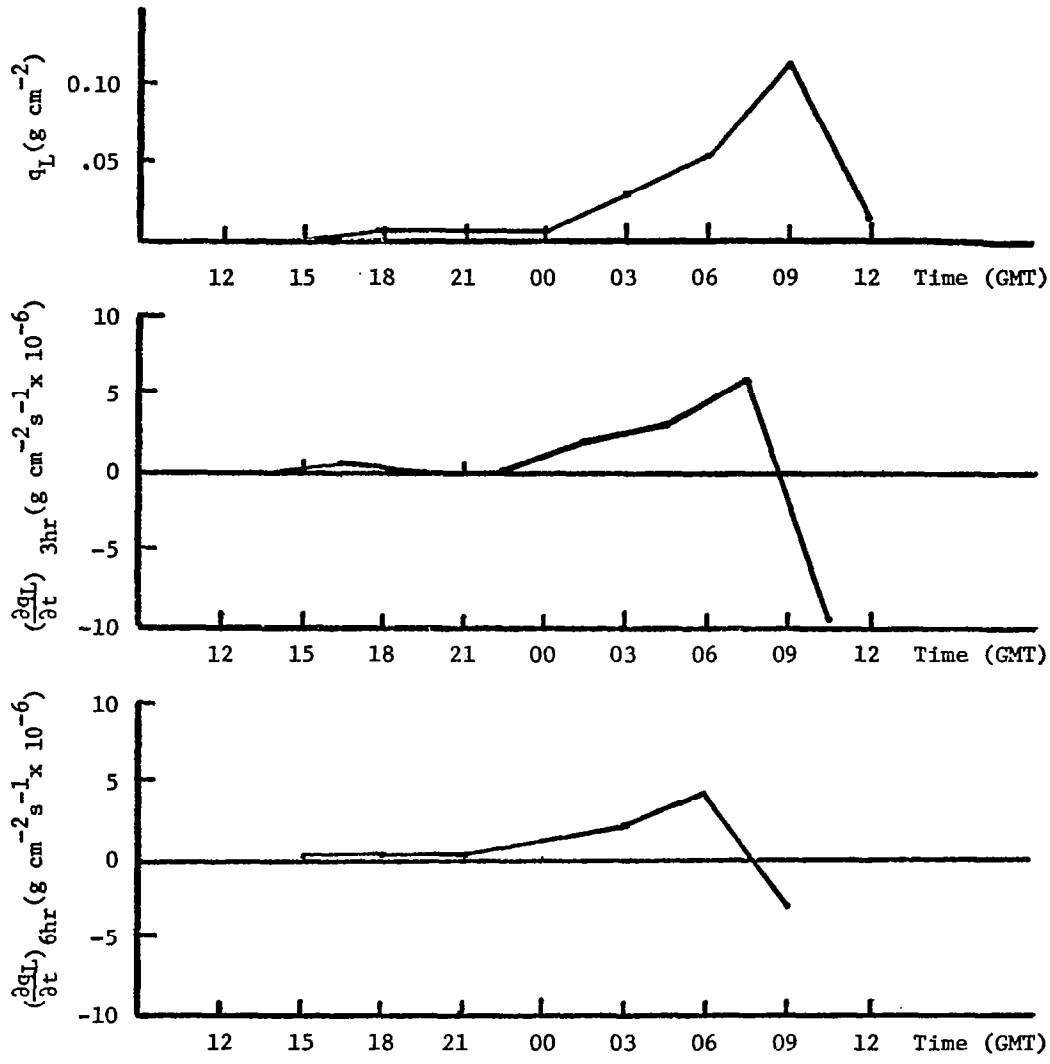

Fig. 22. Moisture content (q_L) and changes in moisture over 3- and 6-hr in the layer 600-500 mb at Stephenville, Texas, on 10-11 April 1979.

the average rate-of-change over the six hours (or twelve hours), but the divergence terms did not represent the average divergence over the same time period.

The analysis method used in this research was devised to circumvent some of the problems of a 6-hr centered difference formulation of the local rate-of-change of moisture. By using the 3-hr difference in moisture, a larger part of the variability in moisture content was retained in the data. This means that there was better resolution of changes in moisture with time. In addition, this average change of moisture in the 3-hr period was compared to average divergence in the same 3-hr period, which means that the divergence and local change terms express simultaneous processes.

One question that comes to mind is that perhaps the arithmetic averages of the divergences measured at the start and end of an observation period do not represent the actual integrated divergences for that time period. Stated another way, are the divergence terms also quite variable over time periods as short as three hours? The comparison of moisture divergence calculated at single time periods with the moisture divergence three hours later showed no major changes occurring in the fields once the convective systems developed (Fig. 23). The changes in divergence seemed to be fairly smooth and continuous, so that the calculated average should be acceptable for use in the moisture budget.

The effect of changing from a 6-hr difference to a 3-hr difference in calculating the local rate-of-change is that the magnitude of the local rate-of-change is increased. The averaging of divergence terms over three hours decreases the magnitudes of these terms. Thus, the effect of the local rate-of-change is magnified in this method as compared to the method used by Scott and Scoggins (1977). The effect is readily seen in the increased influence of local rate-of-change of moisture on the residual term.

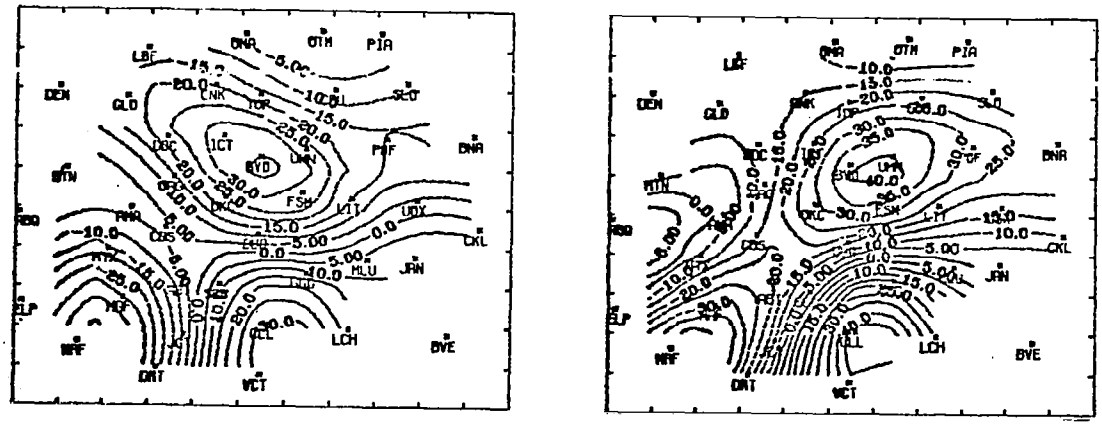

a. 0000 GMT

b. 0300 GMT

c. 0000-0300 GMT

Fig. 23. Comparison of horizontal moisture divergence ($g\ cm^{-2}s^{-1} \times 10^{-6}$) in the 900-750 mb layer computed at observation times with the average value for the time period 0000-0300 GMT on 11 April 1979.

9. CONCLUSIONS

Examination of contoured plots of moisture budget fields calculated from observations taken during two different synoptic situations reveals characteristics of these fields that were similar in all areas of convective activity that were large enough to be resolved by the data. These common features included horizontal moisture convergence in the lowest layers with subsequent upward vertical transport of moisture in the convective areas. Vertical moisture convergence in the lowest layers with subsequent upward vertical transport of moisture in the convective areas. Vertical moisture convergence concentrated this moisture in higher layers where vertical motions decreased with height. The water vapor in higher layers was transported north of storm areas by the southerly winds at those levels. The vapor content in lower layers increased in areas where storms formed, but decreased when storms persisted.

By shortening the time period used in the evaluation of the local rate-of-change term, and averaging the horizontal and vertical divergence terms over the same time period, led to greater emphasis of the effects of the local rate-of-change of moisture than observed in previous studies (e.g., Scott and Scoggins, 1977). Even so, cumulative precipitation totals integrated over the same area as the moisture budget terms were in good agreement with the calculated residual sink term.

REFERENCES

Barnes, S. L., 1964: A technique for maximizing detail in numerical weather map analysis. J. Appl. Meteor. 3, 396-409.

Bradberry, J. S., 1981: Mesoscale structure of an Oklahoma squall line. Mon. Wea. Rev., 109, 1110-1117.

Bradbury, D. L., 1957: Moisture analysis and water budget in three different types of storms. J. Meteor., 14, 559-565.

Cho, H.-R., 1977: Contribution of cumulus cloud life cycle effects to the large scale heat and moisture budget equations. J. Atmos. Sci., 34, 87-97.

Davis, J. G., H. E. Fuelberg, and R. E. Turner, 1978: NASA's AVE VII experiment: 25-mb sounding data. NASA Technical Memorandum TM-78197. NASA Marshall Space Flight Center, Alabama, 218 pp.

Fritsch, J. M., C. F. Chappell, and L. R. Hoxit, 1976: The use of large scale budgets for convective parameterization. Mon. Wea. Rev., 104, 1408-1418.

Fuelberg, H. E., 1974: Reduction and error analysis of the AVE II pilot experiment data. NASA Contractor Report CR-120496. NASA Marshall Space Flight Center, Alabama, 140 pp.

Gerhard, M. L., H. E. Fuelberg, S. F. Williams, and R. E. Turner, 1979: AVE-SESAME I: 25-mb sounding data. NASA Technical Memorandum TM-78256. NASA Marshall Space Flight Center, Alabama, 364 pp.

O'Brien, J. J., 1970: Alternate solutions to the classical vertical velocity problem. J. Appl. Meteor., 9, 197-203.

Ogura, Y., and H.-R. Cho, 1973: Diagnostic determination of cumulus cloud populations from observed large scale variables. J. Atmos. Sci., 30, 1276-1286.

Palmén, E., and E. O. Holopainen, 1962: Divergence, vertical velocity, and conversion between potential and kinetic energy in an extra-tropical diaturbance. Geophysica, 8, 89-113.

Sanders, F., and F. J. Paine, 1975: The structure and thermodynamics of an intense mesoscale convective storm in Okalhoma. J. Atmos. Sci., 32, 1563-1579.

REFERENCES (continued)

Scott, R. W., and J. R. Scoggins, 1977: The moisture budget in relation to convection. NASA Contractor Report CR-2817. NASA Marshall Space Flight Center, Alabama, 88 pp.

Shuman, F. G., 1957: Numerical methods in weather prediction: II Smoothing and filtering. Mon. Wea. Rev., 85, 357-361.

Spar, J., 1953: A suggested technique for quantitative precipitation forecasting. Mon. Wea. Rev., 81, 217-221.

Williams, S. F., and J. R. Scoggins, 1979: Models of the Atmospheric Water Vapor Budget for the Texas HIPLEX Area, Rep. LP-117. Technical Report, TDWR contract Nos. 14-90026 and 14-00003, Texas Department of Water Resources, Austin, Texas, 51 pp.

_____, _____, N. Horvath, and K. Hill, 1980: A preliminary look at AVE-SESAME I conducted on April 10-11, 1979. NASA Technical Memorandum TM-78262. Marshall Space Flight Center, Alabama, 56 pp.

Yanai, M., S. Esbensen, and J.-H. Chu, 1973: Determination of bulk properties of tropical cloud clusters from large scale heat and moisture budgets. J. Atmos. Sci., 30, 611-627.

APPENDIX A

Contoured plots of moisture budget terms for the 900-750 mb and 600-500 mb layers

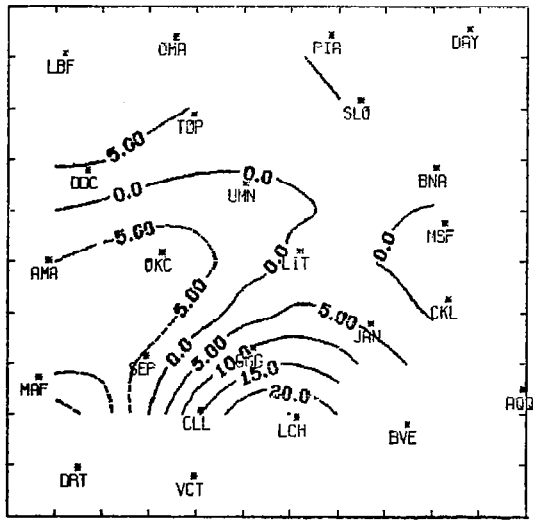

a. 1500-1800 GMT

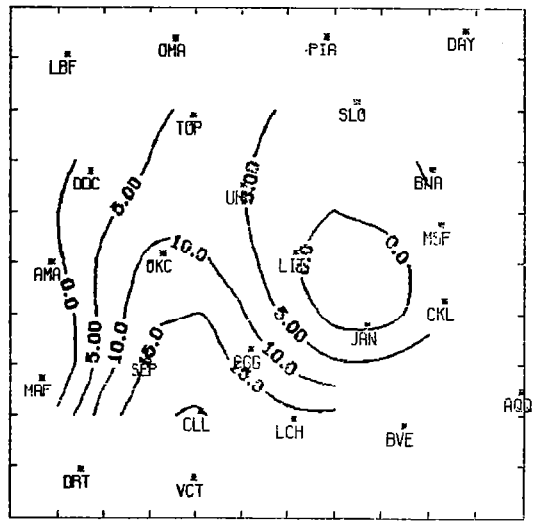

b. 1800-2100 GMT

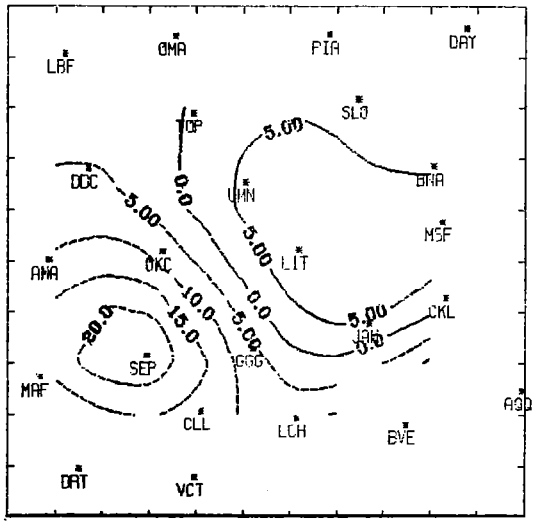

c. 2100-0000 GMT

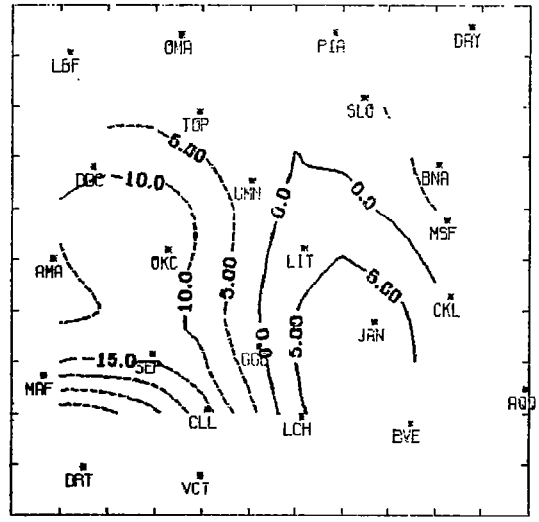

d. 0000-0300 GMT

Fig. A1. Local rate-of-change of moisture (g $cm^{-2}s^{-1}$ x 10^{-6}) in the 900-750 mb layer for 2-3 May 1978.

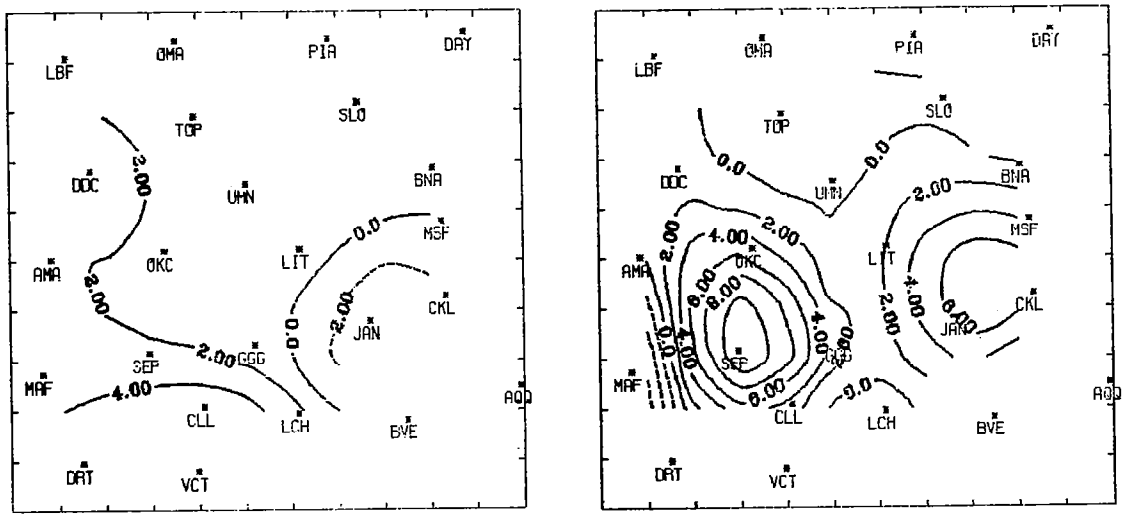

a. 1500-1800 GMT

b. 1800-2100 GMT

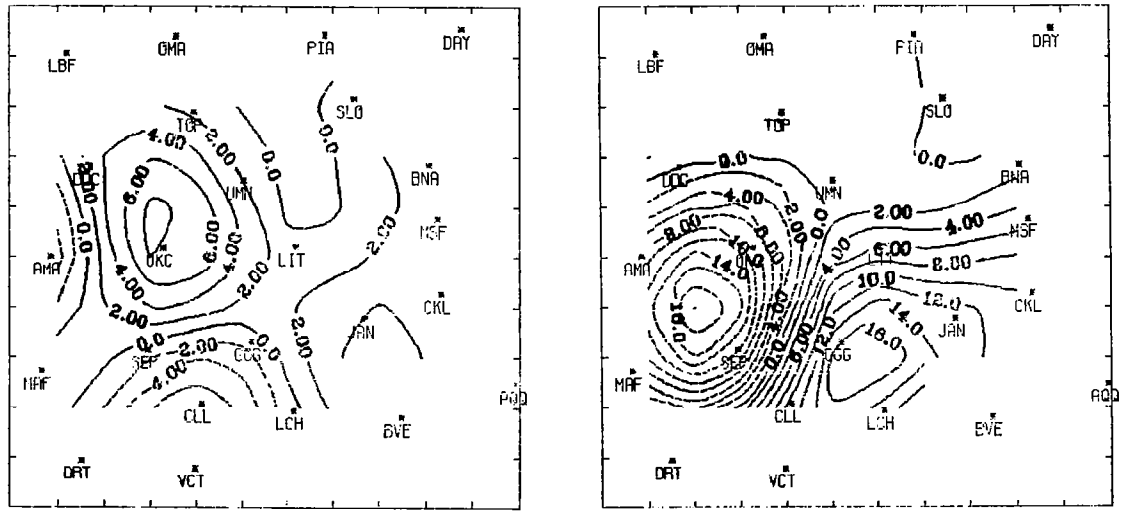

c. 2100-0000 GMT

d. 0000-0300 GMT

Fig. A2. Local rate-of-change of moisture (g $cm^{-2}s^{-1}$ x 10^{-6}) in the 600-500 mb layer for 2-3 May 1978.

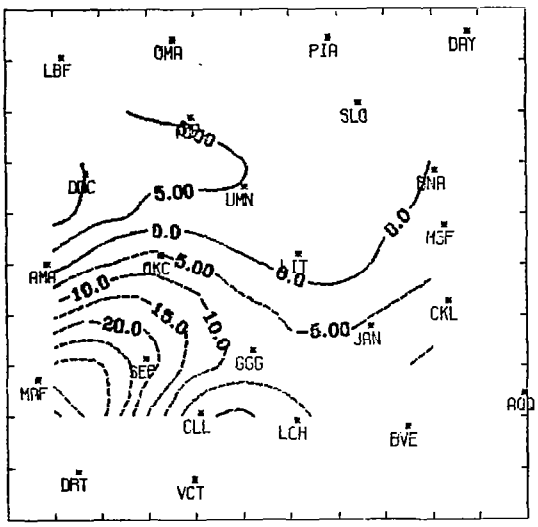

a. 1500-1800 GMT

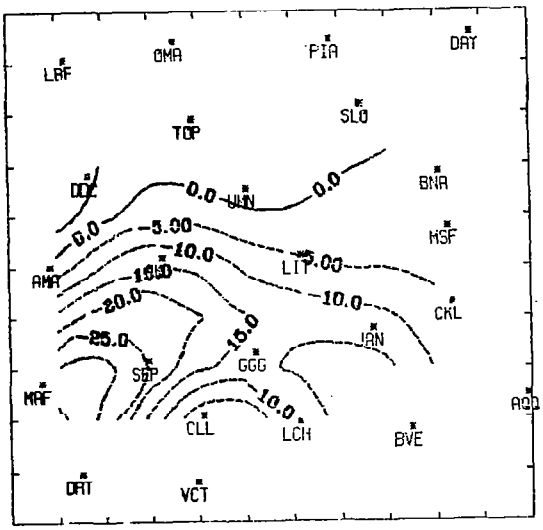

b. 1800-2100 GMT

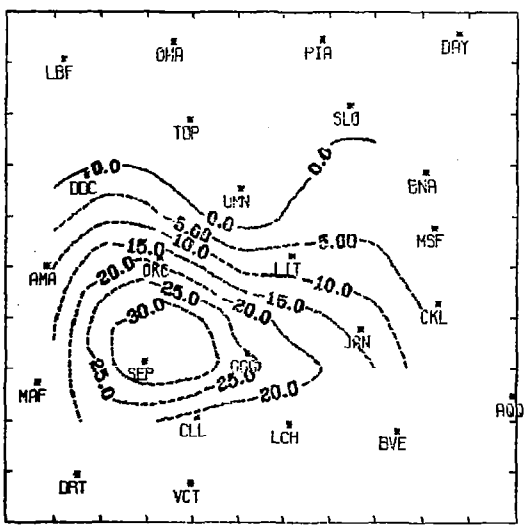

c. 2100-0000 GMT

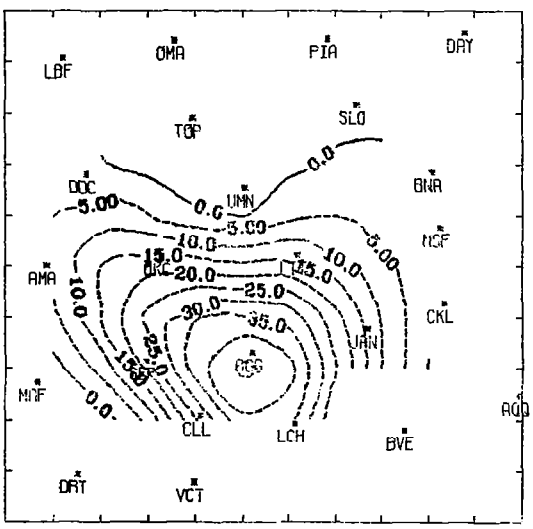

d. 0000-0300 GMT

Fig. A3. Horizontal moisture divergence (g $cm^{-2}s^{-1}$ x 10^{-6}) in the 900-750 mb layer for 2-3 May 1978.

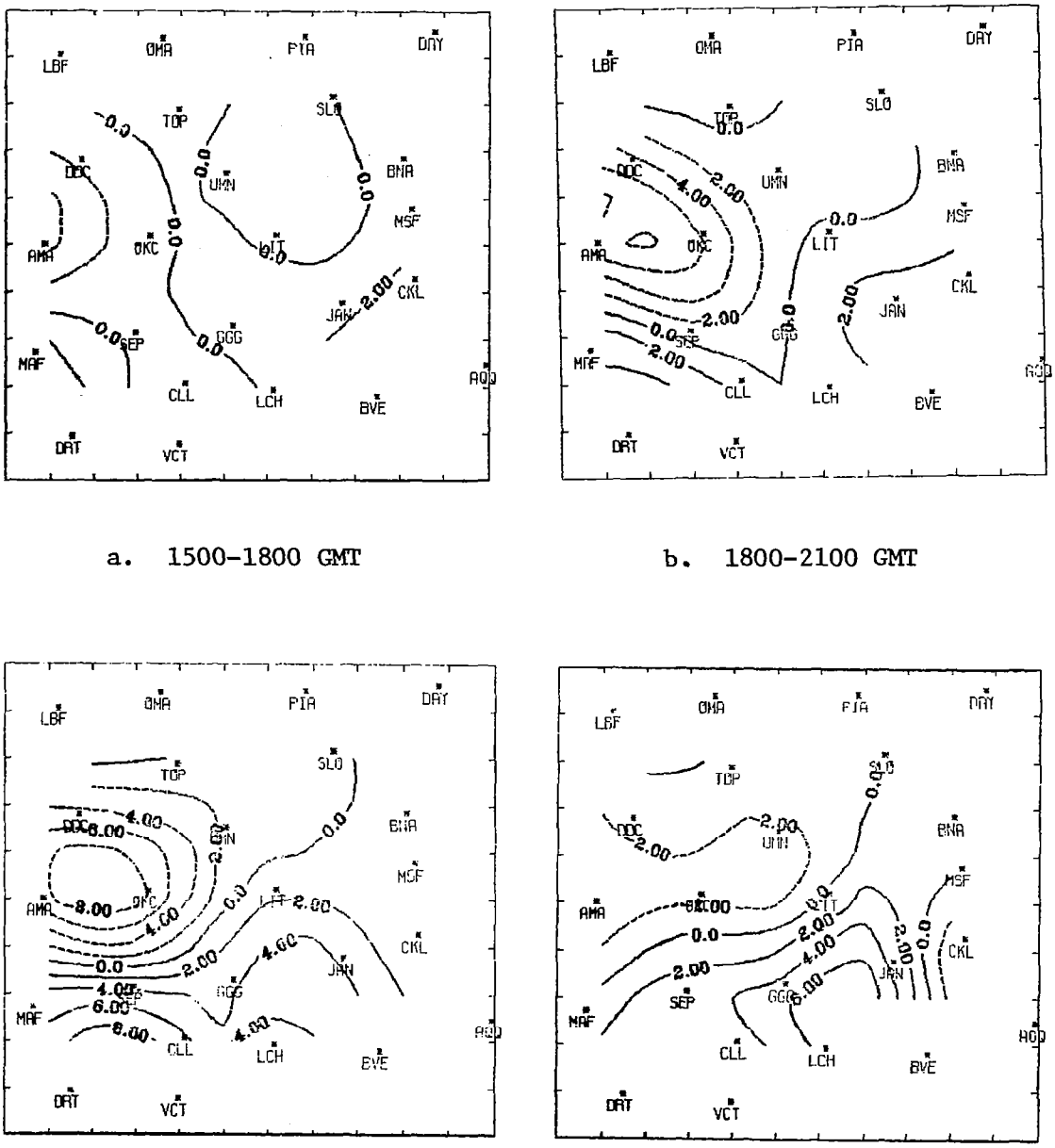

a. 1500–1800 GMT

b. 1800–2100 GMT

c. 2100–0000 GMT

d. 0000–0300 GMT

Fig. A4. Horizontal moisture divergence (g $cm^{-2}s^{-1}x\ 10^{-6}$) in the 600–500 mb layer for 2-3 May 1978.

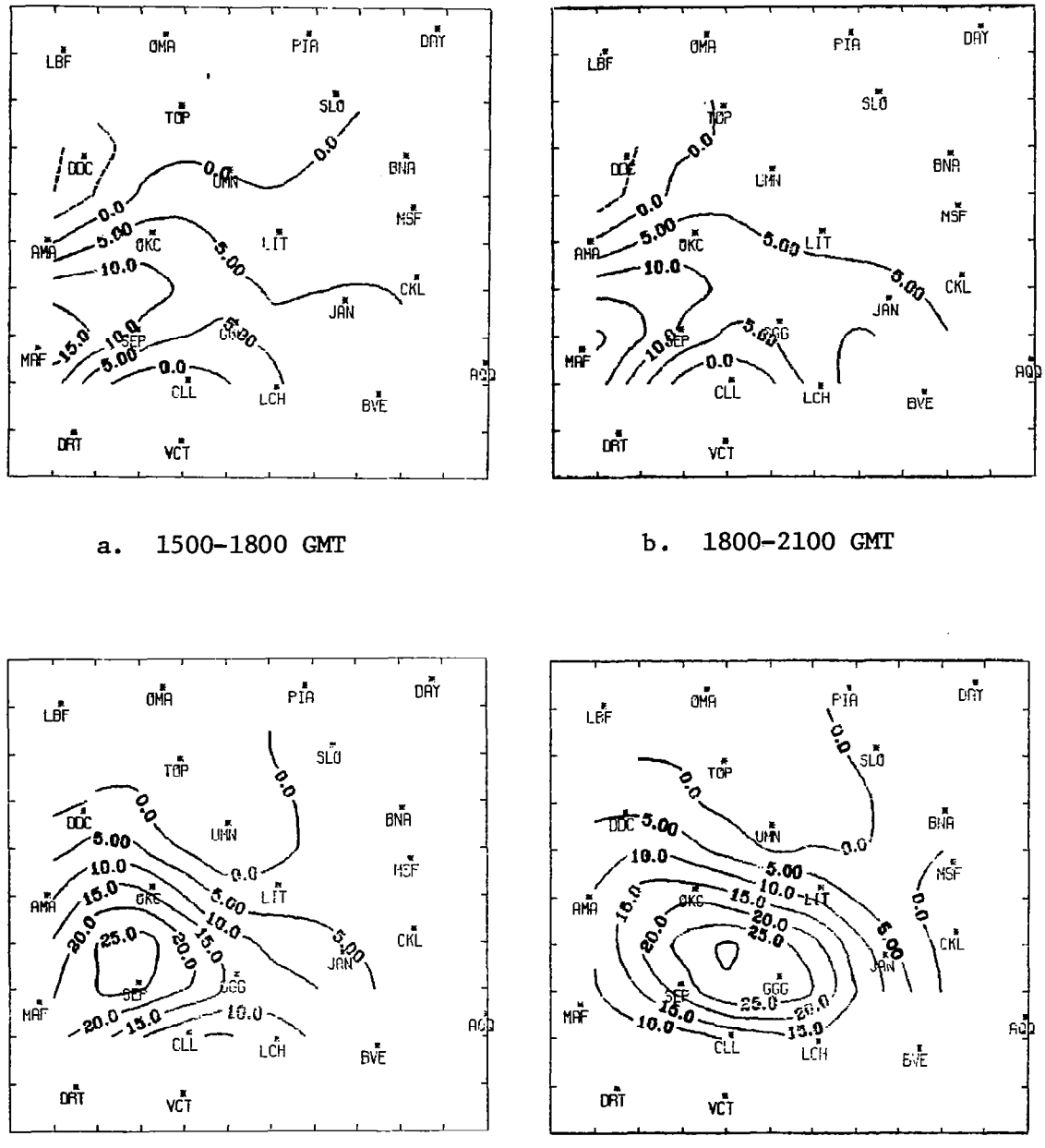

a. 1500-1800 GMT

b. 1800-2100 GMT

c. 2100-0000 GMT

d. 0000-0300 GMT

Fig. A5. Vertical moisture divergence (g $cm^{-2}s^{-1}$ x 10^{-6}) in the 900-750 mb layer for 2-3 May 1978.

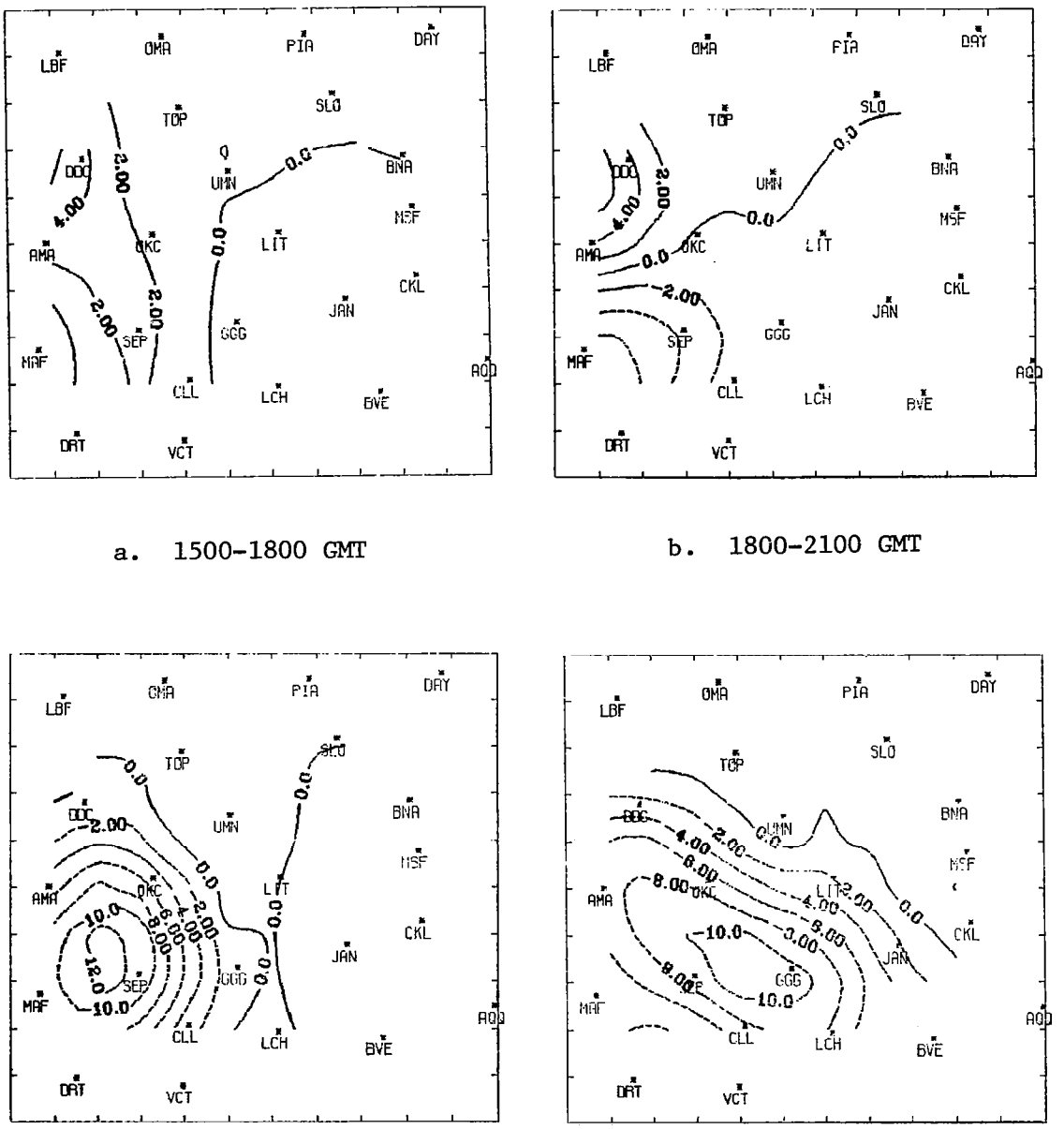

a. 1500-1800 GMT

b. 1800-2100 GMT

c. 2100-0000 GMT

d. 0000-0300 GMT

Fig. A6. Vertical moisture divergence (g $cm^{-2}s^{-1}$ x 10^{-6}) in the 600-500 mb layer for 2-3 May 1978.

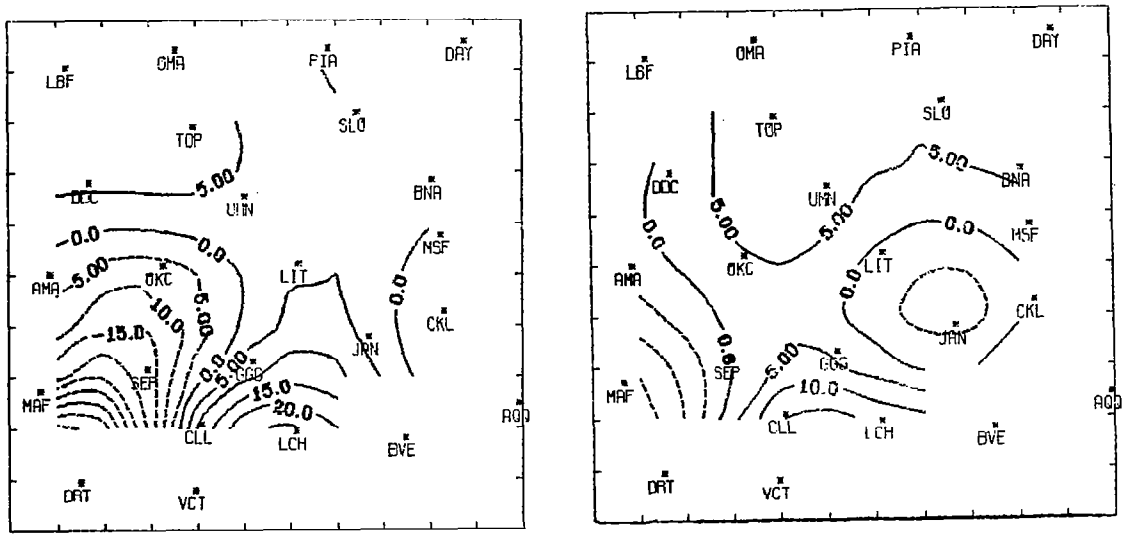

a. 1500-1800 GMT

b. 1800-2100 GMT

c. 2100-0000 GMT

d. 0000-0300 GMT

Fig. A7. Residual (g $cm^{-2}s^{-1}$ x 10^{-6}) in the 900-750 mb layer for 2-3 May 1978.

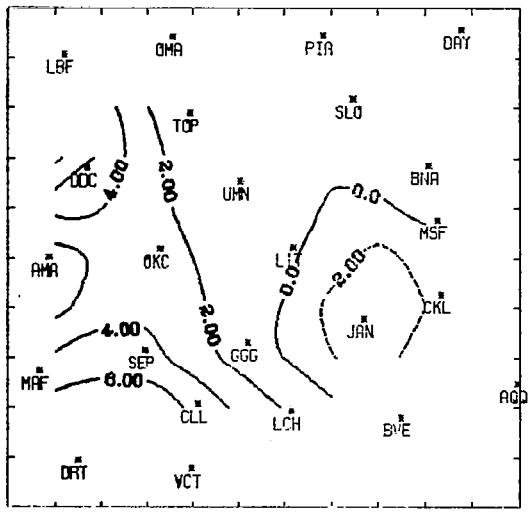

a. 1500-1800 GMT

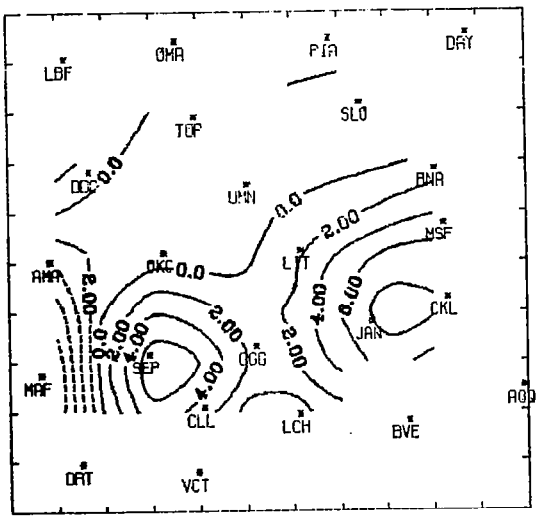

b. 1800-2100 GMT

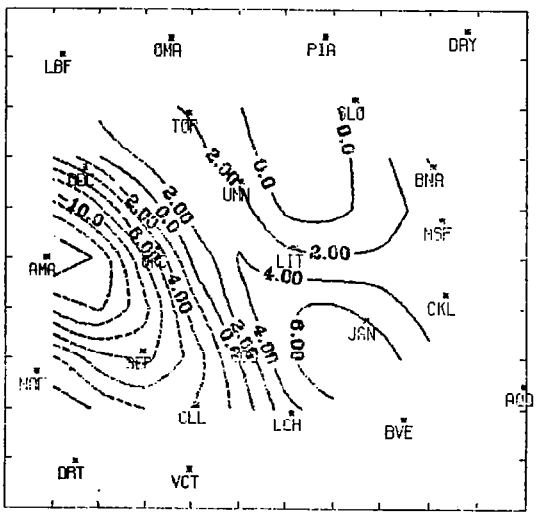

c. 2100-0000 GMT

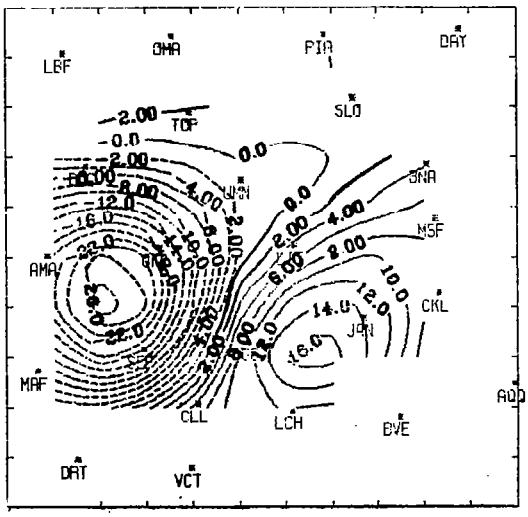

d. 0000-0300 GMT

Fig. A8. Residual (g $cm^{-2}s^{-1}$ x 10^{-6}) in the 600-500 mb layer for 2-3 May 1978.

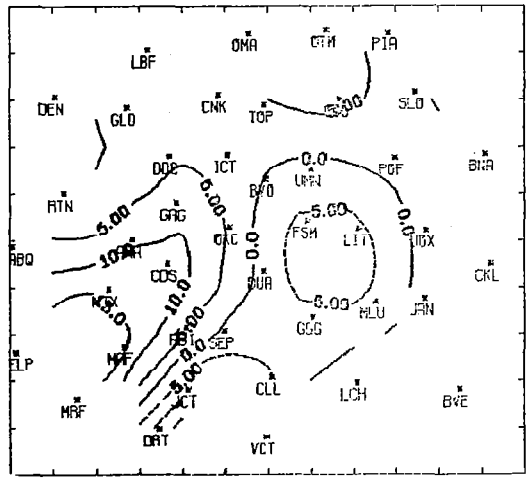

a. 1200-1500 GMT

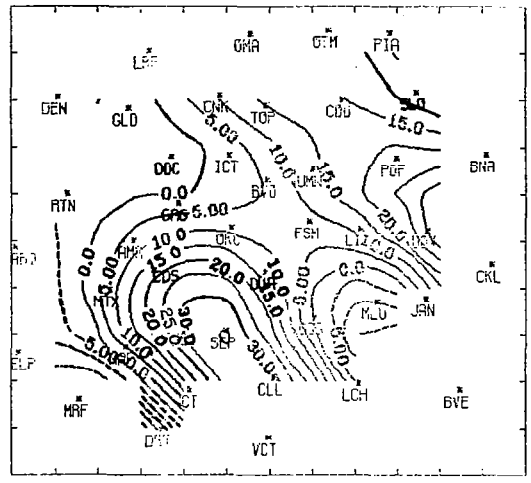

b. 1500-1800 GMT

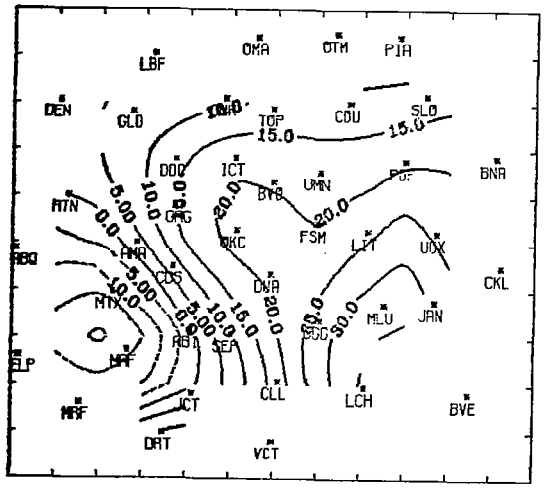

c. 1800-2100 GMT

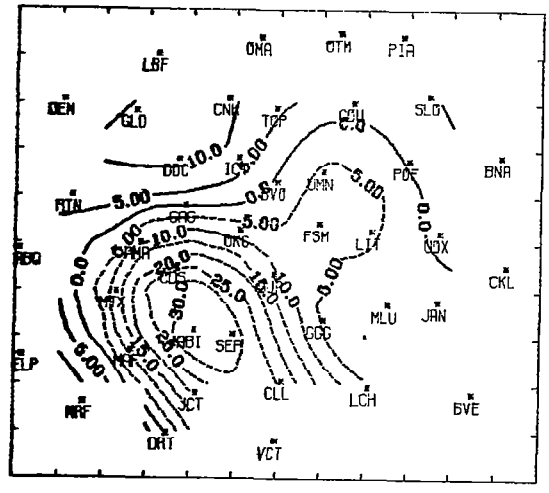

d. 2100-0000 GMT

Fig. A9. Local rate-of-change of moisture ($g\ cm^{-2}s^{-1} \times 10^{-6}$) in the 900-750 mb layer for 10-11 April 1979.

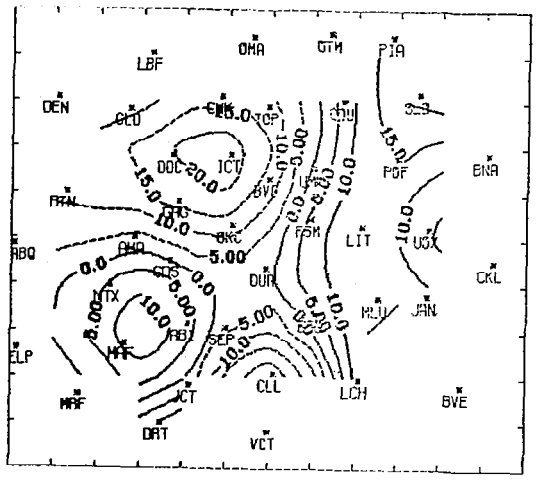

a. 0000-0300 GMT

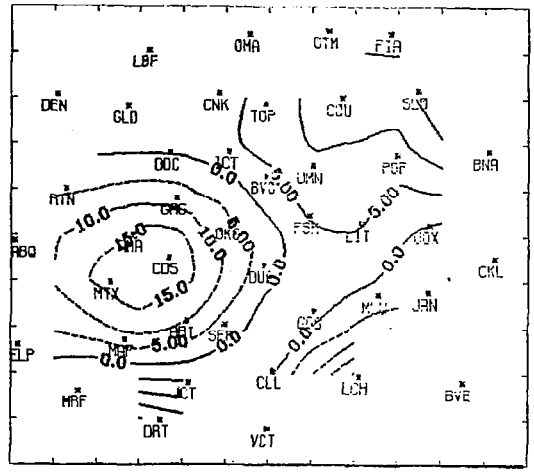

b. 0300-0600 GMT

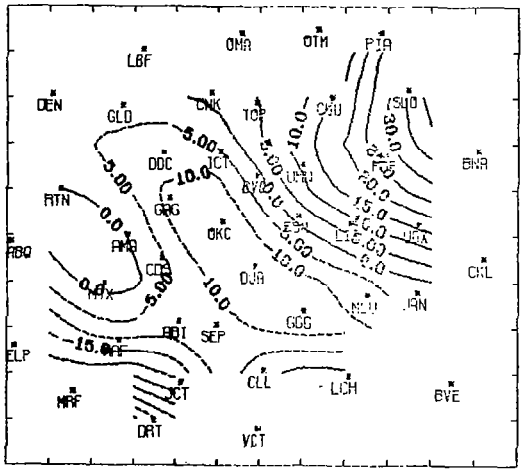

c. 0600-0900 GMT

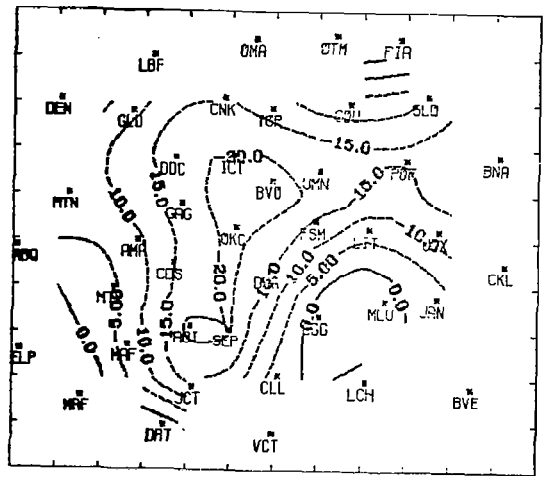

d. 0900-1200 GMT

Fig. A10. Local rate-of-change of moisture (g $cm^{-2}s^{-1}$ x 10^{-6}) in the 900-750 mb layer for 11 April 1979.

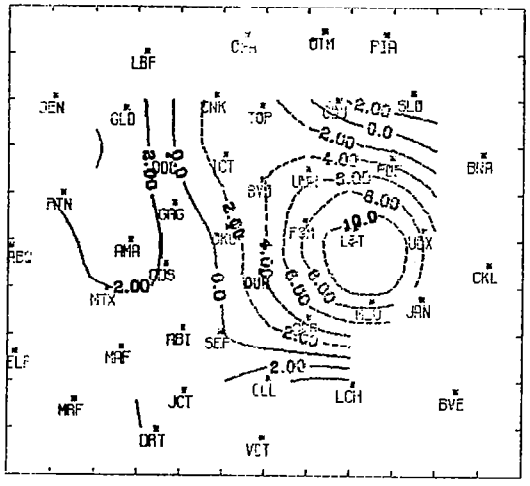

a. 1200-1500 GMT

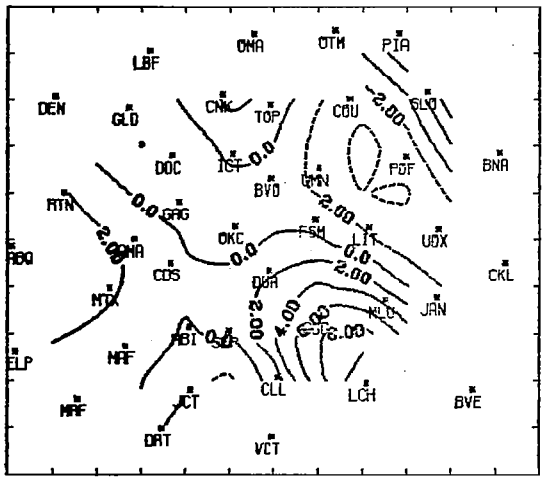

b. 1500-1800 GMT

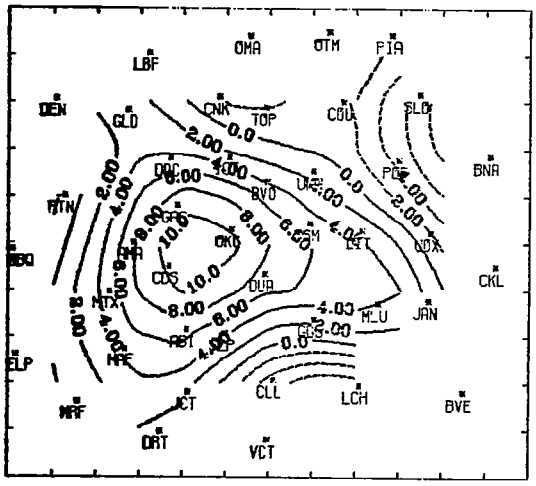

c. 1800-2100 GMT

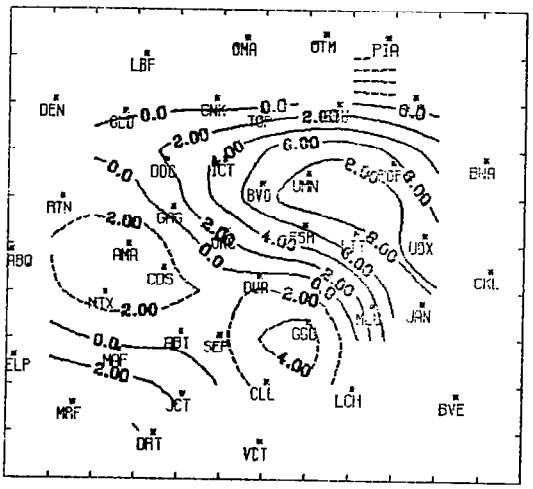

d. 2100-0000 GMT

Fig. A11. Local rate-of-change of moisture (g $cm^{-2}s^{-1}$ x 10^{-6}) in the 600-500 mb layer for 10-11 April 1979.

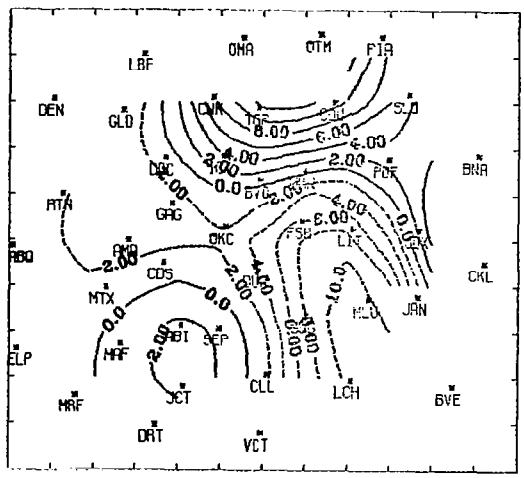

a. 0000-0300 GMT

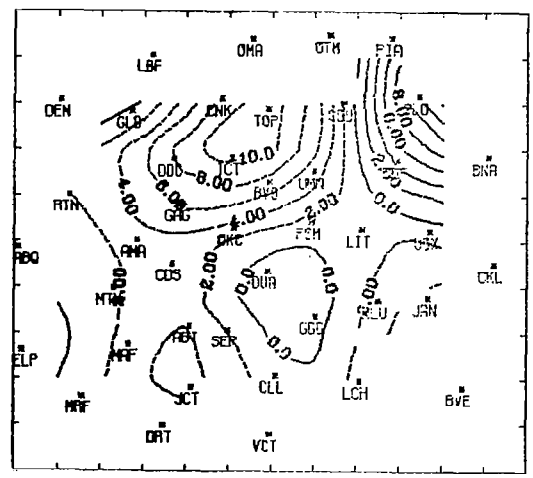

b. 0300-0600 GMT

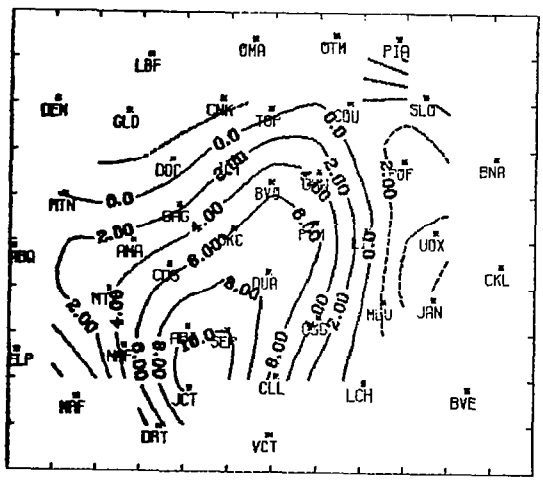

c. 0600-0900 GMT

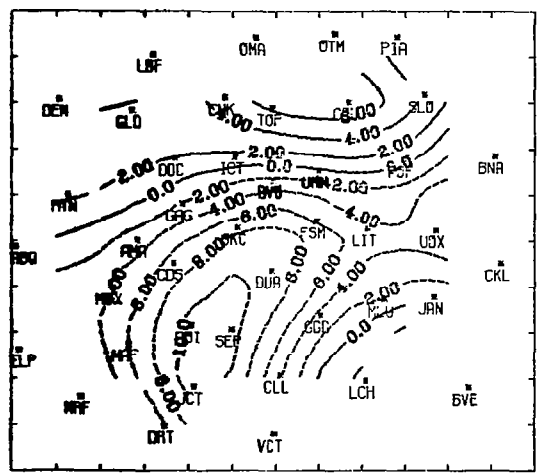

d. 0900-1200 GMT

Fig. A12. Local rate-of-change of moisture (g $cm^{-2}s^{-1}$ x 10^{-6}) in the 600-500 mb layer for 11 April 1979.

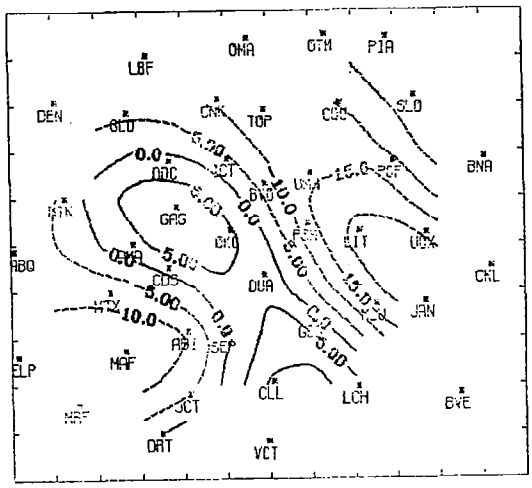

a. 1200-1500 GMT

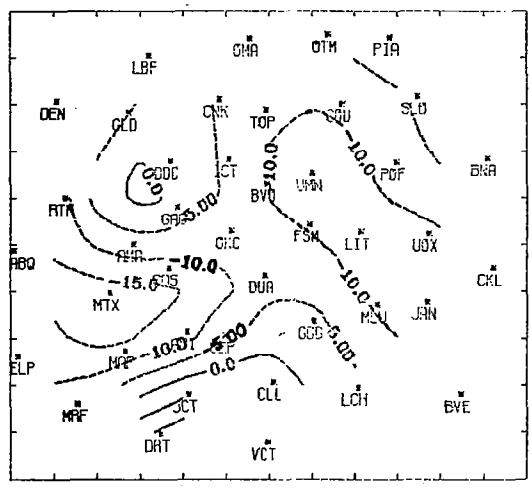

b. 1500-1800 GMT

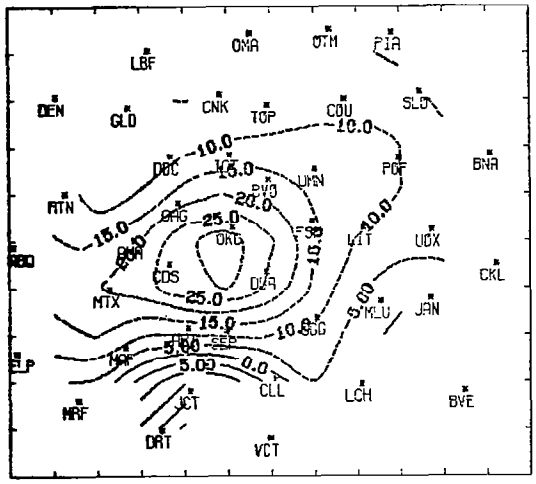

c. 1800-2100 GMT

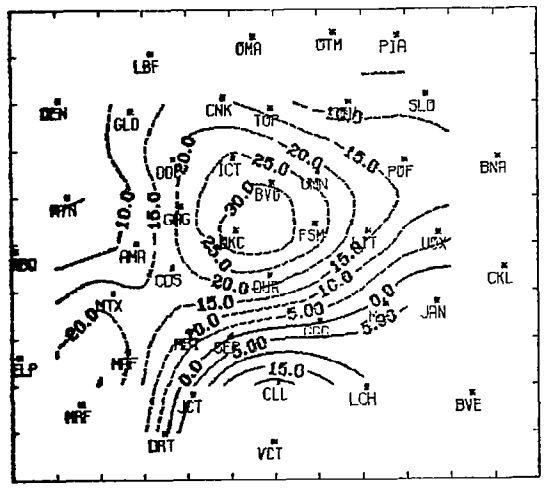

d. 2100-0000 GMT

Fig. A13. Horizontal moisture divergence (g $cm^{-2}s^{-1}$ x 10^{-6}) in the 900-750 mb layer for 10-11 April 1979.

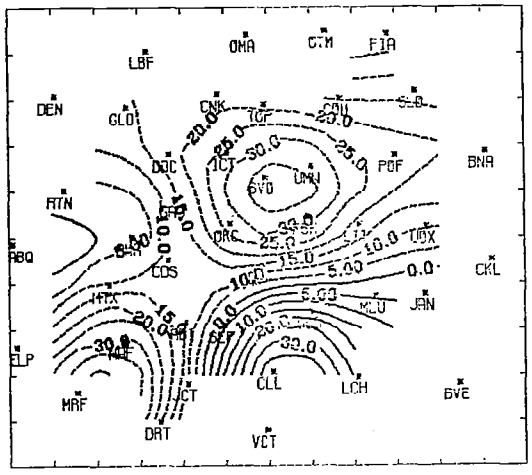

a. 0000-0300 GMT

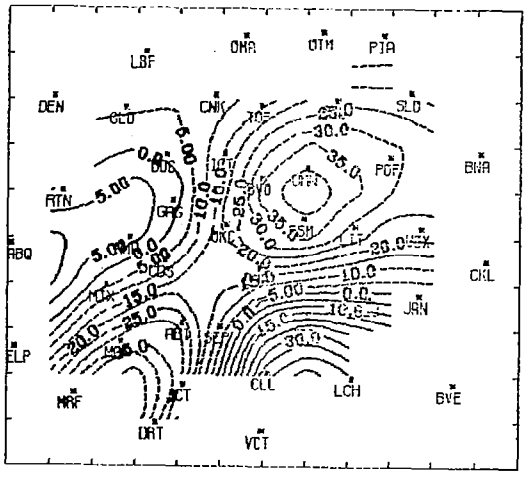

b. 0300-0600 GMT

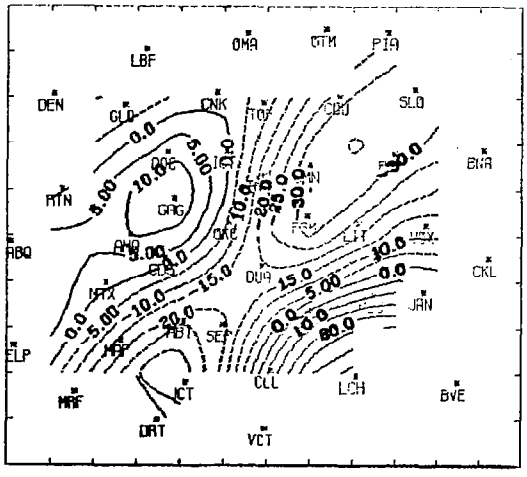

c. 0600-0900 GMT

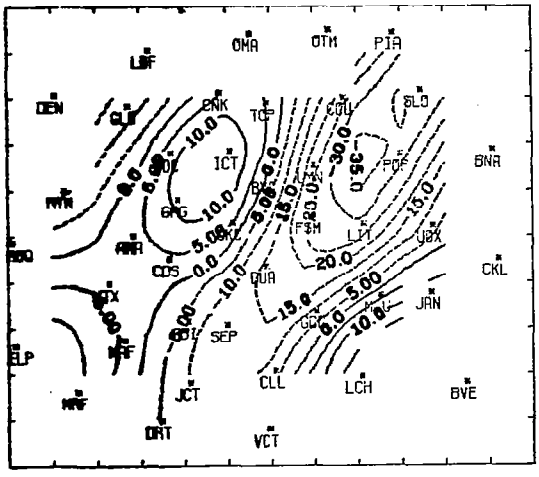

d. 0900-1200 GMT

Fig. A14. Horizontal moisture divergence (g $cm^{-2}s^{-1}$ x 10^{-6}) in the 900-750 mb layer for 11 April 1979.

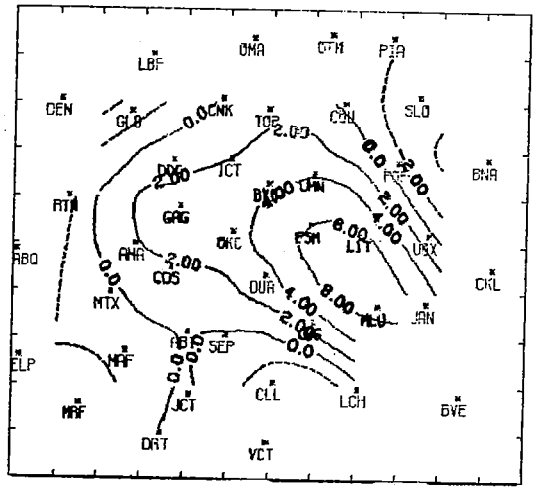

a. 1200-1500 GMT

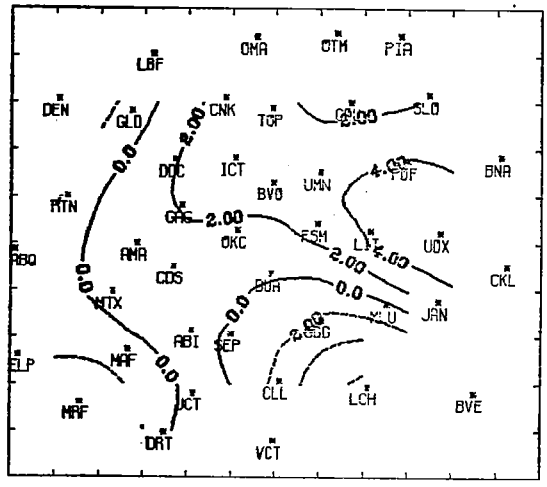

b. 1500-1800 GMT

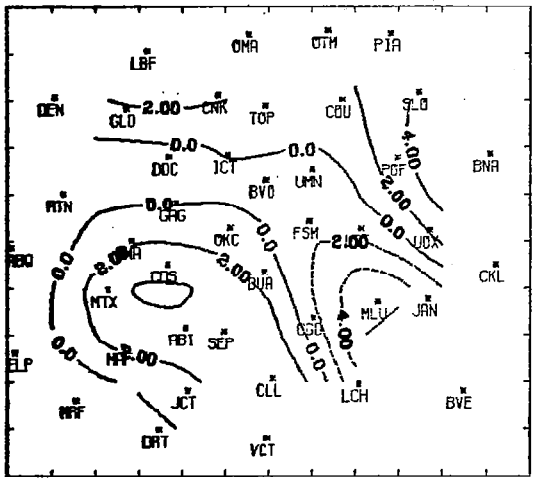

c. 1800-2100 GMT

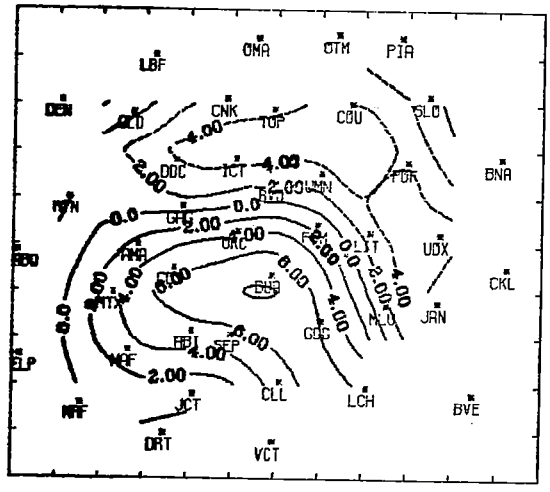

d. 2100-0000 GMT

Fig. A15. Horizontal moisture divergence (g $cm^{-2}s^{-1}$ x 10^{-6}) in the 600-500 mb layer for 10-11 April 1979.

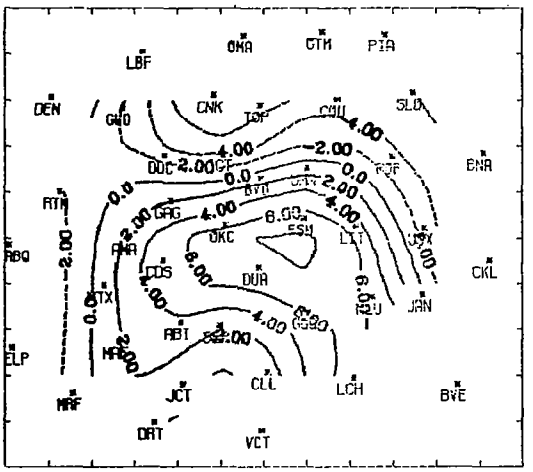

a. 0000-0300 GMT

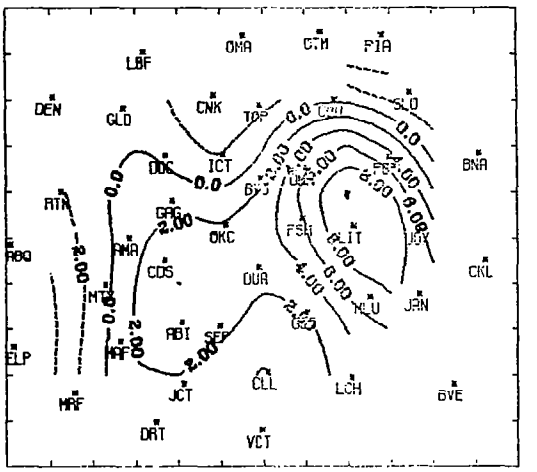

b. 0300-0600 GMT

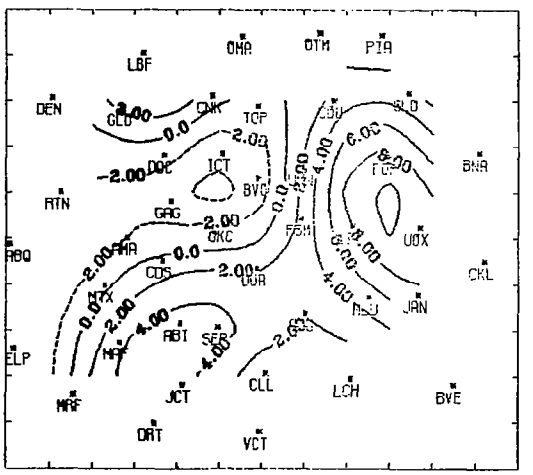

c. 0600-0900 GMT

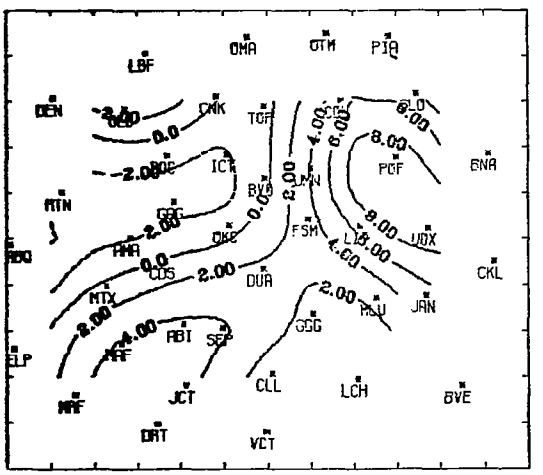

d. 0900-1200 GMT

Fig. A16. Horizontal moisture divergence (g $cm^{-2}s^{-1}$ x 10^{-6}) in the 600-500 mb layer for 11 April 1979.

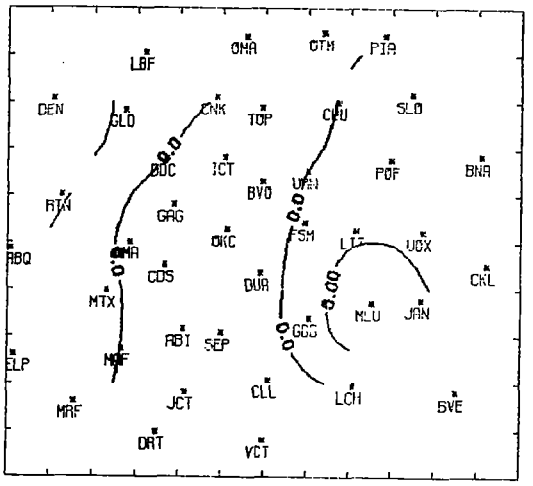

a. 1200-1500 GMT

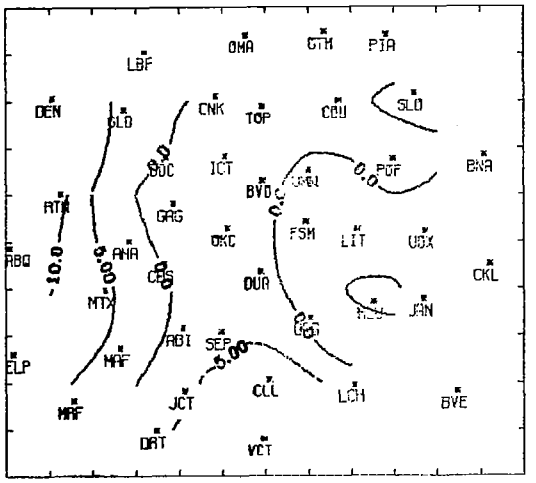

b. 1500-1800 GMT

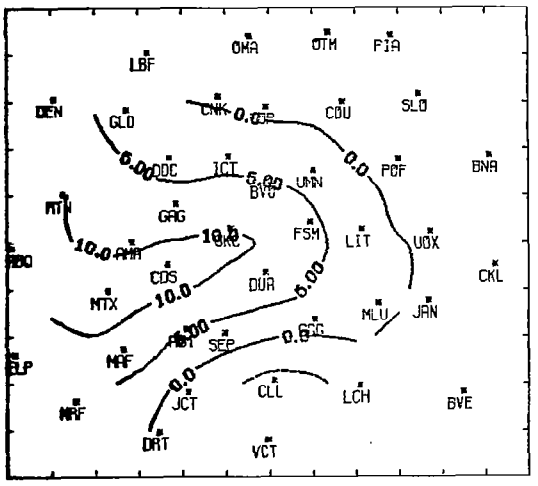

c. 1800-2100 GMT

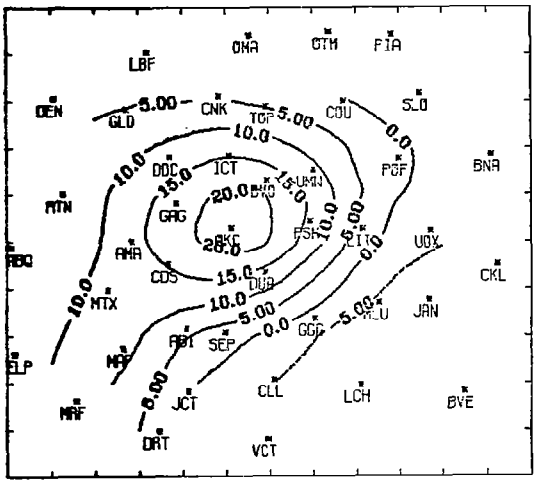

d. 2100-0000 GMT

Fig. A17. Vertical moisture divergence (g $cm^{-2}s^{-1}$ x 10^{-6}) in 900-750 mb layer for 10-11 April 1979.

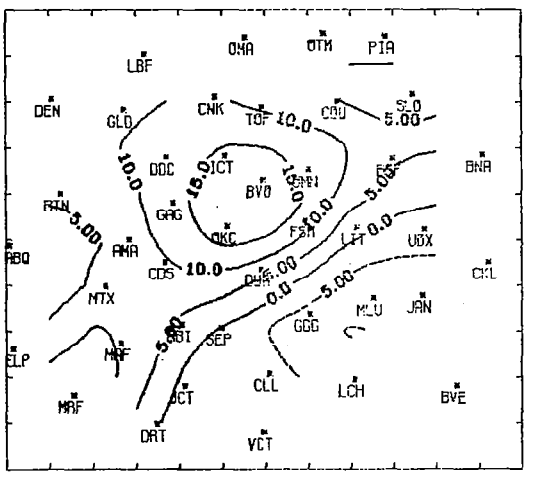

a. 0000–0300 GMT

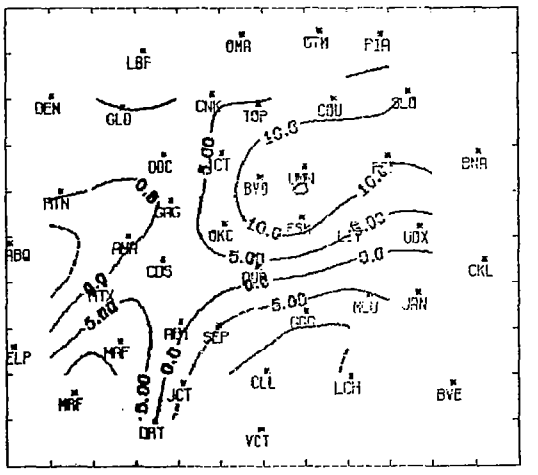

b. 0300–0600 GMT

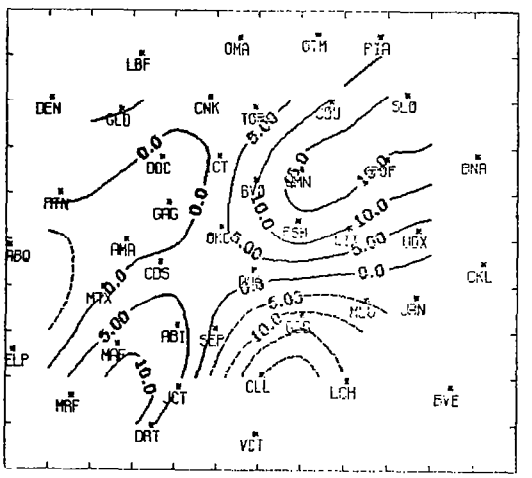

c. 0600–0900 GMT

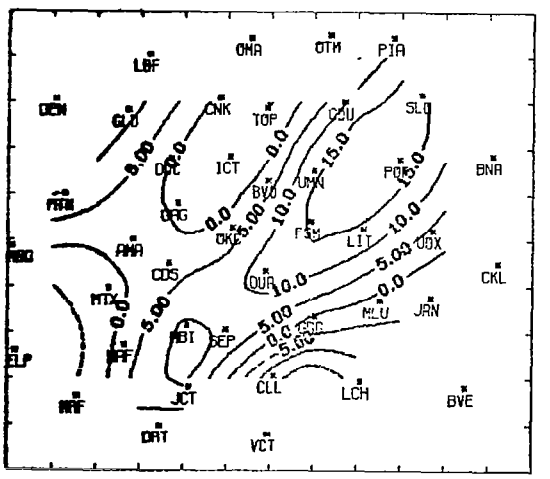

d. 0900–1200 GMT

Fig. A18. Vertical moisture divergence (g $cm^{-2}s^{-1}$ x 10^{-6}) in the 900–750 mb layer for 11 April 1979.

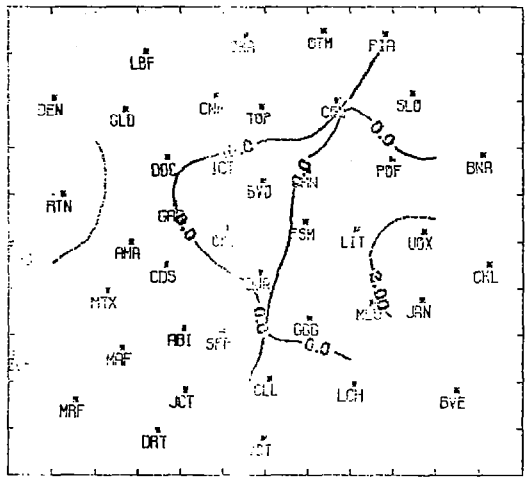

a. 1200-1500 GMT

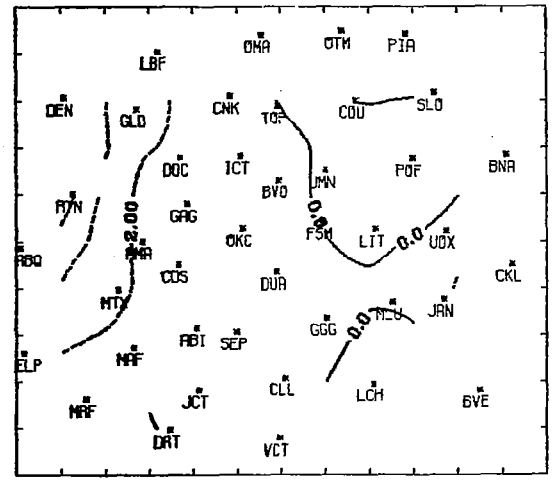

b. 1500-1800 GMT

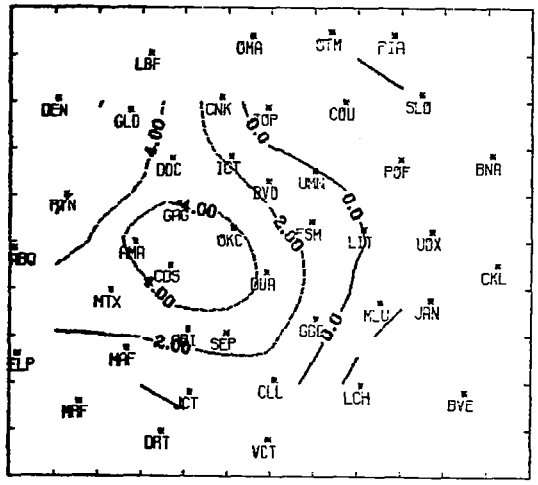

c. 1800-2100 GMT

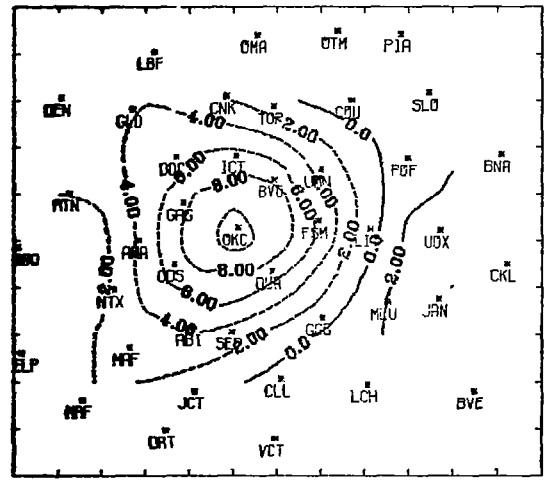

d. 2100-0000 GMT

Fig. A19. Vertical moisture divergence (g $cm^{-2}s^{-1}$ x 10^{-6}) in the 600-500 mb layer for 10-11 April 1979.

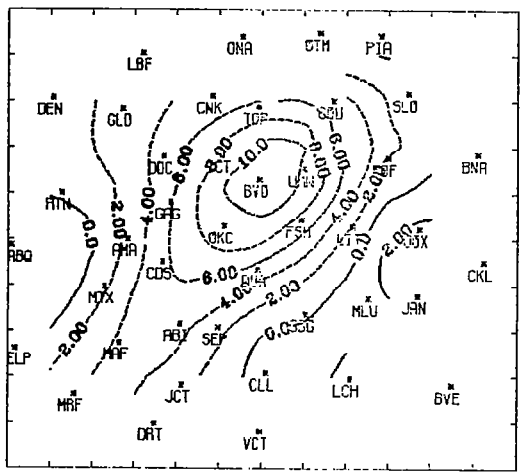

a. 0000-0300 GMT

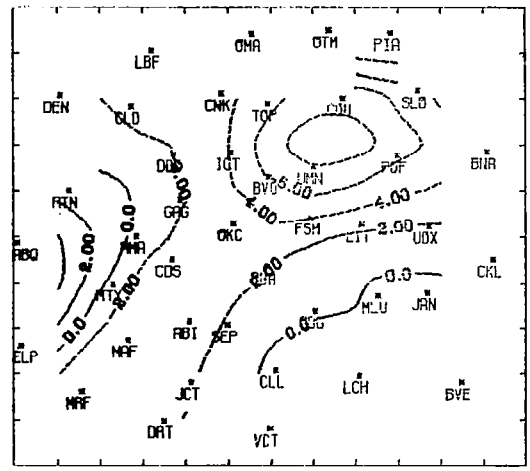

b. 0300-0600 GMT

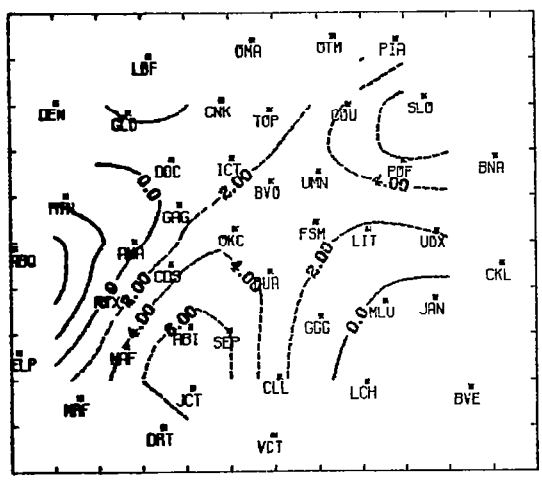

c. 0600-0900 GMT

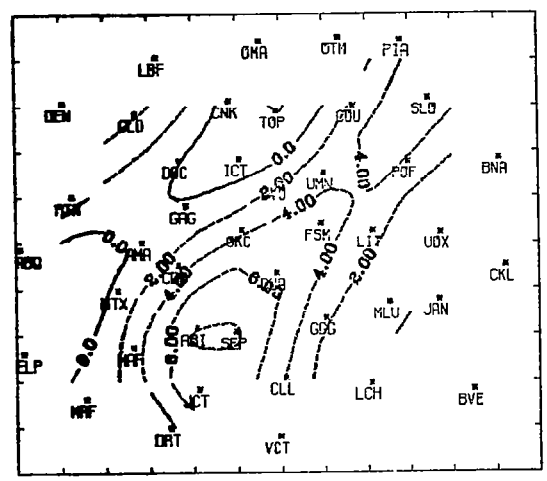

d. 0900-1200 GMT

Fig. A20. Vertical moisture divergence (g $cm^{-2}s^{-1}$ x 10^{-6}) in the 600-500 mb layer for 11 April 1979.

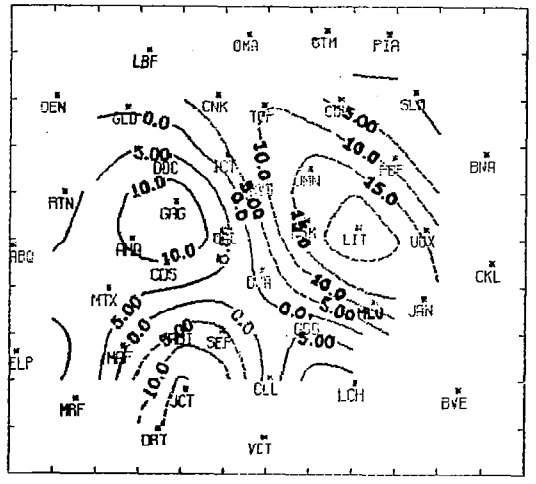

a. 1200-1500 GMT

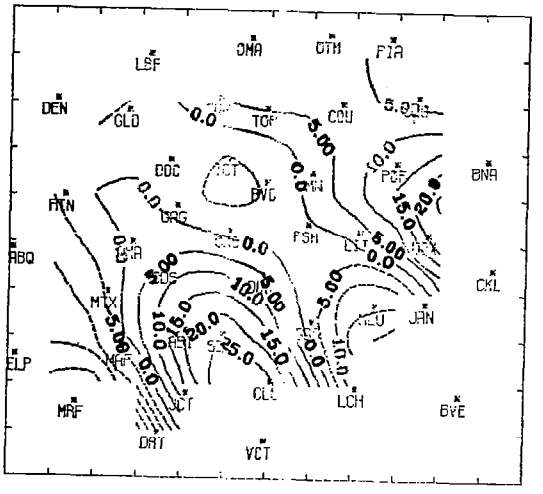

b. 1500-1800 GMT

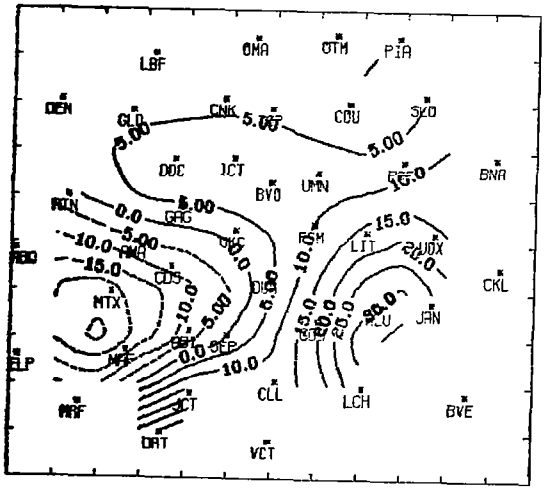

c. 1800-2100 GMT

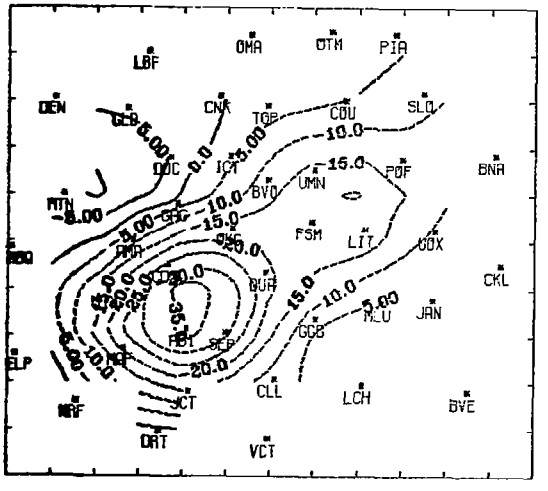

d. 2100-0000 GMT

Fig. A21. Residual (g $cm^{-2}s^{-1}$ x 10^{-6}) in the 900-750 mb layer for 10-11 April 1979.

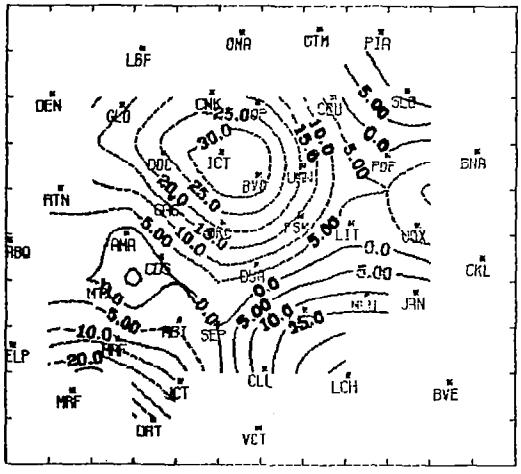

a. 0000-0300 GMT

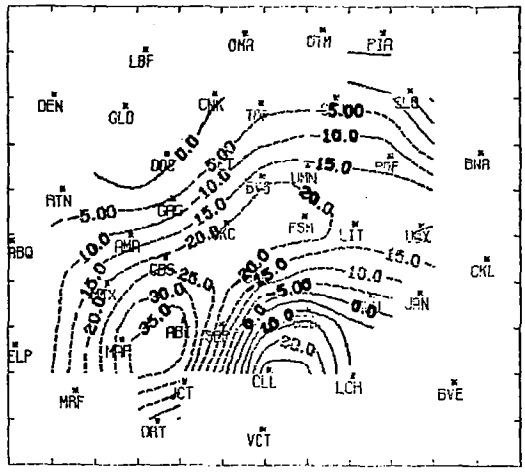

b. 0300-0600 GMT

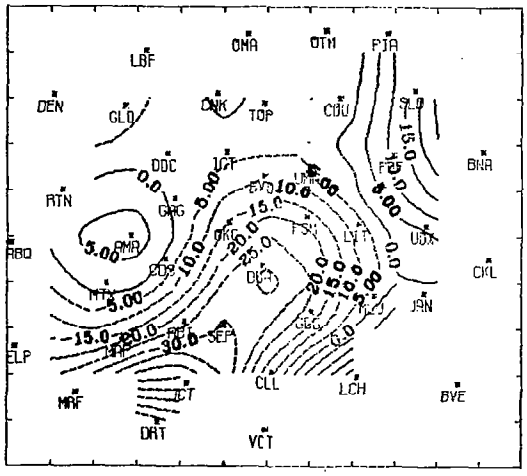

c. 0600-0900 GMT

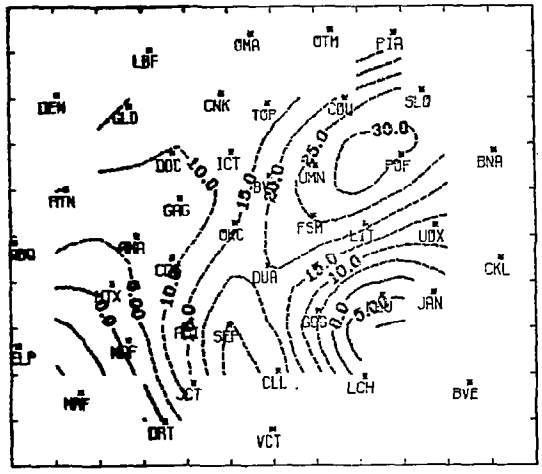

d. 0900-1200 GMT

Fig. A22. Residual (g $cm^{-2}s^{-1}$ x 10^{-6}) in the 900-750 mb layer for 11 April 1979.

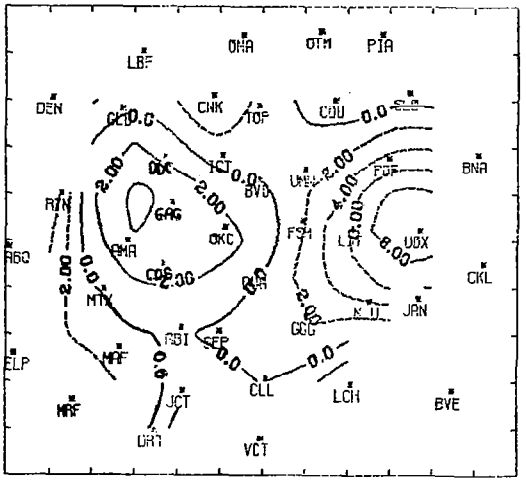

a. 1200-1500 GMT

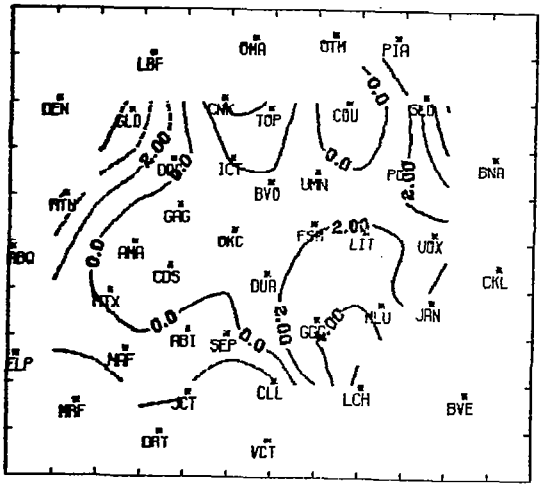

b. 1500-1800 GMT

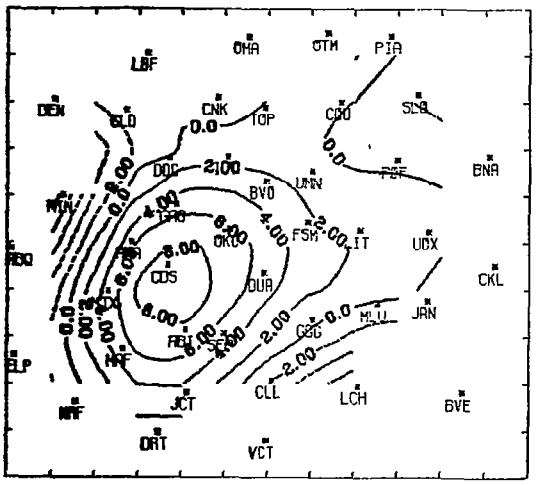

c. 1800-2100 GMT

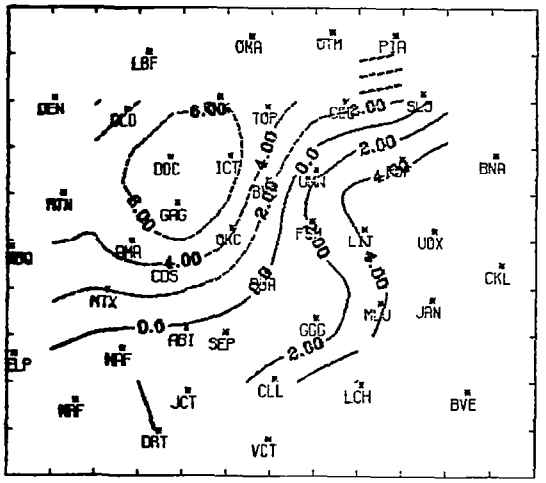

d. 2100-0000 GMT

Fig. A23. Residual (g $cm^{-2}s^{-1}$ x 10^{-6}) in the 600-500 mb layer for 10-11 April 1979.

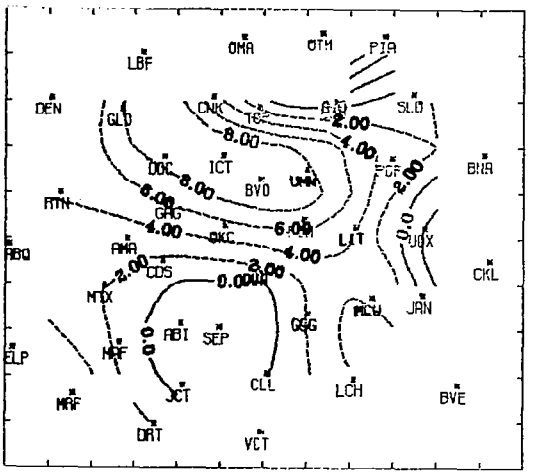

a. 0000-0300 GMT

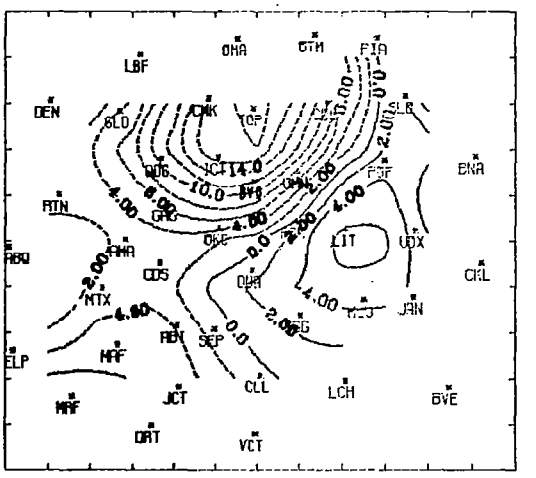

b. 0300-0600 GMT

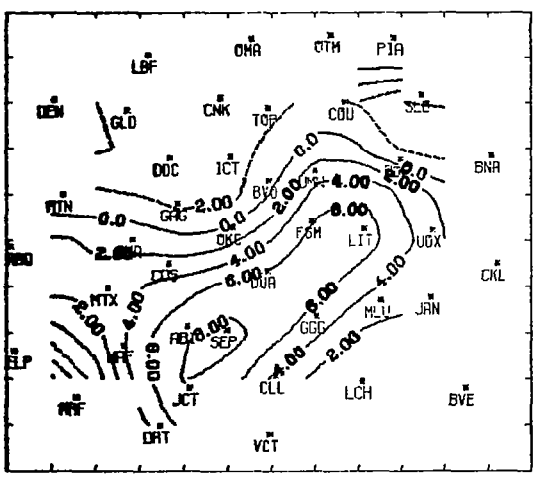

c. 0600-0900 GMT

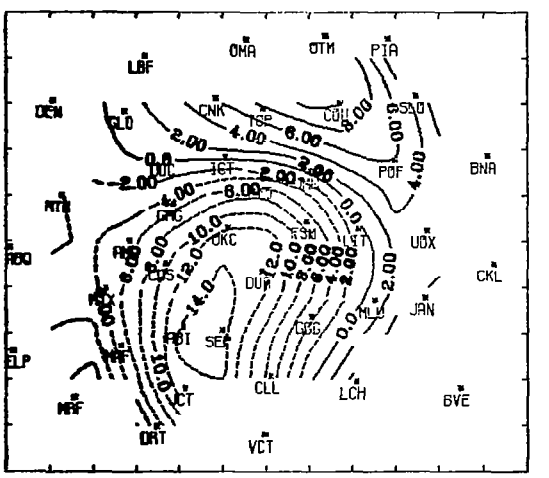

d. 0900-1200 GMT

Fig. A24. Residual (g $cm^{-2}s^{-1}$ x 10^{-6}) in the 600-500 mb layer for 11 April 1979.

APPENDIX B

Radar Summary Charts

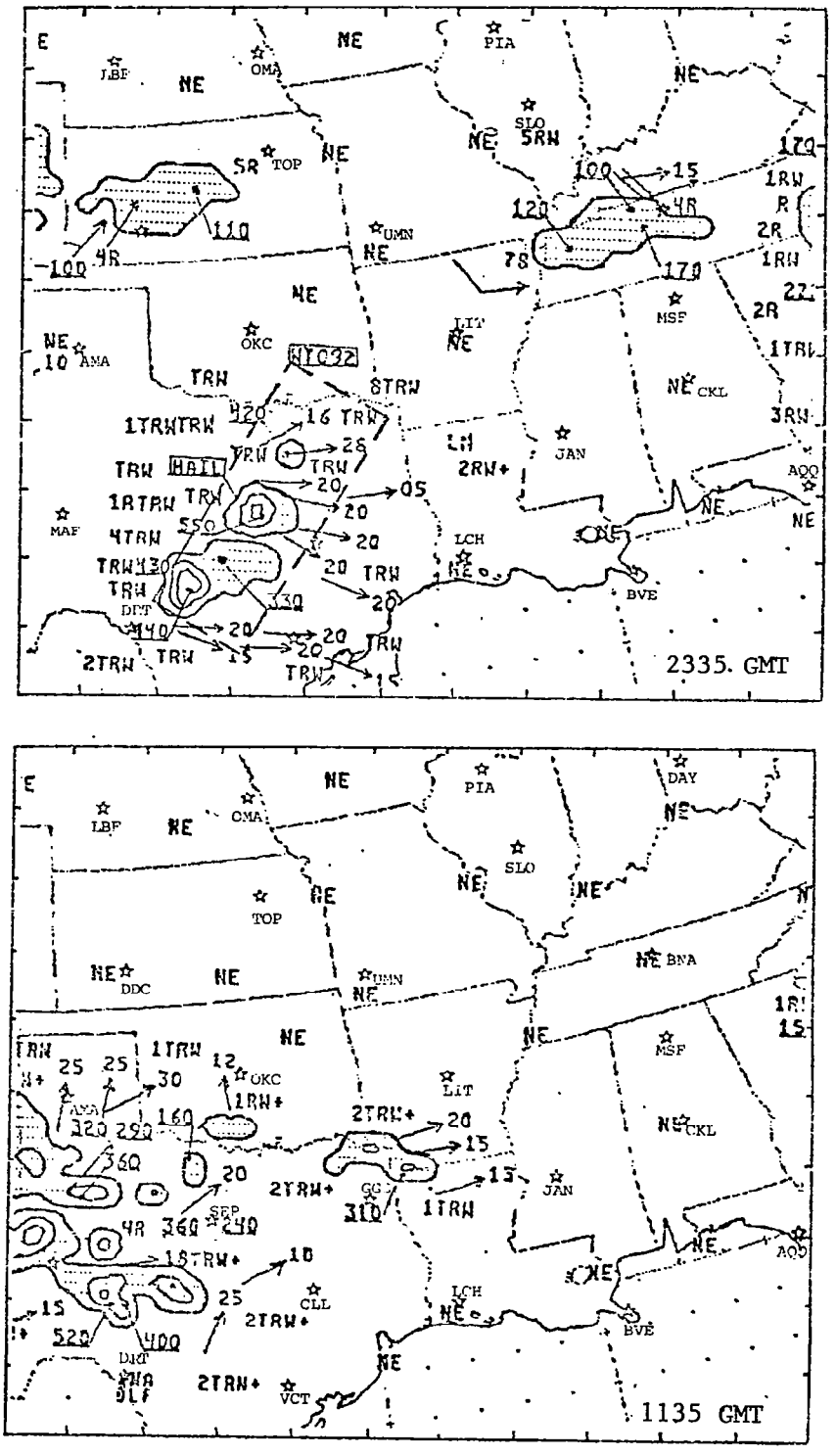

Fig. B1. Radar charts at 2335 GMT on 1 May 1978 and 1135 GMT on 2 May 1978.

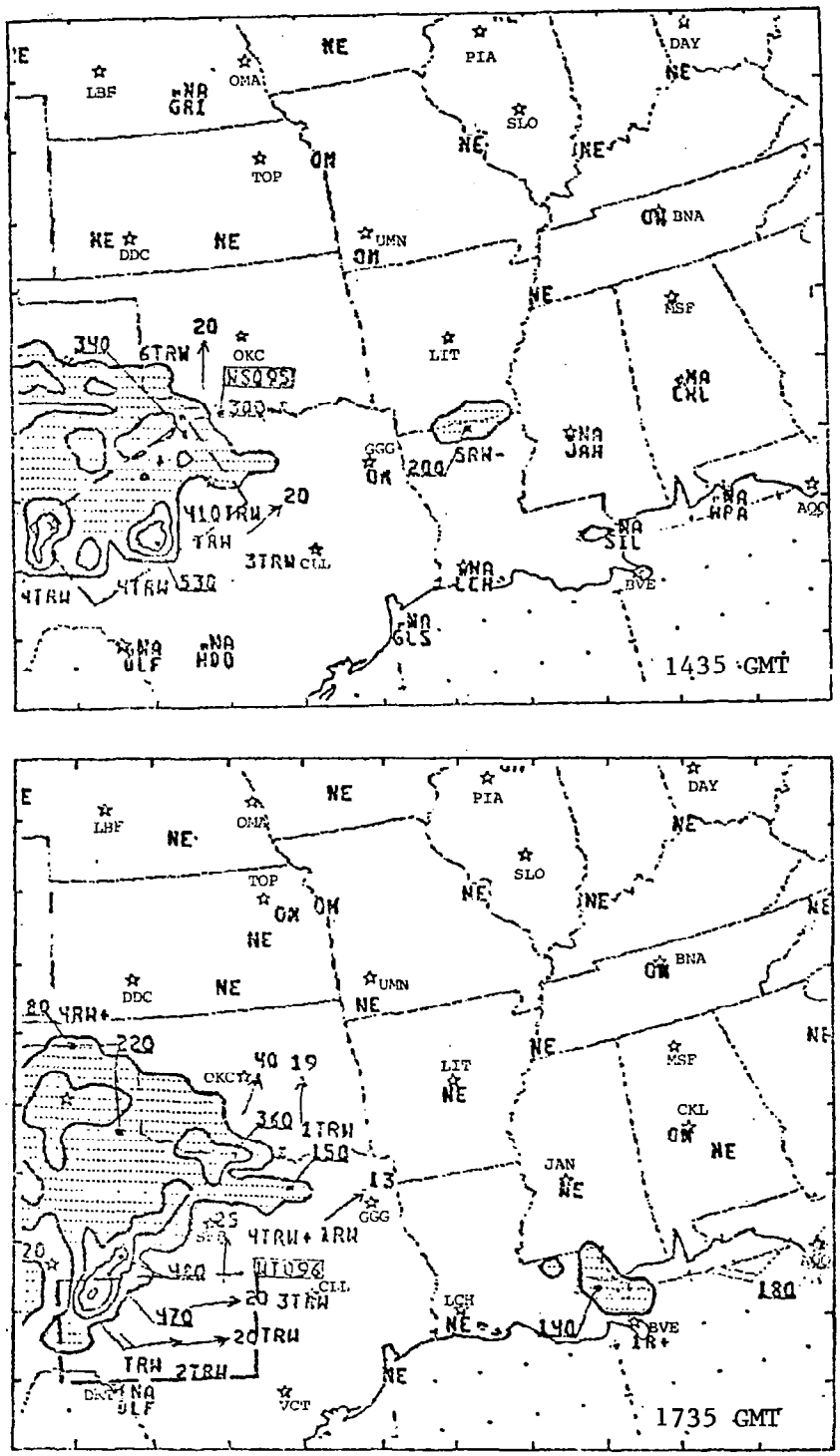

Fig. B2. Radar summary charts at 1435 and 1735 GMT on 2 May 1978.

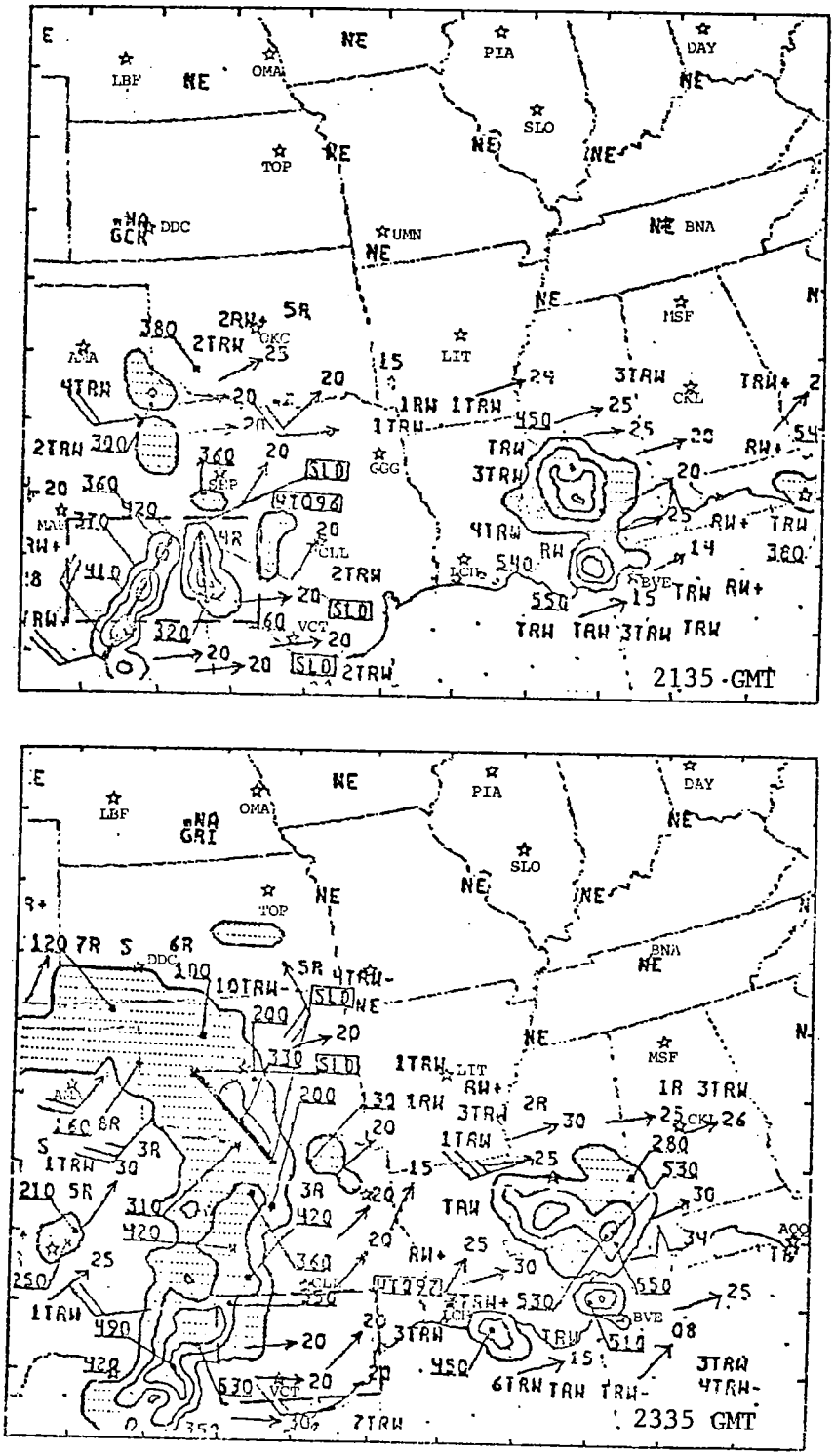

Fig. B3. Radar summary charts at 2135 and 2335 GMT on 2 May 1978.

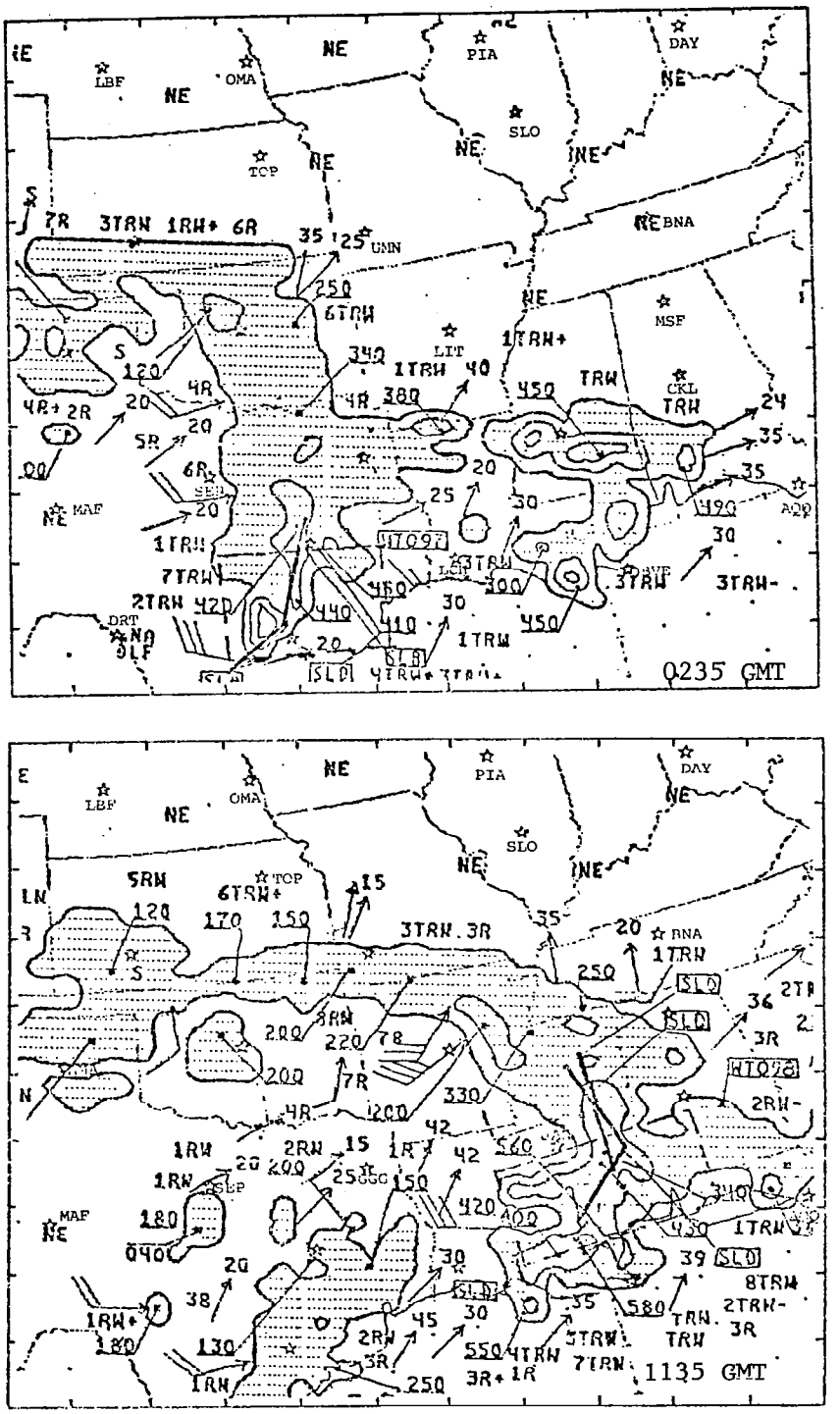

Fig. B4. Radar summary charts at 0235 GMT and 1135 GMT on 3 May 1978.

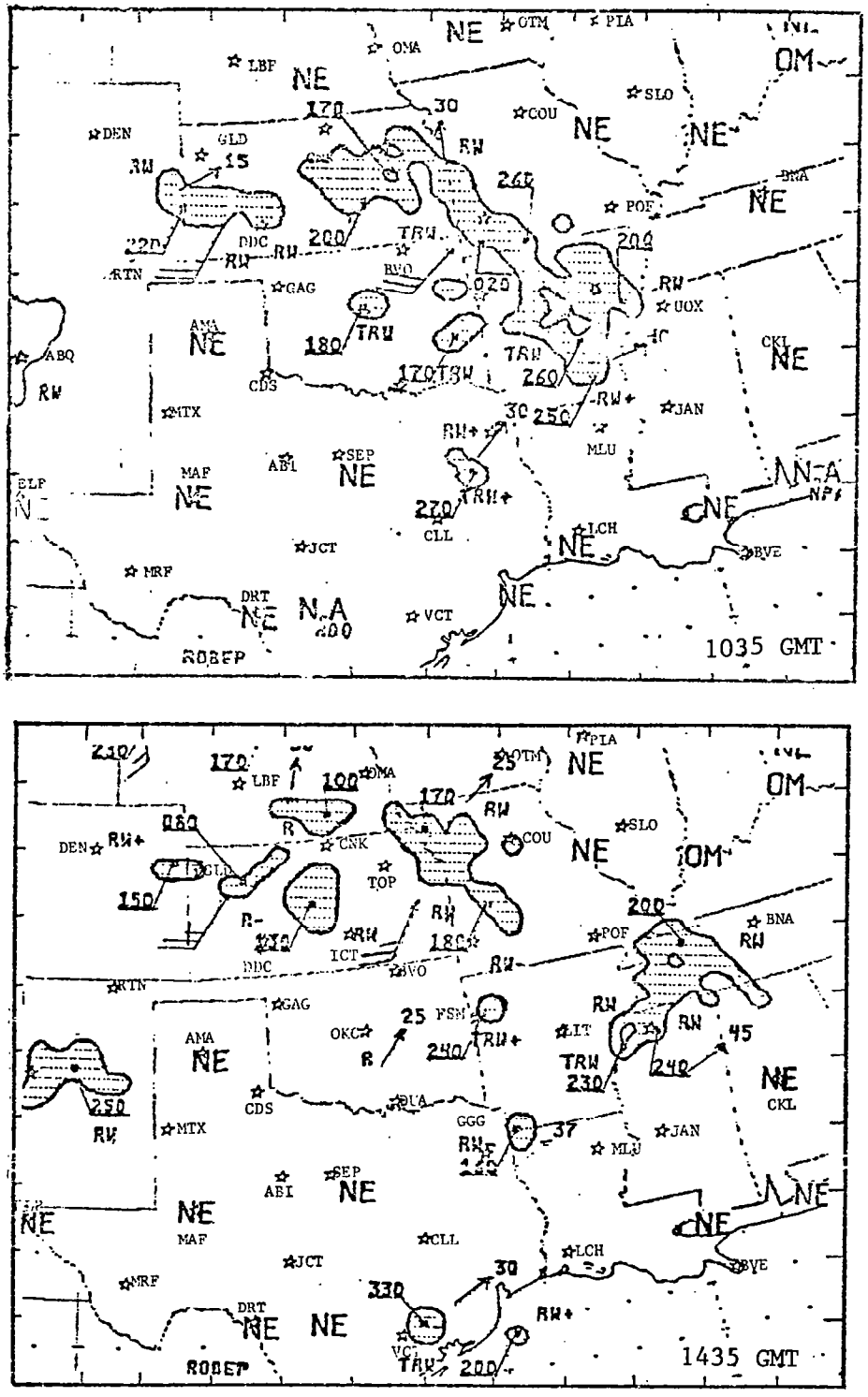

Fig. B5. Radar summary charts at 1035 and 1435 GMT on 10 April 1979.

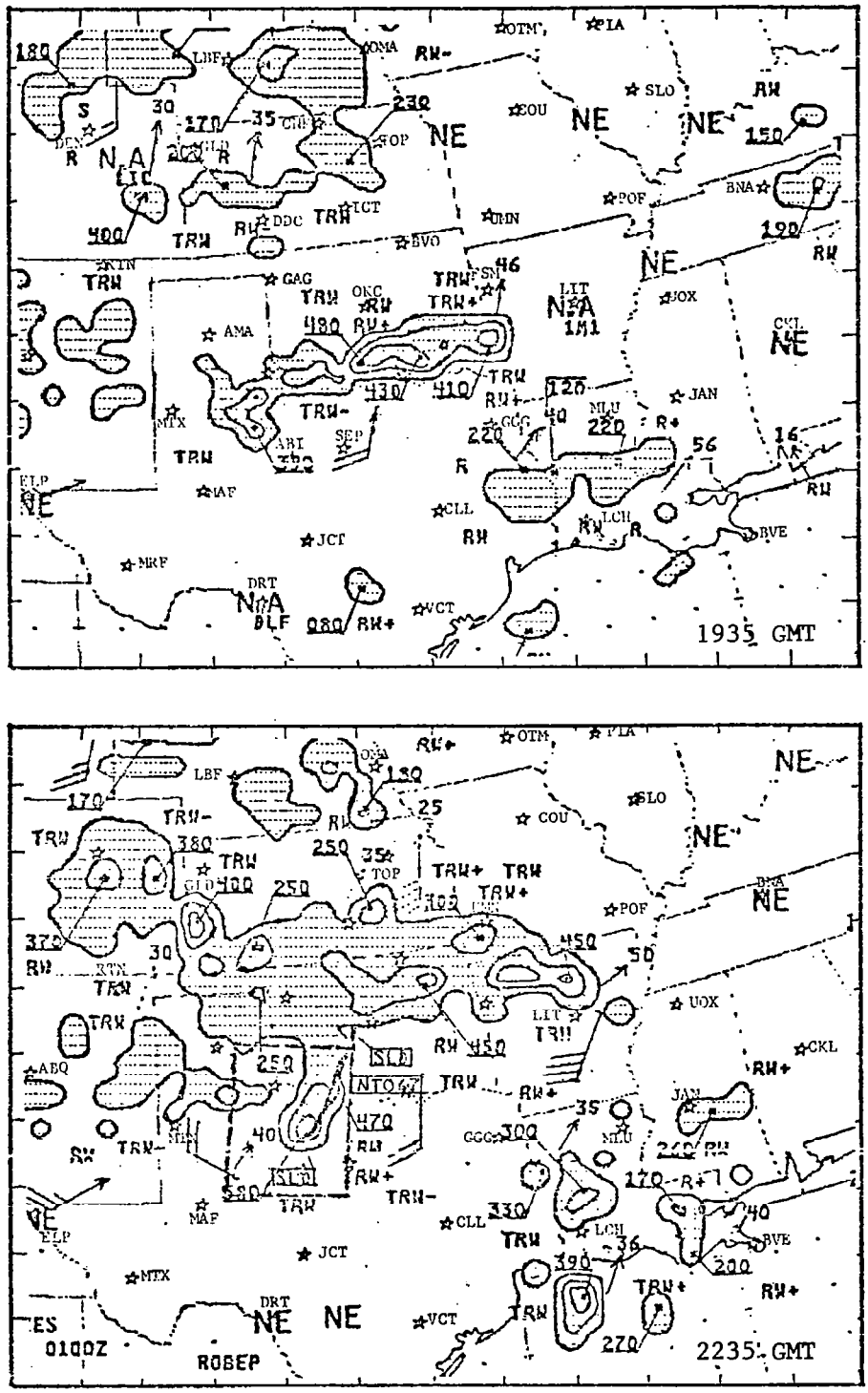

Fig. B6. Radar summary charts at 1935 and 2235 GMT on 10 April 1979.

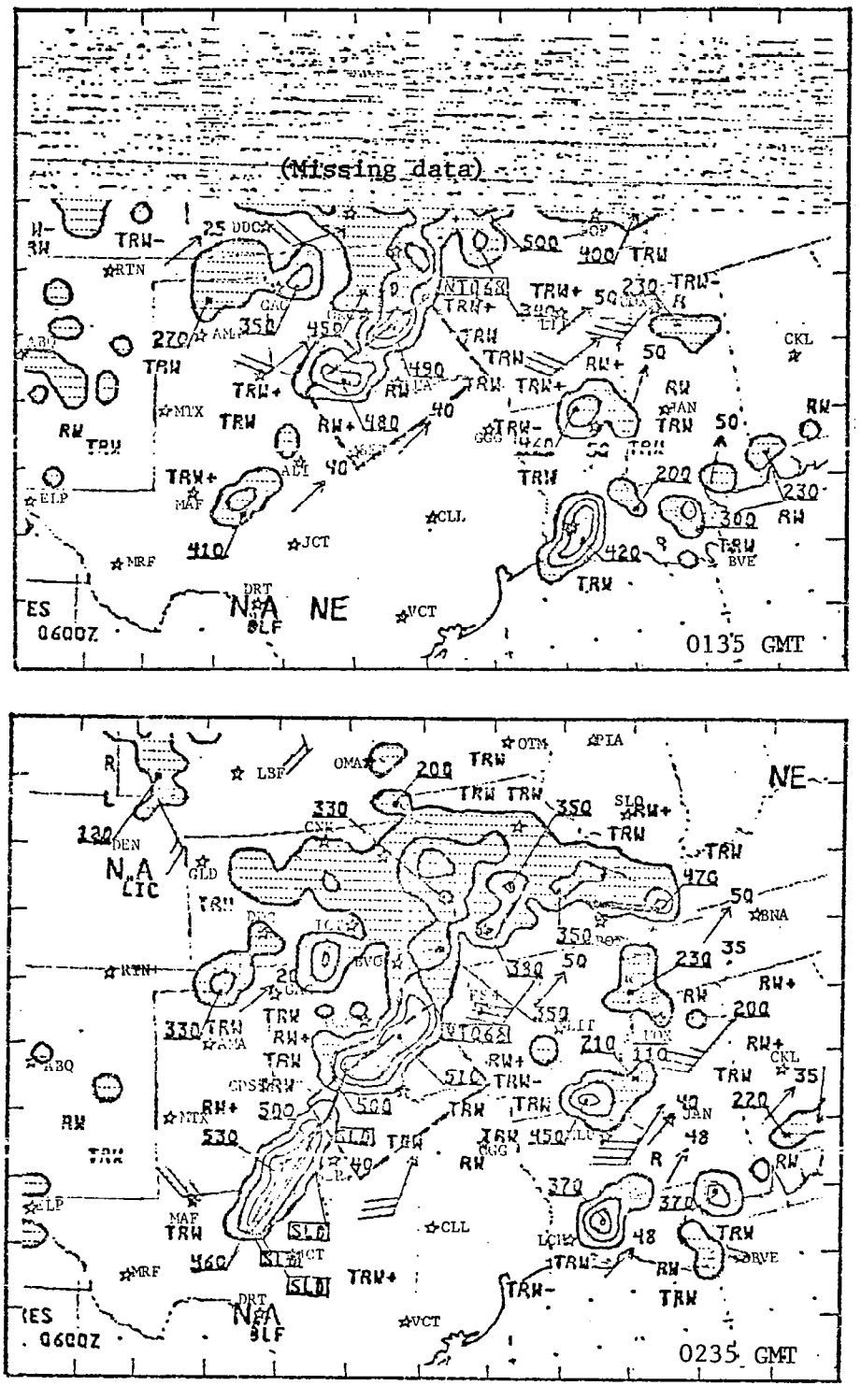

Fig. B7. Radar summary charts at 0135 and 0235 GMT on 11 April 1979.

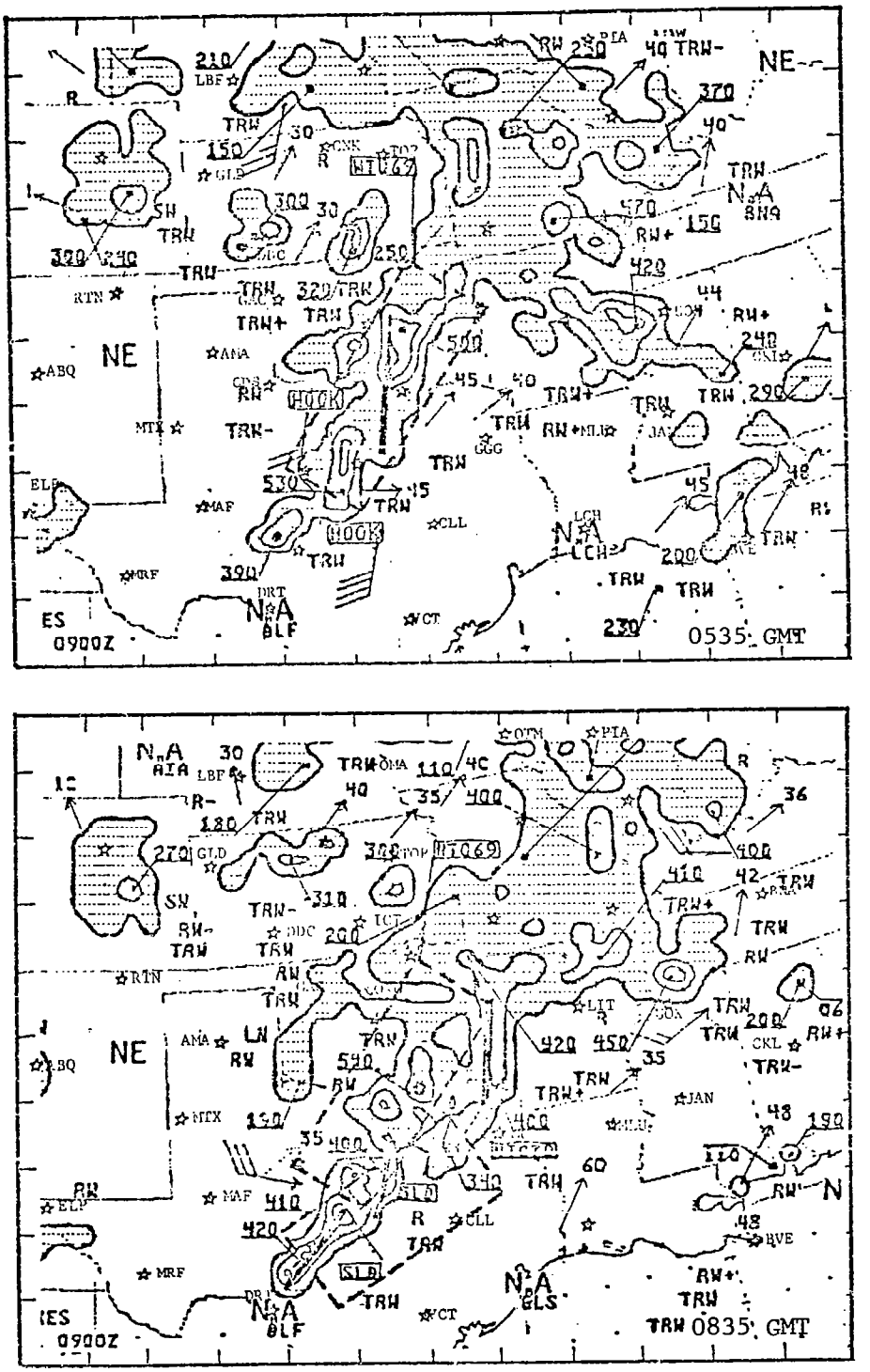

Fig. B8. Radar summary charts at 0535 and 0835 GMT on 11 April 1979.

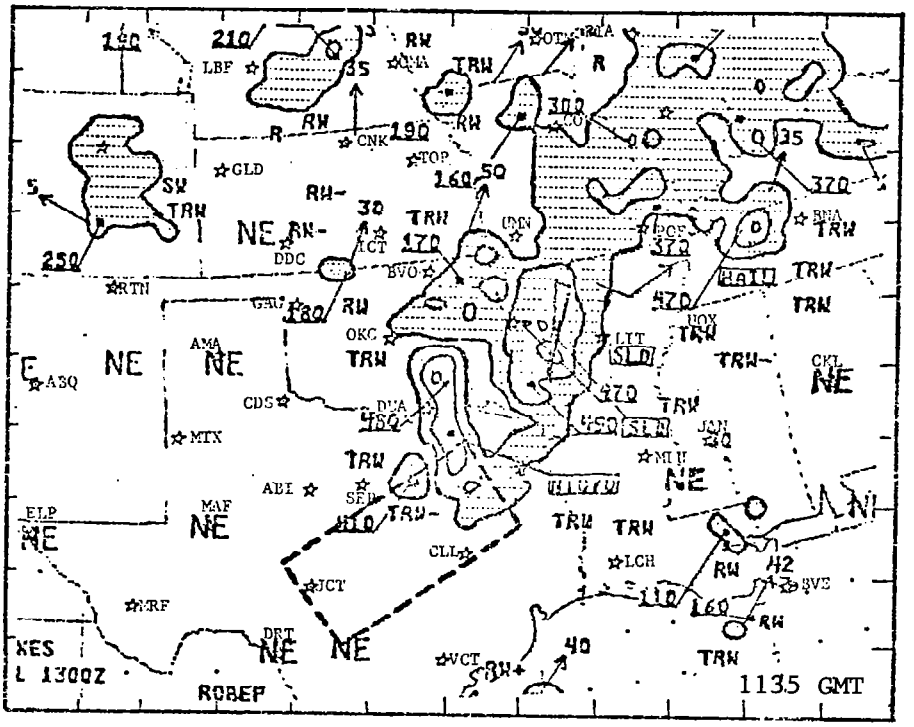

Fig. B9. Radar summary chart at 1135 GMT on 11 April 1979.

1. REPORT NO.	2. GOVERNMENT ACCESSION NO.	3. RECIPIENT'S CATALOG NO.
NASA CR-3542		

4. TITLE AND SUBTITLE	5. REPORT DATE
Moisture Processes Accompanying Convective Activity	April 1982
	6. PERFORMING ORGANIZATION CODE

7. AUTHOR(S)	8. PERFORMING ORGANIZATION REPORT #
Meta E. Sienkiewicz and James R. Scoggins	

9. PERFORMING ORGANIZATION NAME AND ADDRESS	10. WORK UNIT NO.
Department of Meteorology Texas A&M University College Station, Texas 77843	M-378
	11. CONTRACT OR GRANT NO. NAS8-33776
	13. TYPE OF REPORT & PERIOD COVERED
12. SPONSORING AGENCY NAME AND ADDRESS	Contractor Report
National Aeronautics and Space Administration Washington, D.C. 20546	14. SPONSORING AGENCY CODE

15. SUPPLEMENTARY NOTES

Marshall Technical Monitor: Robert E. Turner
Interim Report

16. ABSTRACT

A moisture budget analysis was performed on data collected during the AVE VII (2-3 May 1978) and AVE-SESAME I (10-11 April 1979) experiments. Local rates-of-change of moisture were compared with averaged moisture divergence in the same time period. Results were presented as contoured plots in the horizontal and as vertical cross sections. These results were used to develop models of the distribution of moisture processes in the vicinity of convective areas in two layers representing lower and middle tropospheric conditions. Good correspondence was found between the residual term of the moisture budget and actual precipitation.

17. KEY WORDS	18. DISTRIBUTION STATEMENT
Moisture budget Moisture processes Convective activity Moisture divergence	Unclassified - Unlimited Subject Category 47

19. SECURITY CLASSIF. (of this report)	20. SECURITY CLASSIF. (of this page)	21. NO. OF PAGES	22. PRICE
Unclassified	Unclassified	95	A05

For sale by National Technical Information Service, Springfield, Virginia 22161

NASA-Langley, 1982